Selective Polytopic Protein Degradation by Organelle Membrane Fusion

Erin Kate McNally

A Thesis
In the Department
of
Biology

Presented in Partial Fulfillment of the Requirements
For the Degree of
Doctor of Philosophy (Biology) at
Concordia University
Montréal, Quebec, Canada

August 2017

CONCORDIA UNIVERSITY

SCHOOL OF GRADUATE STUDIES

This is to certify that the thesis prepared

By: **Erin Kate McNally**

Entitled: **Selective Polytopic Protein Degradation by Organelle Membrane Fusion**

and submitted in partial fulfillment of the requirements for the degree of

Doctor Of Philosophy (Biology)

complies with the regulations of the University and meets the accepted standards with respect to originality and quality.

Signed by the final examining committee:

_____ Chair
Dr. Roisin O'Connor

_____ External Examiner
Dr. Christian Rocheleau

_____ External to Program
Dr. Vladimir Titorenko

_____ Examiner
Dr. Alisa Piekny

_____ Examiner
Dr. Michael Sacher

_____ Thesis Supervisor
Dr. Christopher Brett

Approved by _____
Dr. Grant Brown, Graduate Program Director

Thursday, August 17, 2017 _____
Dr. André Roy, Dean
Faculty of Arts and Science

Abstract

Selective Polytopic Protein Degradation by Organelle Membrane Fusion

Erin Kate McNally, Ph.D.

Concordia University, 2017

Lysosomes are dynamic organelles most notably known as the terminal compartments of the endocytic and autophagy pathways in eukaryotic cells. However, lysosome function is not simply for the elimination and catabolism of biomaterials. Rather lysosomes have emerged as critical and dynamic signaling hubs via their ability to sense and provide nutrients, and communicate this information to biosynthetic or metabolic processes. Lysosome physiology relies on membrane transporter activity, best signified by loss-of-function mutations linked to lysosomal storage disorders. These include nutrient transporter proteins that export products of catabolism to the cytoplasm for cellular reuse, as well as Ca^{2+} pumps and transporters important for signaling, and transporters for metal storage and homeostasis. Eukaryotic cells, and their lysosomes, undergo continuous renovation to clear damaged or unused proteins or to alter their proteome accommodating functional changes in response to the environment, physiological cues, or aging. Despite the importance of lysosomal transporters to cell physiology, little is known about their lifetimes and it remains unclear how they are degraded.

Here, I used *Saccharomyces cerevisiae* and its vacuolar lysosome as models to study lysosomal transporter lifetimes and discovered a new cellular protein degradation pathway, the IntraLumenal Fragment (ILF) pathway: During membrane fusion events between lysosomes, transporters are selectively labeled for recognition and sorting by the fusion protein machinery into an area of membrane spanning the apposed organelles. Upon fusion, this membrane and proteins embedded within it are internalized into the lumen as a byproduct for degradation by hydrolases. I find the ILF pathway selectively degrades lysosomal transporters when misfolded, in response to TOR signaling or changes in substrate levels. I also find that protein clients are not limited to lysosomal transporters, as this pathway degrades internalized surface membrane proteins that bypass entry into the canonical MultiVesicular Body pathway, which was previously thought to be the exclusive mechanism for selective surface protein degradation. Finally, I find the ILF pathway cooperates with a second, independent protein degradation

pathway, the vReD pathway, to change the lysosomal membrane proteome. The underlying machinery and transporters studied are evolutionarily conserved, suggesting the ILF pathway contributes to lysosome physiology in all eukaryotic cells.

Acknowledgements

I would like to thank my supervisor Dr. Christopher Brett for giving me the opportunity to complete my Ph.D. research under your supervision and for giving me invaluable guidance and feedback throughout my studies. In addition, I would like to thank my committee members Dr. Alisa Piekny and Dr. Michael Sacher for their support, suggestions and valuable input during my studies.

I also thank the Center for Microscopy and Cellular Imaging at Concordia University, specifically Dr. Christopher Law and Dr. Chloë van Oostende for their constant training, guidance, and assistance.

Thank you to both present and past members of the Brett Lab for providing support both scientifically and personally.

Finally, I thank my family for their unconditional support and encouragement not only throughout my studies but also in everything that I do.

Contribution of Authors

Figure 4: Mahmoud Karim contributed the fusion curve as shown in D.

Figure S2: Mahmoud Karim contributed the fusion curve as shown in D.

Table Of Contents

List of Figures

List of Tables

List of Supplemental Figures

List of Supplemental Movies

Movie S1. Movie of a vacuole fusion event demonstrating the sorting and internalization of Vph1-GFP into the vacuolar lumen.

Movie S2. Movie of a vacuole fusion event demonstrating the exclusion of Fet5-GFP from the boundary membrane although a membrane fragment was formed.

Movie S3. Movie of a vacuole fusion event demonstrating the sorting and internalization of Fth1-GFP into the vacuolar lumen.

Movie S4. Movie of a vacuole fusion event demonstrating the sorting and internalization of Fet5-GFP into the vacuolar lumen after heat stress.

Movie S5. Movie of a vacuole fusion event demonstrating the sorting and internalization of Fth1-GFP into the vacuolar lumen after heat stress.

Movie S6. Movie of a vacuole fusion event demonstrating the sorting and internalization of Fet5-GFP into the vacuolar lumen after cycloheximide treatment.

Movie S7. Movie of a vacuole fusion event demonstrating the sorting and internalization of Fth1-GFP into the vacuolar lumen after cycloheximide treatment.

Movie S8. Movie of a vacuole fusion event demonstrating the sorting and internalization of Hxt3-GFP into the vacuolar lumen when VPS36 is deleted.

Movie S9. Movie of a vacuole fusion event demonstrating the sorting and internalization of Mup1-GFP into the vacuolar lumen when VPS27 is deleted.

Movie S10. Movie of a vacuole fusion event demonstrating the sorting and internalization of Mup1-GFP into the vacuolar lumen when VPS27 is deleted after cycloheximide treatment.

Movie S11. Movie of a vacuole fusion event demonstrating the sorting and internalization of Hxt3-GFP into the vacuolar lumen when VPS36 is deleted after cycloheximide treatment.

Movie S12. Movie of a vacuole fusion event demonstrating the sorting and internalization of Ypq1-GFP into the vacuolar lumen.

Movie S13. Movie of a vacuole fusion event demonstrating the sorting and internalization of Ypq1-GFP into the vacuolar lumen when VPS36 is deleted.

Movie S14. Movie of a vacuole fusion event demonstrating the sorting and internalization of Cot1-GFP into the vacuolar lumen.

Movie S15. Movie of a vacuole fusion event demonstrating the sorting and internalization of Cot1-GFP into the vacuolar lumen when VPS27 is deleted.

Movie S16. Movie of a vacuole fusion event demonstrating the exclusion of Vba4-GFP from the boundary membrane although a membrane fragment was formed.

Movie S17. Movie of a vacuole fusion event demonstrating the sorting and internalization of Vba4-GFP into the vacuolar lumen when VPS36 is deleted.

Movie S18. Movie of a vacuole fusion event demonstrating the exclusion of Vba4-GFP from the boundary membrane although a membrane fragment was formed and the presence of puncta closely apposed to the vacuolar membrane after cycloheximide treatment.

Movie S19. Movie of a vacuole fusion event demonstrating the sorting and internalization of Vba4-GFP into the vacuolar lumen after heat stress.

List of Abbreviations

ATP	adenosine triphosphate
CHX	cycloheximide
CPS	carboxypeptidase S
DAG	diacylglycerol
DDM	*n*-Dodecyl β-D-maltoside
DMSO	dimethyl sulfoxide
DNA	deoxyribonucleic acid
DSC	Defective in SREBP Cleavage
EGO	Exit from G_0
ESCRT	endosomal sorting complexes required for transport
F.I.	fusion inhibitors
FI	fluorescence intensity
FM4-64	*N*-(3-Triethylammoniumpropyl)-4-(6-(4-(Diethylamino) Phenyl) Hexatrienyl) Pyridinium Dibromide (lipophilic dye for fluorescence microscopy)
FRAP	fluorescence recovery after photobleaching
GAP	guanine nucleotide activating protein
rGDI1	recombinant guanine nucleotide dissociation inhibitor
GDP	guanosine diphosphate
GEF	guanine nucleotide exchange factor
GFP	green fluorescence protein
GTP	guanosine triphosphate
GTPase	guanosine triphosphatase
rGyp1-46	GAP catalytically active domain (46) of recombinant GTPase activating protein 1
HOPS	homotypic fusion and vacuole protein sorting
HS	heat stress
ILF	intralumenal fragment
ILV	intralumenal vesicle
LCD	lysosomal cell death
LSDs	lysosomal storage disorders
Mf	mobile fraction

MVB	multivesicular body
NSF	N-ethylmaleimide-sensitive factor
PI(3)P	phosphatidylinositol 3-phosphate
$PI(4,5)P_2$	phosphatidylinositol 4,5-bisphosphate
PUR	puromycin
RAP	rapamycin
RING	really interesting new gene
ROI	region of interest
ROS	reactive oxygen species
SC	synthetic complete
SNARE	soluble N-ethylmaleimide-sensitive factor attachment protein receptor
TFEB	transcription factor EB
TIRF	total internal reflection fluorescence
(m)TOR	(mechanistic) target or rapamycin
mTORC1/2	mechanistic target of rapamycin complex 1/2
Ub	ubiquitin
rVam7	recombinant vam7
VPS	vacuolar protein sorting
vReD	vacuolar membrane recycling and degradation
YPD	yeast extract peptone dextrose

Chapter 1. Introduction

1.1 Lysosome physiology

All eukaryotic cells contain organelles that perform specific functions. Lysosomes are dynamic organelles implicated in a variety of cellular processes including, nutrient sensing through mTOR signaling (Perera and Zoncu, 2016), the storage or metals, ions and amino acids (Li and Kane, 2009), plasma membrane repair (Andrews, 2002), and transcriptional regulation (Settembre et al., 2013). First discovered in 1955 by Belgian biochemist Christian de Duve, the lysosome is perhaps most notably known as the degradative organelle, responsible for the catabolism and recycling of both intracellular and extracellular biomaterials. Important for its degradative function is the acidic lumenal pH – ranging between pH 4.5 and 5.5 – which provides an optimal environment for hydrolase activity. Lumenal acid hydrolases catabolize a wide variety of cellular compartments leading to the production of nutrients such as amino acids, nucleotides, monosaccharides, and fatty free acids, which are exported for cellular reuse by dedicated transporters. Since these transporters support lysosomal function, their lifetimes must be tightly regulated to ensure organelle homeostasis. As with other cellular proteins, lysosomal polytopic proteins are at constant risk of misfolding or aggregating to potentially cause toxicity and disease.

Lysosomes are the terminal hub of multiple trafficking pathways that carry biomaterials destined for degradation. These pathways, including the secretory, endocytic, phagocytic and autophagic membrane-trafficking pathways, are dependent on lysosome function for the degradation of cellular components. Essential for proper lysosome function, there are three specific events that must occur: membrane fusion between the lysosome and various transport vesicles, the catabolism of biomaterials, and the export of nutrients for cellular reuse. First, in order for lysosomes to receive incoming biomaterials, the lysosome must undergo a *membrane fusion* event with transport vesicles encapsulating biomaterials from within the cell, through autophagy or from outside the cell, via endocytosis and the MultiVesicular Body pathway. Once within the lysosomal lumen, biomaterials are exposed to lumenal acid hydrolases, such as proteases and lipases, for *catabolism* into their constituents, including amino acids, lipids, and nucleotides. Once degraded, these nutrients are *exported* back out into the cytoplasm for reuse by the cell through resident lysosomal membrane transporters. These lysosomal transporter proteins are thus essential for lysosomal function as they also regulate the lumenal environment and contribute to cellular signaling.

For example, the V-type H^+-ATPase drives lumenal acidification required for the proper maturation and function of acid hydrolases that degrade proteins, lipids and DNA into their constituents (Tarsio, et al., 2011). In turn, these constituents are returned to the cytoplasm for reuse through the activities of other transporters that mobilize nucleotides (ENT3) (Song et al., 2014), amino acids (SLC38A9, PQLC2) (Jung et al., 2015; Jezegou et al., 2013), lipids (NPC1, CLN3) (Ko, et al., 2001), and other metabolites and macromolecules (e.g. ABCB6) (Kiss et al., 2015). Lysosomes are also critical for cellular Ca^{2+} signaling (TRPML1) (Wang et al., 2015) and storage of divalent metals – including Zn^{2+} by ZnT2 (Hennigar and Kelleher, 2015), Cu^{2+} by SLC31A2 (Schweigel-Rontgen, 2014) and iron by NRAMP2/DMT1 (Ehrnstorfer et al., 2011) – essential cofactors for many cellular enzymes. Due to their importance to lysosome physiology, mutations that target many of these transporters underlie human diseases related to lysosome dysfunction, classified as lysosomal storage disorders. These include mucolipidosis type IV linked to TRPML1 (Waller-Evans and Lloyd-Evans, 2015), juvenile neuronal ceroid lipofuscinosis (or Batten disease) linked to CLN3 (Arlt et al., 2011), or Niemann-Pick disease type C linked to NPC1 (Berger et al., 2005). Despite the fact that lysosomal transporters are critical for cellular homeostasis and their lifetimes must be tightly regulated, these proteins are understudied leading to the pivotal question: *How are resident lysosomal polytopic proteins turned over by degradation?*

1.2 ESCRT-dependent degradation of polytopic proteins

One possibility is that lysosomal polytopic proteins use the canonical cellular protein degradation pathway known to control lifetimes of polytopic proteins that relies on lysosome function, the MultiVesicular Body (MVB) pathway (**Figure 1A**). Surface polytopic proteins, such as receptors or transporters, are responsible for diverse physiology, including cellular growth and differentiation, the immune response, and neurotransmission (Raiteri and Raiteri, 2015). As such, their lifetimes are tightly regulated through the biosynthesis of new proteins as well as the removal and degradation of existing proteins via endocytosis and the MVB pathway. Since their discovery, how ESCRTs (Endosomal Sorting Complexes Required for Transport) function in regulating protein turnover has been extensively studied. With a few exceptions, ESCRT-dependent protein sorting into the MVB pathway relies on cargo protein ubiquitylation, a universal signal for protein degradation (MacDonald et al, 2012). These proteins are

ubiquitinated primarily through the coordinated action of an E3-ubiquitin ligase and an E4-adaptor protein, either constitutively (i.e. Ste3-GFP; Davis et al., 1993), in response to protein misfolding (Keener and Babst, 2013), TOR activation (MacGurn et al., 2011), or due to changes in cognate substrate levels (i.e. Mup1-GFP; MacDonald et al., 2012). Once ubiquitinated, proteins are internalized by endocytosis and sent to endosomal membranes, where they are recognized and interact with ESCRT machinery that function sequentially to sort and package protein cargoes into intralumenal vesicles (ILVs) (Raiborg and Stenmark, 2009; Henne et al., 2011). After multiple rounds of this process, a mature MVB forms that upon fusing with the lysosome, deposits protein-laden vesicles within the lumen for degradation by lumenal acid hydrolases.

The ESCRT protein machinery are evolutionarily conserved and function sequentially to drive surface protein recognition and sorting. This sorting machinery is comprised of five protein complexes (ESCRT-0, ESCRT-I, ESCRT-II, ESCRT-III and the Vps4 complex) that initially reside in the cytoplasm, but are successively recruited to the endosomal membrane for assembly and to facilitate protein sorting and MVB genesis.

The ESCRT-0 complex initiates the MVB pathway and is a heterodimer consisting of Vps27 (Vacuole Protein Sorting) and Hse1 (Henne et al., 2011). ESCRT-0 localizes to endosomal membranes where both subunits can recognize and engage ubiquitylated plasma membrane polytopic proteins, or 'cargoes'. ESCRT-0 also recruits the ESCRT-1 complex, comprised of Vps23, Vps28, Vps37, and Mvb12, through its interaction with Vps23. ESCRT-I, through the UEV (Ubiquitin E2 Variant) domain of Vps23, binds ubiquitylated protein cargoes and recruits ESCRT-II via the interaction between Vps28 and Vps36. ESCRT-II, comprised of Vps36, Vps22, and Vps25, propagates ubiquitylated protein sorting through Vps36 and recruits ESCRT-III with the interaction between Vps25 and Vps20. The ESCRT-III complex, consisting of Vps20, Snf7, Vps24 and Vps2, is required for the final steps of the MVB sorting, cargo protein sequestration, and MVB vesicle formation. Snf7 sequesters cargo proteins into membrane patches to initiate MVB formation and Vps2 recruits the Vps4 complex consists of three subunits, Vps4, Vps60 and Vta1, for final scission of the invaginated membrane, via the ATPase activity of Vps4, and creation of the intralumenal vesicle and ESCRT disassembly. Unlike the other ESCRT

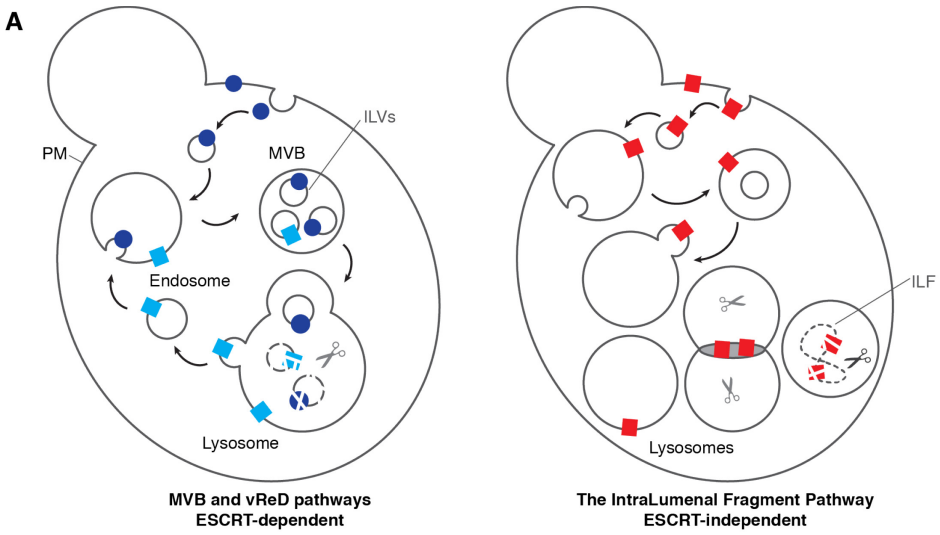
A
PM
MVB
ILVs
Endosome
Lysosome
MVB and vReD pathways
ESCRT-dependent
ILF
Lysosomes
The IntraLumenal Fragment Pathway
ESCRT-independent

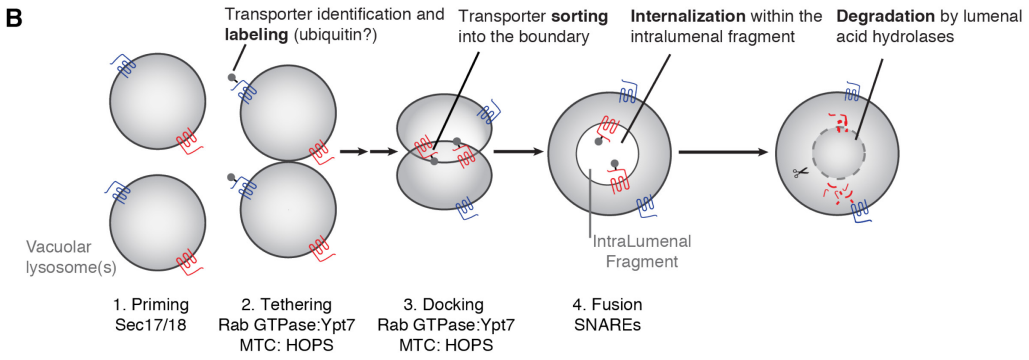
B
Transporter identification and labeling (ubiquitin?)
Transporter sorting into the boundary
Internalization within the intralumenal fragment
Degradation by lumenal acid hydrolases
Vacuolar lysosome(s)
IntraLumenal Fragment
1. Priming
Sec17/18
2. Tethering
Rab GTPase:Ypt7
MTC: HOPS
3. Docking
Rab GTPase:Ypt7
MTC: HOPS
4. Fusion
SNAREs

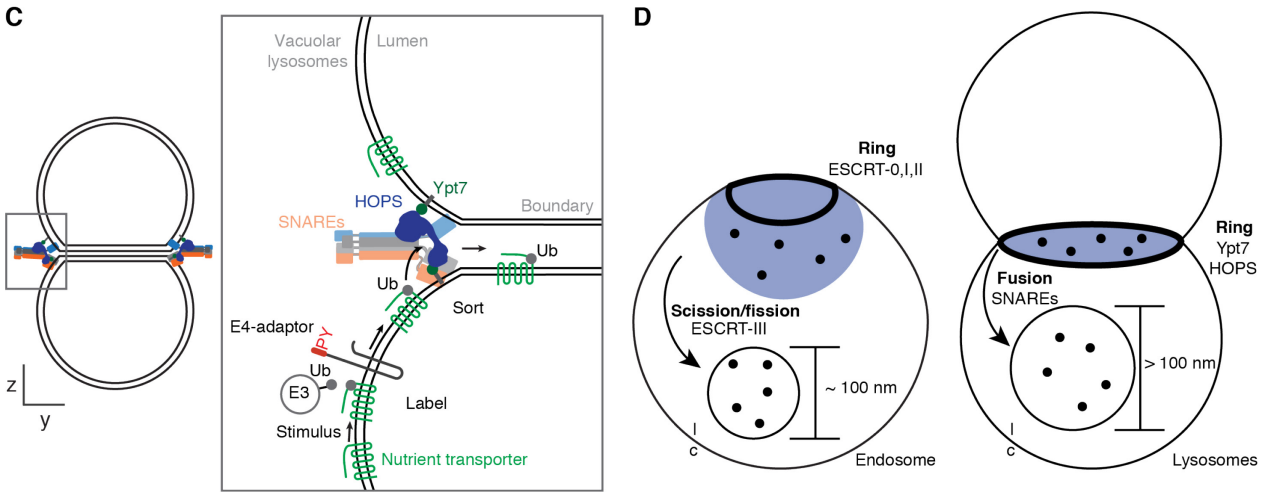
C
Vacuolar lysosomes
Lumen
Ypt7
HOPS
SNAREs
Boundary
Ub
Ub
Sort
E4-adaptor
Ub
E3
Label
Stimulus
Nutrient transporter
z
y
D
Ring
ESCRT-0,I,II
Scission/fission
ESCRT-III
~ 100 nm
Endosome
Ring
Ypt7
HOPS
Fusion
SNAREs
> 100 nm
Lysosomes

Figure 1. Summary of the canonical ESCRT-dependent pathway and the ESCRT-independent, IntraLumenal Fragment pathway for polytopic protein degradation

(A) Cartoon models of key stages in ESCRT-dependent (MVB and vReD) and ESCRT-independent (ILF) protein degradation pathways. Surface polytopic proteins (dark blue) and lysosomal polytopic proteins (light blue) are sent to the endosome for sorting into ILVs by ESCRT machinery before deposition within the lysosomal lumen for degradation. Surface or lysosomal polytopic proteins (red) are present within the boundary membrane and internalized as an ILF for degradation within the lysosomal lumen. **(B)** Stages of homotypic membrane fusion demonstrating how the ILF pathway accommodates lysosomal polytopic protein sorting and internalization. **(C)** Working model describing how lysosomal nutrient transporters are labeled with ubiquitin for selective sorting into the boundary membrane in the ILF pathway. Upon stimulation, nutrient transporters are labeled with ubiquitin through coordination of an E3 Ubiquitin-ligase and an E4-adaptor protein. Once ubiquitinated, the membrane fusion machinery – including SNARE proteins, the Rab GTPase Ypt7, and the HOPS tethering complex – recognize and bind the protein for active sorting into the boundary membrane for subsequent internalization into the lysosomal lumen and exposure to lumenal acid hydrolases for degradation upon lipid bilayer fusion. The membrane fusion machinery concentrates at the vertex domain of docked organelles to facilitate fusion, thus they are in an ideal location to regulate polytopic protein sorting as the vertex surrounds the boundary membrane in a ring. Additionally, three of the six HOPS subunits contain RING (Really Interesting New Gene)-like motifs that when in complex form a predicted ubiquitin-binding domain. **(D)** Cartoon comparing polytopic protein sorting at the endosome and lysosome. At the endosome, proteins undergo ESCRT-dependent sorting into a ring surrounding the nascent ILV prior to a membrane scission event mediated by the ESCRT-III complex for ILV genesis. At the lysosomal membrane, the membrane fusion machinery including Ypt7 and HOPS assemble in a vertex ring surround the boundary membrane for protein sorting prior to SNARE-mediated membrane fusion and internalization of the boundary as an ILF. Black dots represent polytopic proteins. PM: Plasma membrane MVB: MultiVesicular Body. ILVs: Inralumenal vesicles. ILF: Intralumenal fragment. MTC: multisubunit tethering complex. HOPS: homotypic fusion and vacuole protein sorting. SNAREs: soluble NSF attachment protein receptor. Ub: ubiquitin. Ypt7: Rab GTPase. PY: PY-motif. E3: E3-ubiquitin ligase. l = lumen. c = cytoplasm.

complexes, none of the ESCRT-III subunits contain ubiquitin-binding domains, rather they are thought to function as the membrane scission (or fission) machinery. These subunits can oligomerize into spiral-shaped polymers capable of deforming endosomal membranes into inward budding tubular structures (Mageswaran et al., 2014), allowing for the final scission of the invaginated membrane and creation of the intralumenal vesicle. Together, the ESCRT complexes form a concentric ring or circle to concentrate cargo proteins for their internalization into nascent ILVs (**Figure 1D**; Piper et al., 1995; Urbanowski and Piper, 2001; Babst et al., 2002; Katzmann et al., 2003; Nickerson et al., 2007; Teis et al., 2009; Shields and Piper, 2012; Vild et al., 2015).

Recently Scott Emr and colleagues proposed an ESCRT-dependent mechanism, termed the vReD (Vacuole membrane REcycling and Degradation) pathway, capable of degrading lysosomal transporter proteins in response to changes in cognate substrate levels. Here, instead of entering the MVB pathway from the surface, lysosomal transporter proteins are sent directly from the lysosome (vacuole) to the endosome for ESCRT-dependent sorting and ILV packaging (**Figure 1A**). In their founding publication, the authors demonstrated that Ypq1, a vacuolar amino acid transporter protein, is ubiquitinated and sent through a retrograde trafficking pathway to the MVB when cells are starved of lysine. Briefly, Ypq1 is ubiquitinated by the E3-ligase Rsp5 and E4 adaptor protein Ssh4, where it is sorted into patches on the vacuolar membrane. These patches then bud off of the membrane as post-vacuolar compartments where the ESCRT-machinery can further package Ypq1 into ILVs creating a mature MVB. Upon fusion between the MVB and the vacuole, Ypq1-containing ILVs are deposited within the lumen for degradation (Li et al., 2015a). Shortly after characterizing the selective degradation of Ypq1, the authors published a similar story for the turnover of Cot1 – a zinc transporter – in response to changes in zinc levels. Here, Cot1 is ubiquitinated by the E3-ligase Tul1 and the DSC (Defective in SREBP Cleavage) complex when cells are grown in the absence of zinc (Li et al., 2015b).

While the vReD pathway represents the first descriptions of how vacuolar lysosome polytopic proteins can be degraded, Ypq1 and Cot1 are the only known cargoes and authors admit that other transporters (e.g. Fth1, Vph1, Fet5, Ncr1, Ycf1 and Vba4; Li et al., 2015a,b) do not use this pathway for degradation upon substrate manipulation. Additionally, the authors only observe protein degradation by the vReD pathway in response to substrate chelation or addition and have yet to identify any lysosomal proteins constitutively degraded by this pathway and the

ESCRT machinery. It is known that cells survive when components of the ESCRT machinery are impaired, suggesting another pathway for vacuolar lysosome transporter degradation exists within the cell. One cellular process that may accommodate the topological challenge of internalizing lysosomal polytopic proteins for degradation is through homotypic lysosome (lysosome-lysosome) membrane fusion.

1.3 Vacuolar lysosome membrane fusion

When degradative processes were first discovered, membrane fragments present within the lysosomal lumen were also identified, which facilitate lipid and protein catabolism. These fragments are known to result from two main cellular protein degradation pathways, autophagy and endocytosis, that terminate with a heterotypic membrane fusion event between their respective transport vesicle and the lysosome. However, when components of these pathways are impaired, lumenal membrane fragments persist, suggesting another process exists that results in lipid fragment formation. Based on current knowledge, there is one cellular event that may result in lumenal fragment formation and intrinsically could accommodate the turnover of lysosomal polytopic proteins: the process of *homotypic lysosome membrane fusion*.

Around the same time that the molecular machinery responsible for selective down-regulation of surface transporters was first discovered, Wickner, Merz and colleagues demonstrated that upon fusion of two vacuolar lysosomes, a portion of the membrane is internalized into the lumen as a byproduct of the reaction (Wang et al., 2002) using *Saccharomyces cerevisiae* and its vacuolar lysosome as models. This process of homotypic membrane fusion has been very well characterized and occurs in four distinct subreactions: priming, tethering, docking, and fusion (**Figure 1B**).

Priming prepares vacuoles for the fusion reaction by disassembling cis-SNARE (Soluble N-ethylmaleimide-sensitive factor (NSF) Attachment REceptor) complexes, to ensure that individual SNARE proteins will interact and form new complexes in trans, a prerequisite for fusion. This stage is initiated by the ATPase activity of Sec18 (NSF homologue) to release Sec17 (a cis-SNARE chaperone and α-SNAP homologue) and disassemble the cis-SNARE complex (Eitzen et al., 2000; Wickner and Haas, 2000; Wang et al., 2003b). This disassembly frees individual SNARE proteins (Vam3, Vit1, Vam7, and Nyv1) and the HOPS (HOmotypic vacuole

fusion and Protein Sorting) tethering holocomplex from their complexed state to allow for the formation of new SNARE complexes on apposed organelle membranes.

Tethering, a prerequisite for membrane fusion, occurs when apposing membranes make initial contact and establish a site for formation of the vertex domain. This step requires the Rab GTPase Ypt7 (Rab 7 homolog) to associate with HOPS, its effector. HOPS is comprised of a class C core complex (Vps11, 16, 18, and 33) with two accessory proteins (Vps39 and 41; Nickerson et al., 2009), and this Rab-mediated step tethers membranes reversibly.

Docking occurs as the vertex domain expands radially, forming the boundary membrane – the area of membrane within the vertex of apposed vacuoles (Wang et al., 2002). During this stage, the membrane fusion machinery – including Ypt7, HOPS, and SNARE proteins – accumulate and assemble into an expanding ring that stabilizes contact at the vertex between apposed membranes (Wickner and Haas, 2000; Wickner, 2010). Ypt7 localizes to the vertex domain and functions to recruit additional fusion machinery to stabilize this site in support of fusion. In order to recruit additional machinery, Ypt7 must first be activated, or converted from a GDP-bound state to a GTP-bound state by its guanine nucleotide exchange factor (GEF), the Mon1-Ccz1 complex (Wang et al., 2003a; Nordmann et al., 2010; Kiontke et al., 2017). GEFs are thus critical activators of fusion reactions, by coupling Rab activation with recruitment to cognate membranes. In its active state, Ypt7 binds and recruits HOPS to the vertex, which in cooperation with other machinery components, ensures fidelity of the membrane fusion event by creating a physical link between the two apposed membranes. Other effectors of docking include Gyp3 and Gyp7, both Rab GTPase-activating proteins (GAPs) that inactivate Ypt7 through GTP hydrolysis, and a GDP dissociation inhibitor (GDI) chaperone, which extracts inactive Rab (Ypt7:GDP) and retains it in the cytoplasm (Eitzen et al., 2000; Cabrera and Ungermann, 2013).

As docking proceeds, trans-SNARE complexes within this assembly progressively twist into stable helical bundles (or SNARE pins) that drives lipid bilayers together leading to complete membrane *fusion.* This trans-SNARE pairing involves the binding of three Q-SNAREs (Vam3, Vti1 and Vam7) with one R-SNARE (Nyv1), and renders the fusion reaction irreversible (Wickner, 2010). SNAREs are categorized based on the residue they contribute to the 'zero-layer', or the center of the helical bundle (glutamine (Q) or arginine (R)), which generates polar interactions to ensure proper SNARE assembly (Baker et al., 2015). SNARE assembly also requires Sec1/Munc18 (SM) proteins that interact with individual SNAREs, as well as with

partial or complete complexes. Recent evidence suggests that Vps33, a SM protein and subunit of HOPS, orchestrates SNARE pairing by binding to two SNARE proteins (Nyv1 and Vam3 via their SNARE motifs), one from each apposed membrane, to act as a template for generating partially zippered SNARE complex intermediates (Baker et al. 2015). Once SNARE complexes are fully zippered, they bring apposed membranes in close proximity to promote lipid bilayer merger for full membrane fusion and lumenal content mixing.

Importantly, the boundary membrane is internalized as an intralumenal fragment and degraded as a byproduct of this fusion event (Wang et al., 2002). Topologically, formation of this intralumenal fragment is analogous to genesis of intralumenal vesicles within the MultiVesicular Body pathway (**Figure 1D**), which accommodates exposure of internalized surface transporters to acid hydrolases for degradation. Although fusion proteins are spared from internalization upon fusion, it was previously unclear whether polytopic proteins can be selectively sorted into the boundary membrane, where they would be degraded as a byproduct of organelle fusion.

Thus, we hypothesized that the process of homotypic organelle membrane fusion could accommodate the selective turnover of lysosomal polytopic proteins upon internalization of the boundary membrane fragment after fusion. Using *S. cerevisiae*, we examined polytopic protein membrane localization or sorting, internalization, and degradation upon organelle fusion within cells as well as using purified organelles. In summary, we discovered a new cellular degradation pathway, which we named the IntraLumenal Fragment pathway (**Figure 1A** and **B**), that selectively degrades lysosomal membrane proteins as well as surface proteins in response to protein misfolding, TOR signaling, and changes in cognate substrate levels.

1.4 ESCRT-dependent and –independent pathways coordinate function for cellular protein turnover

Until now, the ESCRT machinery and the MultiVesicular Body pathway represented the only known mechanism for the regulated turnover of polytopic proteins, post-endoplasmic reticulum exit. However, when key components of the ESCRT machinery are impaired, cells still survive and known MVB cargo proteins are still degraded, although less efficiently. Since both the quality and the quantity of polytopic proteins is essential for proper cellular function, it seems likely that eukaryotic cells would not exclusively rely on one core mechanism for the degradation of these proteins. The IntraLumenal Fragment (ILF) pathway represents a completely new and

different mechanism than the canonical ESCRT-dependent pathway for polytopic protein degradation. While there are clear differences between these processes, they perform analogous roles in protein catabolism, relying on distinct molecular machinery for protein sorting and internalization at their respective cellular locations. Both contribute to the degradation of a variety of cellular cargoes in response to protein misfolding, changes in substrate levels and TOR (target of rapamycin) signaling. Ultimately, ESCRT-dependent and ESCRT-independent pathways complement each other by remodeling membrane protein landscapes to preserve organelle identity and maintain cellular proteostasis. These findings are summarized in **Table 1** and **Figure 1**.

Both ESCRT-dependent and –independent pathways accommodate the degradation of a variety of protein cargoes. While the primary function of the MVB pathway is to down-regulate surface polytopic proteins, evidence exists that ESCRTs can sort and package lysosomal polytopic proteins (via the vReD pathway), soluble proteins and biosynthetic proteins (i.e. carboxypeptidase S (CPS) Tran et al., 2009; Mageswaran et al., 2014; Feyder et al., 2015). It has yet to be elucidated if the ILF pathway can selectively degrade non-polytopic proteins. However, if soluble or membrane-associated proteins localize to lysosomal membranes, the ILF pathway likely can accommodate their internalization and degradation.

The majority of ESCRT client proteins undergo ubiquitylation either at the plasma membrane (i.e. surface polytopic proteins) or at endosomal membranes (i.e. biosynthetic proteins) prior to sorting by the ESCRT complexes. Several ubiquitin-binding domains or motifs have been identified in ESCRT-0 (Vps27 and Hse1), ESCRT-I (Vps23 and Mvb12), and ESCRT-II (Vps36) complexes, highlighting that the earlier stages of ESCRT trafficking are important for cargo protein binding and sorting. Similarly in the vReD pathway, lysosomal membrane proteins are first labeled with ubiquitin prior to packaging into the post-vacuolar compartments for ESCRT-mediated sorting and degradation. Since the ILF pathway selectively sorts and degrades polytopic proteins, a labeling mechanism likely exists. Based on these studies as well as the extensive literature detailing other eukaryotic protein degradation pathways, we speculate that ubiquitin is the label to identify proteins for degradation in the ILF pathway (**Figure 1B** and **C**). In this work we have shown that the ILF pathway recognizes and degrades misfolded proteins, which are typically labeled with ubiquitin (Claessen et al., 2011; Keener and Babst, 2013; Zhao et al., 2013; Fang et al., 2014). Nutrient transporters degraded by this pathway can be

Table 1. Summary of the MultiVesicular Body and IntraLumenal Fragment pathways

	ESCRT-dependent MultiVesicular Body	**ESCRT-independent IntraLumenal Fragment**
Cargoes		
Lysosome polytopic	✓	✓
Surface polytopic	✓	✓
Membrane-associated	×	✓
Soluble cytoplasmic	✓	×
Biosynthetic	✓	**?**
Lipids (selective)	×	**?** (DAG)
Labeling and sorting		
Ubiquitin label	✓	**?**
E3-ligase	✓	✓
E4-adaptor	✓	✓
Sorting	ESCRT-0-II	HOPS (Ypt7)
ILV/ILF formation		
Compartment	Endosome Plasma membrane	Vacuolar lysosome Endosome?
Change in membrane morphology	Scission (Fission)	Fusion
Number of compartments required	1	2
Size of product	~ 100 nm	> 100 nm
Catalytic machinery	ESCRT-III	SNAREs

ubiquitylated and interact with the ubiquitylation machinery based on results from genome-wide studies (Urbanowski and Piper, 2001; Peng et al., 2003). Additionally, E3-ubiquitin ligases and E4-adaptor proteins are capable of ubiquitylating lysosomal proteins in the vReD pathway (Li et al., 2015a,b) and through our own observations are important for protein degradation by the ILF pathway (unpublished data). Lastly, the ILF pathway can accommodate the sorting and degradation of surface proteins, and vReD client proteins, if they avoid packaging into intralumenal vesicles (but are still labeled with ubiquitin), thus it is likely that protein labeling and sorting in the ILF pathway is ubiquitin-dependent as well.

Based on these observations and what we know about the ILF pathway, we propose a model for the ubiquitin-dependent sorting and internalization of lysosomal polytopic proteins in the ILF pathway (**Figure 1C**). First, a stimulus, such as heat stress, triggers the ubiquitination of a lysosomal membrane protein through coordination of an E3-ubiquitin ligase and E4-adaptor protein. Once ubiquitinated, the protein must be actively sorted into the boundary membrane for subsequent internalization into the lysosomal lumen upon fusion. We speculate that the membrane fusion machinery – including the Rab GTPase Ypt7 and the HOPS tethering complex – facilitate protein recognition and sorting as they localize to the vertex domain of docked vacuoles (Wang et al., 2002; Wickner, 2010) and are thus in a location capable of regulating boundary membrane protein composition. Additionally, we have shown that impairing Ypt7 function inhibits protein sorting, internalization, and degradation (**Figures 7, 10, 11, 12, 18, S6, S9** and **S11**), and that these proteins are actively sorted in a molecular sieving mechanism during vertex ring expansion (**Figures 8**). Furthermore, three of the six subunits of the HOPS tethering complex (Vps39, Vps18, and Vps11) contain partial RING (Really Interesting New Gene)-like motifs that when in complex form a predicted ubiquitin-binding domain (Nickerson et al., 2009). Similar to the how the numerous ubiquitin-binding domains of the ESCRT machinery sort surface proteins in the MVB pathway (Nickerson et al., 2007; Henne et al., 2011; Shields and Piper, 2012) these HOPS subunits could recognize and sort ubiquitinated lysosomal proteins into the boundary for subsequent internalization as the intralumenal fragment and degradation by lumenal acid hydrolases.

Once cargo proteins are efficiently sorted into ILVs or into the boundary membrane, the limiting membrane must undergo a change in morphology to allow for subsequent protein degradation. In the MVB pathway, the ESCRT-III complex facilitates the final scission between

the nascent ILV and the endosomal membrane for cargo internalization and MVB maturation. Additionally, homologs of ESCRT-III subunits and Vps4 are implicated in other membrane scission or fission events, such as cell division in Archaea (Samson et al., 2008) and cytokinesis in mammals (Carlton and Martin-Serrano, 2007). Similarly, in the ILF pathway SNARE proteins are the catalytic machinery responsible for membrane fusion and the internalization of the boundary as an intralumenal membrane fragment. SNAREs are found in all eukaryotic organisms and are recognized as the key components of protein complexes that mediate and drive membrane fusion events at distinct subcellular locations. SNARE-mediated membrane fusion events are implicated in both endocytic and exocytic trafficking pathways, thus they are essential for a variety of cellular processes including cell growth, membrane repair, cytokinesis, hormone secretion and synaptic transmission (Fasshauer et al., 1998; Hong, 2005; Wickner and Schekman, 2008). While both processes generate a similar product to topologically accommodate protein internalization, ILVs are much smaller than ILFs, typically being around 100 nm in diameter.

Despite clear mechanistic differences between ESCRT-dependent and –independent pathways, they both are capable of accommodating the topological challenge of internalizing polytopic proteins for degradation. Thus, both pathways are equally important for cellular homeostasis by remodeling protein landscapes to allow for organelle adaptation in response to intracellular and extracellular cues.

Chapter 2. Selective Lysosomal Transporter Degradation by Organelle Membrane Fusion

2.1 Abstract

Lysosomes rely on their resident transporter proteins to return products of catabolism to the cell for reuse, and for cellular signaling, metal storage and maintaining the lumenal environment. Despite their importance, little is known about the lifetime of these transporters or how they are regulated. Using *Saccharomyces cerevisiae* as a model, we discovered a new pathway intrinsic to homotypic lysosome membrane fusion that is responsible for their degradation. Transporter proteins are selectively sorted by the docking machinery into an area between apposing lysosome membranes, which is internalized and degraded by lumenal hydrolases upon organelle fusion. These proteins have diverse lifetimes that are regulated in response to protein misfolding, changing substrate levels or TOR activation. Analogous to endocytosis for controlling surface protein levels, the "intralumenal fragment pathway" is critical for lysosome membrane remodeling required for organelle function in context to cellular protein quality control, ion homeostasis and metabolism.

2.2 Introduction

All eukaryotic organisms use organelles called lysosomes to recycle biomaterials. To receive incoming biomaterial, lysosomes must fuse with encapsulated compartments containing proteins, DNA, damaged organelles, or cellular debris packaged within through autophagy or collected from outside the cell by endocytosis. Fusion events expose the biomaterials to lumenal hydrolases for catabolism and once degraded, resident lysosomal transporters translocate the constituents from the lumen to the cytoplasm for reuse by the cell. These transporters include nucleotide transporters ENT3 (Song et al., 2014), amino acid transporters SLC38A9 (Jung et al., 2015), lipid transporters NPC1 (Berger et al., 2005) and transporters for metabolites and macromolecules, e.g. ABCB6 (Kiss et al., 2015). Lysosomes are also critical for storage of divalent metals – including zinc by ZnT2 (Hennigar and Kelleher, 2015), copper by SLC31A2 (Schweigel-Rontgen, 2014) and iron by NRAMP2/DMT1 (Ehrnstorfer et al., 2011) – essential cofactors for many cellular enzymes. Because of their importance to lysosome physiology, mutations that target many of these transporters, channels and pumps underlie human lysosomal storage disorders, such as mucolipidosis type IV (TRPML1; Waller-Evans and Lloyd-Evans,

2015) or Niemann-Pick disease type C (NPC1; Berger et al., 2005). Despite being critical for lysosome function and their relationship with human disease, we know little about how these transporters are regulated or degraded.

Most polytopic proteins, after passing endoplasmic reticulum quality control, are degraded by the MultiVesicular Body (MVB) pathway. This pathway mediates the ubiquitin-dependent downregulation of surface transporters and receptors (Katzmann et al., 2001; Babst, 2011) either constitutively (e.g. Ste3; Davis et al., 1993) or in response to cellular cues, such as changes in substrate levels (e.g. Mup1; MacDonald et al., 2012) or upon protein misfolding (e.g. Fur4; Keener and Babst, 2013). A critical step in the MVB pathway is the inward budding of the membrane, which results in formation of intralumenal vesicles (ILVs) within the MVB. Importantly, surface proteins targeted for downregulation are sorted into the ILVs where upon heterotypic fusion between the MVB and the lysosome, the protein laden ILVs are delivered to the lysosomal lumen for exposure to acid hydrolases and degradation (Katzmann et al., 2001; Shields and Piper, 2012).

MVB formation and protein sorting are achieved through the sequential function of a multisubunit machinery comprised of the endosomal sorting complex required for transport (ESCRT) complexes. Recently, Emr and colleagues demonstrated that some resident lysosomal membrane proteins utilize components of the MVB pathway machinery for degradation using *Saccharomyces cerevisiae* as a model (Li et al., 2015a,b). While this is the first description of a mechanism for lysosomal polytopic proteins degradation, the authors disclose that this process, termed vReD (vacuolar membrane REcycling and Degradation), does not regulate the lifetimes of other yeast transporters and pumps, e.g. Vph1 (subunit of the V-ATPase), Fth1 (iron transporter) and Vba4 (cationic amino acid transporter). Additionally, cells survive and divide when key components of the ESCRT machinery are eliminated or dysfunctional (Mageswaran et al., 2015). Thus it is possible that eukaryotic cells have an additional ESCRT-independent pathway to degrade polytopic proteins. If so, this new degradation pathway must possess ESCRT-independent mechanisms that recognize and sort labeled polytopic proteins into an area of membrane that is internalized within the lysosomal lumen for exposure to acid hydrolases for degradation. Based on current knowledge, there is a cellular event that may fulfill all criteria: the process of homotypic lysosome membrane fusion.

Lysosomes are dynamic organelles constantly undergoing cycles of fission and homotypic fusion to retain copy number and accommodate organelle inheritance (de Duve and Wattiaux, 1966; Wickner and Haas, 2000). Homotypic vacuolar lysosome fusion requires a sequential series of four distinct subreactions: priming, tethering, docking and fusion: *Priming* involves the disassembly of *cis*-SNARE complexes, which ensures that individual SNARE proteins will interact to form new complexes in *trans*, a prerequisite for fusion. *Tethering* occurs when apposing membranes make first contact, which requires active Ypt7, a Rab-GTPase, and the HOPS (HOmotypic vacuole fusion and Protein Sorting) tethering holocomplex. *Docking* is operationally defined as the period between tethering and lipid bilayer fusion. During this stage, fusogenic lipids and proteins assemble into an expanding ring that stabilizes contact at the vertex between apposing membranes (Wickner and Haas, 2000; Wang et al., 2002; Fratti et al., 2004). Here, *trans*-SNARE complexes within this assembly progressively twist into stable helical bundles that drive lipid bilayers together leading to complete membrane *fusion.* Importantly, the area of membrane and embedded proteins within the vertex ring, called the boundary, is internalized as a byproduct of this fusion event (Wang et al., 2002). Topologically, formation of this intralumenal fragment is analogous to genesis of intralumenal vesicles in the MVB pathway, which accommodates exposure of membrane proteins to hydrolases for degradation. Although fusion proteins are spared upon fusion, it was previously unclear whether vacuolar polytopic proteins can be selectively sorted into the boundary. If so, then this process could accommodate their internalization into the lumen for subsequent degradation. Thus we hypothesize that resident lysosomal membrane proteins may be selectively sorted into the boundary, internalized and degraded upon homotypic vacuole fusion.

2.3 Materials and Methods

2.3.1 Yeast strains and materials

Yeast strains used in this study are listed in **Table 2**. Biochemical and yeast growth reagents were purchased from either Sigma-Aldrich, Invitrogen or BioShop Canada Inc. Proteins used include recombinant Gdi1 purified as previously described (Brett and Merz, 2008), recombinant Gyp1-46 purified as previously described (Eitzen et al. 2000), and recombinant soluble Qc-SNARE Vam7 purified as previously described (Schwartz and Merz, 2009). Reagents used in fusion reactions were prepared in 20 mM Pipes-KOH, pH 6.8, and 200 mM sorbitol.

2.3.2 Microscopy

Images were acquired with a Nikon Eclipse TiE inverted microscope equipped with either a motorized laser TIRF illumination unit, Photometrics Evolve 512 EM-CCD camera, CFI ApoTIRF 1.49 NA 100x objective lens, and 488 nm or 561 nm (50 mW) solid-state lasers or Agilent MLC400 Monolithic Laser Combiner unit, Andor Ixon3 512 EM-CCD camera, CFI Plan Apo Lambda 1.49 NA 100x objective lens, and Diode 488 nm or 561 nm (100mW) lasers. Both systems are operated with Nikon Elements software. Cross sectional images were recorded 1 μm into the sample and resulting micrographs were deconvolved using AutoQuant X3 (Media Cybernetics) and processed using ImageJ software (National Institutes of Health) and Adobe Photoshop CC. GFP fluorescence intensity profiles were generated using ImageJ software.

Live yeast cells were stained with FM4-64 using a pulse-chase method as previously described (Brett et al., 2008). Where indicated, cells were incubated at 37 °C for 30 minutes for heat stress and with 100 μM cycloheximide or puromycin for 90 minutes after FM4-64 staining. Time-lapse videos were acquired at 30°C using a Chamlide TC-N incubator (Live Cell Instruments) with cells plated on coverslips coated with concanavalin-A (1 mg/ml in 50 mM HEPES, pH 7.5, 20 mM CaAcetate, 1 mM $MnSO_4$). Approximately 150 vacuole fusion events were observed.

2.3.3 Vacuole isolation and homotypic vacuole fusion

Vacuoles were isolated from yeast cells as previously described (Haas, 1995). Fusion reactions were prepared using 6 μg of vacuoles isolated from GFP derivative strains in standard fusion reaction buffer with 0.125 M KCl, 5 mM $MgCl_2$, 1 mM ATP and 10 μM CoA. Vacuolar membranes stained with FM4-64 by treating vacuoles with 3 μM FM4-64 for 10 minutes at 27 °C. Reactions were incubated at 27 °C for 60 minutes, unless otherwise noted, and placed on ice prior to visualization by microscopy. For examining the contribution of the fusion machinery, vacuoles were incubated in the absence (CTL) or presence of 3.2 μM Gyp1-46, 4 μM rGdi, or 100 nM rVam7 (in the absence of ATP). For heat stress treatment, vacuoles were pretreated for 5 minutes at 37 °C before addition to the fusion reaction and incubation for 30 minutes at 27 °C. Where indicated, vacuoles were pretreated with 7 μM Rapamycin or DMSO, 100 μM cycloheximide or 100 μM puromycin for 15 minutes at 27 °C and incubated for an additional 15 minutes with the fusion reaction.

Vacuole content mixing was assessed using a complementary, split β-lactamase based assay (Jun and Wickner, 2007). Data shown was normalized to values obtained at 120 minutes under standard fusion conditions (n = 3).

To assess protein exclusion during vertex expansion, isolated vacuoles were stained with FM4-64 and reactions were prepared by mixing vacuole populations, 3 µg of either Vps33-GFP or Fet5-GFP with 3 µg of DKY6281, and were incubated for 0-60 minutes.

2.3.4 Fluorescence Recovery After Photobleaching (FRAP)

FRAP experiments were conducted using vacuoles isolated from yeast strains expressing Fth1-GFP, Vph1-GFP and Vps33-GFP or lacking a GFP tag (DKY6281 stained with FM4-64). Fusion reactions were incubated at 27 °C for 10 minutes or 60 minutes prior to imaging using a Nikon Eclipse TiE inverted microscope equipped with Laser Scanning C2 Confocal system and an CFI ApoTIRF 1.49 NA 100x objective lens. ROIs were first scanned using a 488 nm laser (3-5% power) for five cycles to establish the prebleached fluorescence intensity. ROIs were then photobleached for three cycles using 100% 488 nm laser power. ROI fluorescence intensity was then recorded every 20 seconds for 10 minutes at 3-5% laser power of the 488 nm laser using a dichroic 525/50 561LP nm emission filter. FM4-64 FRAP experiments were conducted as described except with a dichroic 447/60 nm emission filter. Unprocessed data obtained as mean fluorescence values measured were corrected with respect to background fluorescence intensity and spontaneous photobleaching and then were normalized with respect to fluorescence intensity of prebleached images. Mobile fraction (Mf) values were calculated by fitting experimental values with the equation: $Mf = (F_{end} - F_{post})/(F_{pre} - F_{post})$. Where F_{pre} corresponds to prebleach fluorescence, F_{post} to fluorescence intensity after photobleaching and F_{end} to recovered fluorescence intensity. Fluorescence intensity curves and Mf values are means ± SEM.

2.3.5 pHluorin-based assay

Ecleptic pHluorin was cytoplasmically tagged to lysosomal membrane proteins (see Prosser et al., 2010). Fusion reactions (15 µl) were prepared using 6 µg of isolated vacuoles and standard reaction buffer. Reactions were transferred to black 96-well conical-bottom microtiter plates with 15 µl of reaction buffer titrated to different pH values. pHluorin fluorescence (λ_{ex} = 480 nm; λ_{em} = 515 nm) was recorded every two minutes for 90 minutes using a BioTek Synergy H1 plate

reading flourometer. Data shown are representative traces with values normalized to time zero, n≥6.

2.3.6 Western blot analysis

Fusion reactions were prepared from isolated vacuoles as previously described, expect where noted for altered buffer pH. Where indicated, samples were pretreated with rapamycin, cycloheximide, puromycin, or at 37 °C as previously described. Reactions were incubated at 27 °C followed by addition of protease inhibitors (6.7 μM leupeptin, 33 μM pepstatin, 1 mM PMSF and 10.7 mM AEBSF), 1% DDM and 5X laemmli sample buffer. To solubilize membrane proteins but avoid aggregation due to boiling, reactions were incubated at 27 °C for 10 minutes prior to running on an SDS-Page gel. Samples were probed for α-GFP or α-Vph1 (Abcam, Cambridge, UK). All samples were repeated at least three times. Gels were imaged using GE Amersham Imager 600 by chemiluminescence and prepared using Adobe Photoshop and Illustrator CC software.

Table 2. Yeast strains used in Chapter 2

Strain	Genotype	Source
BY4741	*MATα his3-Δ1 leu2-Δ0 met15-Δ0 ura3-Δ0*	Huh et al., 2003
Fet5-GFP	BY4741, *Fet5-GFP::HIS3MX*	Huh et al., 2003
Fth1-GFP	BY4741, *Fth1-GFP::HIS3MX*	Huh et al., 2003
Vph1-GFP	BY4741, *Vph1-GFP::HIS3MX*	Huh et al., 2003
Cot1-GFP	BY4741, *Cot1-GFP::HIS3MX*	Huh et al., 2003
Sna4-GFP	BY4741, *Sna4-GFP::HIS3MX*	Huh et al., 2003
Ncr1-GFP	BY4741, *Ncr1-GFP::HIS3MX*	Huh et al., 2003
Ybt1-GFP	BY4741, *Ybt1-GFP::HIS3MX*	Huh et al., 2003
Ycf1-GFP	BY4741, *Ycf1-GFP::HIS3MX*	Huh et al., 2003
Vps33-GFP	BY4741, *Vps33-GFP::HIS3MX*	Huh et al., 2003
Fth1-pHluorin	BY4741, *Fth1-pHluorin::KanMX*	This study
Fet5-pHluorin	BY4741, *Fet5-pHluorin::KanMX*	This study
Fth1-GFP:*vps27Δ*	Fth1-GFP*::HIS3MX, vps27Δ::KanMX*	This study
Fth1-GFP:*vps23Δ*	Fth1-GFP*::HIS3MX, vps23Δ::KanMX*	This study
Fth1-GFP:*vps36Δ*	Fth1-GFP:: *HIS3MX, vps36Δ::KanMX*	This study
Fet5-GFP:*vps27Δ*	Fet5-GFP::*HIS3MX, vps27Δ::KanMX*	This study
Fet5-GFP:*vps23Δ*	Fet5-GFP::*HIS3MX, vps23Δ::KanMX*	This study
Fet5-GFP:*vps36Δ*	Fet5-GFP::*HIS3MX, vps36Δ::KanMX*	This study
Fth1-GFP:*atg1Δ*	Fth1-GFP::*HIS3MX, atg1Δ::KanMX*	This study
Fth1-GFP:*atg7Δ*	Fth1-GFP::*HIS3MX, atg7Δ::KanMX*	This study
Fet5-GFP:*atg1Δ*	Fet5-GFP::*HIS3MX, atg1Δ::KanMX*	This study
Fet5-GFP:*atg7Δ*	Fet5-GFP::*HIS3MX, atg7Δ::KanMX*	This study
BJ3505	*MATa Δpep4::HIS3 prb1-Δ1.6R HIS3 lys2–208 trp1-Δ101 ura3–52 gal2 can1*	Haas et al., 1994
DKY6210	*MATα leu2-3 leu2-112 ura3-52 his3- Δ200 trpl-Δ901 lys2-801 suc2-Δ9 pho8::TRP1*	Haas et al., 1994
Fth1-GFP	BJ3505, *Fth1-GFP::KanMX*	This study
Fet5-GFP	BJ3505, *Fet5-GFP::KanMX*	This study
Vph1-GFP	SEY6210, *pep4Δ::His3, GFP::TRP1*	Wang et al., 2002

2.4 Results

2.4.1 Polytopic proteins are selectively sorted for degradation during homotypic lysosome fusion

To test our hypothesized model of lysosomal polytopic protein degradation (**Figure 2A**) we examined the sorting (membrane distribution), internalization and degradation of eight GFP-tagged lysosomal polytopic proteins during homotypic fusion events using *Saccharomyces cerevisiae* and its vacuolar lysosome as models, as the underlying machinery and transporters are largely evolutionarily conserved. To begin, we monitored the distribution of GFP-tagged transporter proteins on the vacuole membrane over time during homotypic vacuole fusion within live *S. cerevisiae* cells (**Figure 2B, movies S1-S3**). We first confirmed that Vph1, the stalk domain of the V-ATPase complex, was uniformly distributed on the lysosomal membrane during fusion and, as a consequence, internalized (Wang et al., 2002). Then we made two striking observations: (1) The lysosomal multi-copper oxidase Fet5 (Urbanowski and Piper, 1999) was excluded from the boundary membrane of docked organelles and spared from being internalized upon fusion, despite formation of a lumenal lipid membrane fragment. (2) The lysosomal iron transporter Fth1 accumulated within the boundary and was internalized upon lysosome fusion. We conducted similar studies with five other GFP-tagged resident polytopic proteins (**Figure 2C**) and classified their sorting phenotypes as either uniformly distributed (Vph1), excluded from (Fet5; Ybt1 and Ycf1, ABC-C transporters; the sterol transporter Ncr1) or enriched within (Fth1; the zinc transporter Cot1; and Sna4, an E3-Ub ligase adaptor protein) the boundary membrane during lysosome fusion. These data demonstrate that protein sorting is selective and highlights the dependence of this process on intralumenal membrane fragment formation during organelle fusion. As such, we named this new cellular protein degradation pathway the IntraLumenal Fragment (ILF) pathway.

To further study the molecular basis of the ILF pathway, we isolated vacuolar lysosomes from yeast cells and conducted *in vitro* fusion reactions (Wickner, 2010). We first confirmed our initial findings, whereby the same sorting phenotypes were observed *in vitro* as *in vivo* for all GFP-tagged polytopic proteins studied (**Figure 3A**). This important result indicates that all molecular machinery necessary for protein sorting and internalization during fusion co-purifies with the organelles. Next, to examine the sorting process in more detail, we quantified GFP fluorescence within the boundary on organelles undergoing fusion *in vitro* (**Figures 3B** and **3C**).

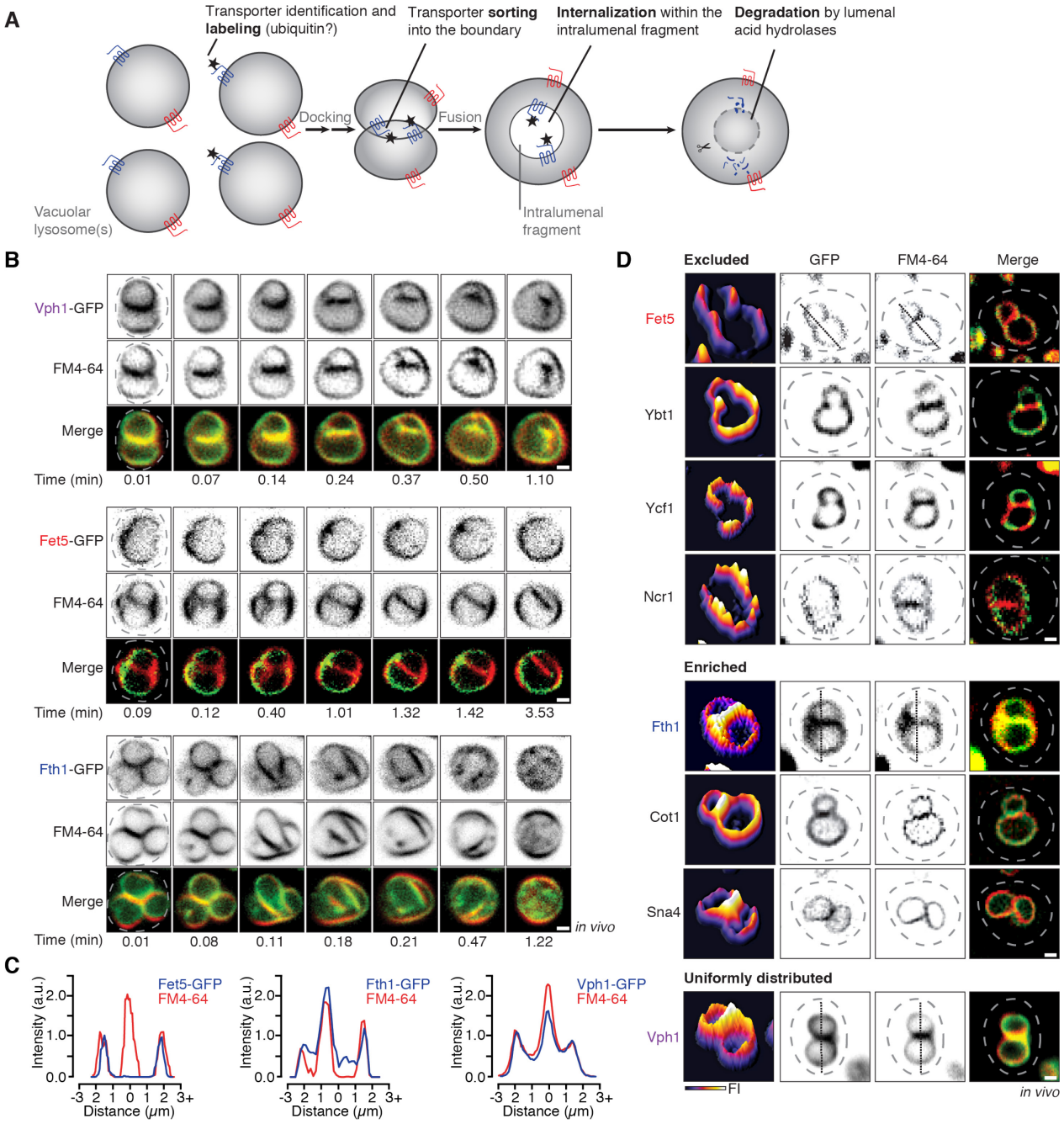
A
Transporter identification and labeling (ubiquitin?)
Transporter sorting into the boundary
Internalization within the intralumenal fragment
Degradation by lumenal acid hydrolases
Docking
Fusion
Vacuolar lysosome(s)
Intralumenal fragment
B
Vph1-GFP
FM4-64
Merge
Time (min)
0.01 0.07 0.14 0.24 0.37 0.50 1.10
Fet5-GFP
FM4-64
Merge
Time (min)
0.09 0.12 0.40 1.01 1.32 1.42 3.53
Fth1-GFP
FM4-64
Merge
Time (min)
0.01 0.08 0.11 0.18 0.21 0.47 1.22
in vivo
C
Fet5-GFP
FM4-64
Fth1-GFP
FM4-64
Vph1-GFP
FM4-64
Intensity (a.u.)
2.0
1.0
0.0
-3 2 1 0 1 2 3+
Distance (μm)
D
Excluded
GFP
FM4-64
Merge
Fet5
Ybt1
Ycf1
Ncr1
Enriched
Fth1
Cot1
Sna4
Uniformly distributed
Vph1
FI
in vivo

Figure 2. Polytopic proteins are selectively sorted for degradation during homotypic lysosome fusion within live cells

(A) Working model describing how lysosomal membrane proteins are selectively sorted into the boundary for internalization into the vacuolar lumen and subsequent degradation by the IntraLumenal Fragment (ILF) pathway. **(B)** Images from time-lapse videos of live yeast cells undergoing vacuole fusion *in vivo*, expressing Vph1-GFP, Fet5-GFP or Fth1-GFP stained with FM4-64 to label the vacuolar membrane. See also **movies S1-S3**. **(C)** Line-scan analysis of Fet5-GFP, Fth1-GFP or Vph1-GFP along dotted line illustrating GFP (blue) or FM4-64 (red) fluorescence distribution (same images as shown in **D**). **(D)** Micrographs of yeast cells expressing eight different GFP-labeled lysosomal polytopic proteins illustrating the three sorting phenotypes by the ILF pathway; excluded, enriched or uniformly distributed. Dotted lines outline each cell as observed by DIC. GFP fluorescence intensity profile plots (left panel). Scale bars, 1 μm (*in vivo*).

As compared to Vph1-GFP fluorescence, which is uniformly distributed on the boundary and outer membranes, Fet5-GFP is clearly expelled from the boundary, whereas Fth1-GFP concentrates within apposed boundary membranes as the fusion reaction progresses. Results from these experiments also offer evidence that support the internalization of boundary-localized polytopic proteins (**Figures 3D** and **3E**): As compared to Vph1-GFP, there is no lumenal accumulation of Fet5-GFP (even at 120 minutes when most vacuoles have fused; Merz and Wickner, 2004) but more accumulation of lumenal Fth1-GFP as the fusion reaction progresses, consistent with their sorting phenotypes. When internalized within the lumen, the membrane fragment and polytopic proteins embedded within it are exposed to lysosomal acid hydrolases for degradation. Thus, we conducted western blot analysis to detect cleavage of GFP from the polytopic proteins by lumenal proteases (**Figure 3F**; Li et al., 2015a). Consistent with the results of our micrographic analysis, less GFP was cleaved from Fet5 and more was cleaved from Fth1 as compared to Vph1 after the fusion reaction progressed for 120 minutes. This approach also allowed us to more accurately measure rates of protein turnover as it eliminates the impact of new protein delivery to the isolated lysosomal vacuoles during study, since polysomes and components of the secretory system are absent from the preparation (Cabrera and Ungermann, 2008). Deleting the *PEP4* and *PRB1* genes encoding critical lumenal proteases prevented GFP cleavage, further validating our model of the ILF pathway and highlighting the ability to selectively control polytopic protein lifetimes on lysosomal membranes. Furthermore, it suggests that lysosomes, and possibly other organelles, have the capability to remodel the protein landscape within their membranes with every fusion event. Two questions immediately arose upon making this exciting discovery: What is the function of the ILF pathway? What mechanisms underlie this process?

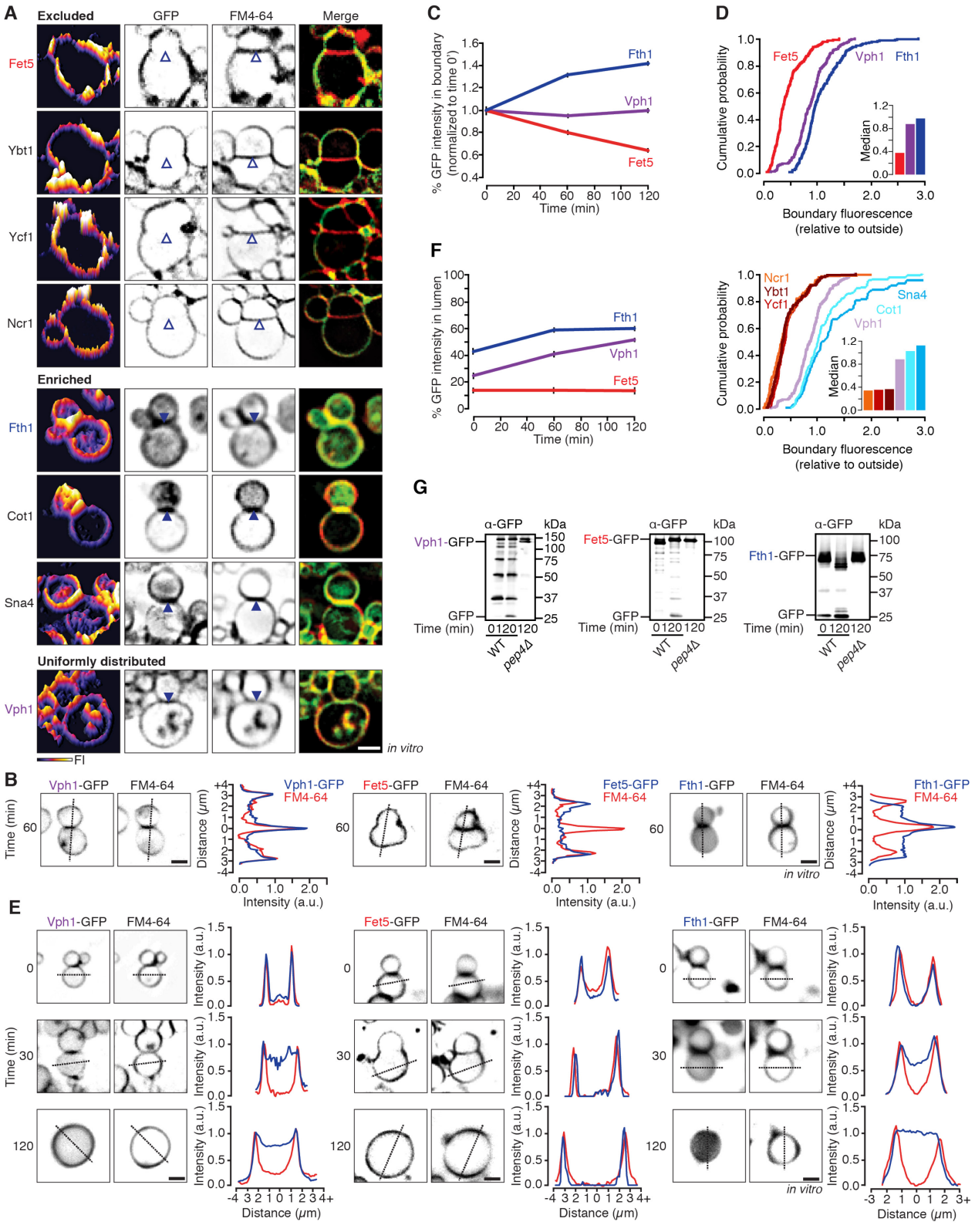
A
Excluded
GFP
FM4-64
Merge
Fet5
Ybt1
Ycf1
Ncr1
Enriched
Fth1
Cot1
Sna4
Uniformly distributed
Vph1
FI
in vitro
C
% GFP intensity in boundary (normalized to time 0')
Time (min)
Fth1
Vph1
Fet5
D
Cumulative probability
Boundary fluorescence (relative to outside)
Median
Fet5
Vph1
Fth1
Ncr1
Ybt1
Ycf1
Sna4
Cot1
F
% GFP intensity in lumen
G
α-GFP
kDa
Vph1-GFP
Fet5-GFP
Fth1-GFP
GFP
Time (min)
WT
pep4Δ
B
Time (min)
Vph1-GFP
FM4-64
Fet5-GFP
Fth1-GFP
Distance (μm)
Intensity (a.u.)
in vitro
E
Time (min)
Intensity (a.u.)
Distance (μm)

Figure 3. Polytopic proteins are sorted for degradation during lysosome fusion *in vitro*

(A) Micrographs of isolated vacuoles expressing a different GFP-labeled membrane protein stained with FM4-64 under standard fusion conditions. Boundaries containing (closed) or lacking (open arrowheads) GFP fluorescence are indicated. **(B)** Membrane distribution of Vph1-GFP, Fet5-GFP or Fth1-GFP on isolated vacuoles at 60 minutes into the fusion reaction highlighting GFP localization in the boundary with line-scan analysis highlighting GFP fluorescence in the boundary. **(C)** Percent of GFP fluorescence in the boundary observed over the course of the *in vitro* fusion reaction calculated from micrographic data ($n \geq 168$). **(D)** Cumulative probability curves of GFP fluorescence intensity within the boundary membrane (relative to outside) for all proteins tested *in vitro*. **(E)** Membrane distribution of Vph1-GFP, Fet5-GFP or Fth1-GFP on isolated vacuoles at 0, 30 and 120 minutes into the fusion reaction with line-scan analysis indicating GFP fluorescence in the lumen Associated GFP lumenal fluorescence intensity measurements are shown in **(F)** ($n \geq 168$). **(G)** Western blots comparing Vph1-GFP, Fet5-GFP and Fth1-GFP degradation kinetics in wild type (WT) or *pep4*Δ*prb1*Δ (*pep4*Δ) strains *in vitro*. Scale bars, 2 μm (*in vitro*).

2.4.2 The ILF pathway mediates quality control of lysosomal polytopic proteins

A primary function of cellular protein degradation pathways is to clear misfolded or damaged proteins, a vital quality control mechanism within all eukaryotic cells (Chen et al., 2011; Babst, 2014; Fang et al., 2014). Thus, we hypothesized that one function of the ILF pathway may be to clear damaged polytopic proteins from vacuolar lysosome membranes. To test this hypothesis, we first treated live yeast cells with heat stress, a known trigger of protein misfolding or damage (e.g. Keener and Babst, 2013), and studied its effect on the distribution of GFP-labeled polytopic proteins during vacuole fusion (**Figure 4A, movies S4** and **S5**). As predicted, Fet5-GFP (an excluded protein) was shunted to the boundary and internalized within the lumen when cells were heat stressed, whereas Fth1-GFP (an enriched protein) continued to be cleared from the lysosome membrane. Indeed, all polytopic proteins tested were sorted into the boundary and internalized regardless of their sorting phenotypes (**Figure 4B**), suggesting that the ILF pathway functions to clear misfolded lysosomal proteins within cells.

We next repeated these experiments using isolated vacuolar lysosomes and made similar findings (**Figure 4C**), confirming the molecular machinery required to sense and sort misfolded polytopic proteins co-purifies with the organelles. Because heat stress could also cause misfolding of fusogenic proteins, we measured homotypic vacuole fusion using a lumenal content mixing assay (Jun and Wickner, 2007) and confirmed that heat stress does not completely block the fusion reaction *in vitro* suggesting the machinery is intact (**Figure 4D**). To better assess protein sorting in response to heat stress, we next used micrographs shown in **Figures 3A** and **4C** to calculate the proportion of docked vacuoles that contained Fet5-GFP or Fth1-GFP within their boundary membranes (**Figure 4E**). As expected, more Fet5-GFP was sorted into the boundary upon heat stress, whereas Fth1-GFP was enriched in the boundary under both conditions. Together, these results demonstrate that misfolded polytopic proteins are sorted into the ILF pathway for clearance.

To demonstrate that damaged proteins within the boundary are indeed internalized upon fusion, we used micrographs shown in **Figures 3A** and **4C** to calculate the proportion of total Fet5-GFP or Fth1-GFP fluorescence found within the lumen of vacuoles after fusion occurred (**Figure 4F**). As predicted, protein damage induced by heat stress increased lumenal levels of both proteins, suggesting their internalization by the ILF pathway. We next replaced cytoplasmic GFP tags with pHluorin, a pH-sensitive variant, and monitored fluorescence (an indicator of

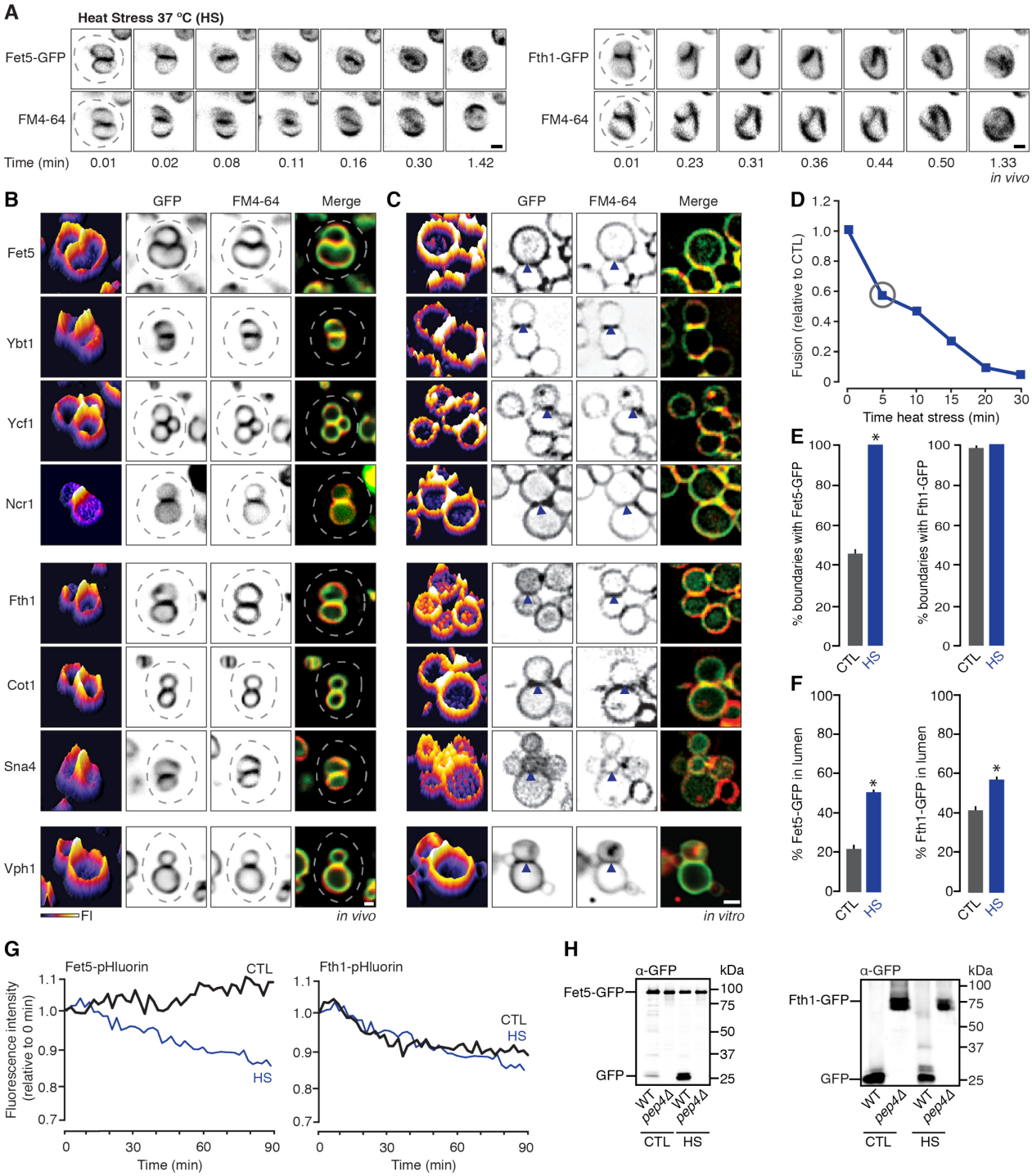
A
Heat Stress 37 °C (HS)
Fet5-GFP
FM4-64
Time (min)
0.01
0.02
0.08
0.11
0.16
0.30
1.42
Fth1-GFP
FM4-64
0.01
0.23
0.31
0.36
0.44
0.50
1.33
in vivo
B
GFP
FM4-64
Merge
Fet5
Ybt1
Ycf1
Ncr1
Fth1
Cot1
Sna4
Vph1
FI
in vivo
C
GFP
FM4-64
Merge
in vitro
D
Fusion (relative to CTL)
Time heat stress (min)
E
% boundaries with Fet5-GFP
% boundaries with Fth1-GFP
CTL
HS
F
% Fet5-GFP in lumen
% Fth1-GFP in lumen
CTL
HS
G
Fet5-pHluorin
Fth1-pHluorin
CTL
HS
Fluorescence intensity (relative to 0 min)
Time (min)
H
α-GFP
kDa
Fet5-GFP
GFP
Fth1-GFP
WT
pep4Δ
CTL
HS

Figure 4. The ILF pathway degrades misfolded lysosomal proteins

(A) Images from time-lapse videos of vacuole fusion events within cells expressing Fet5-GFP or Fth1-GFP after heat stress (HS). Micrographs of docked vacuoles expressing eight different polytopic proteins tagged with GFP after HS imaged *in vivo* **(B)** or *in vitro* **(C)**. **(D)** *In vitro* homotypic vacuole fusion measured using a lumenal enzyme complementation assay after isolated organelles were pretreated at 37 °C for indicated times. Grey circle indicates time of HS used in all other *in vitro* experiments shown. **(E)** Percent of boundaries observed containing Fet5-GFP or Fth1-GFP and **(F)** GFP fluorescence intensity within the lumen of docked vacuoles 60 minutes into the fusion reaction based on micrographic analysis ($n \geq 360$). **(G)** Relative pHluorin fluorescence of isolated vacuoles expressing Fet5-pHluroin or Fth1-pHluorin under standard conditions (CTL) or after heat stress (HS). **(H)** Western blot analysis of Fet5-GFP or Fth1-GFP degradation after vacuole isolated from WT or *pep4*Δ*prb1*Δ cells were permitted to fuse for 120 minutes under control conditions (CTL) or after HS. Scale bars, 1 μm (*in vivo*) or 2 μm (*in vitro*); *, $P < 0.05$. See also **Figure S1** and **movies S4** and **S5**.

internalization) during the course of the vacuole fusion reaction *in vitro*. Our reasoning was that because the lumenal pH is lower (pH 5; Brett et al., 2005) than the reaction buffer (pH 6.8), a drop in fluorescence intensity occurs upon internalization of pHluorin-tagged proteins (**Figure S1**). As predicted, Fth1-pHluorin but not Fet5-pHluorin fluorescence was quenched over time under control conditions (**Figure 4G**), consistent with Fet5 being spared and Fth1 internalized during fusion. However, the fluorescence of both pHluorin-tagged proteins was quenched under heat stress, confirming that damaged polytopic proteins are internalized within the vacuole lumen during fusion.

Finally, to confirm that these internalized proteins are degraded, we conducted western blot analysis after fusion reactions progressed for 120 minutes (**Figure 4H**). We observed that pretreating the vacuoles with heat stress increased the cleavage of Fet5-GFP, consistent with it being shunted to the boundary and internalized under these conditions. Whereas, heat stress had a minimal effect on Fth1-GFP cleavage as it is internalized under both conditions. GFP cleavage was abolished when PEP4 and PRB1 were deleted, confirming that observed proteolysis is conducted by lumenal acid hydrolases. Taken together, these findings demonstrate that the ILF pathway is responsible for clearing misfolded lysosomal polytopic proteins from membranes and thus contributes to cellular protein quality control.

2.4.3 TOR activation by cycloheximide triggers protein degradation by the ILF pathway

Because some lysosomal polytopic proteins studied were readily internalized and others were spared during organelle fusion under control conditions, we reasoned that they had different lifetimes. To better assess their rates of turnover, we employed a classic pulse-chase approach that involves treating live cells with the protein translation inhibitor cycloheximide and then monitored protein degradation by fluorescence microscopy (Watanabe-Asano et al., 2014). We predicted that when translation is blocked, levels of proteins that are enriched within the boundary would be depleted (as proteins degraded during lysosome fusion events would not be replenished) whereas levels of excluded proteins would persist over time. However, when we treated live yeast cells with low concentrations of cycloheximide (100 µM for 90 minutes), we observed sorting of all GFP-tagged polytopic proteins studied into the ILF pathway (**Figures 5A** and **5B, movies S6** and **S7**), including Fet5-GFP and other proteins that are normally spared. To better understand the basis of this preliminary observation, we repeated this experiment with

isolated organelles that do not co-purify with polysomes, ER or ribosomal components that are known targets of cycloheximide (Schneider-Poetsch et al., 2010, Cabrera and Ungermann, 2008). Again, to our surprise, cycloheximide caused the immediate sorting (**Figures 5C** and **S2**), internalization (**Figures 5D** and **S2**) and degradation (**Figures 5E** and **S2**) of all lysosomal polytopic proteins studied during organelle fusion *in vitro*. Although perplexing, these results suggest that cycloheximide has secondary targets on lysosomes that trigger polytopic protein degradation by the ILF pathway.

Cycloheximide (CHX) is similar to many other bioactive compounds that do not target ribosomes, and it has been reported to have off-target effects for decades (e.g. MacDonald and Ellis, 1969; McMahon, 1975). In fact, surface polytopic protein degradation is also triggered by cycloheximide, supposedly through the TOR (Target Of Rapamycin) signaling pathway (MacGurn et al., 2011), which releases amino acids from lysosomal stores to accommodate protein translation by ribosomes (Loewith and Hall, 2011). Although somewhat controversial, this finding may explain our observations, especially since the TOR signaling machinery functions on lysosome membranes, co-purifies with vacuolar lysosomes, and is known to mediate major changes in lysosome physiology that could involve restructuring the protein content of lysosomal membranes (Settembre et al., 2013). Thus, to test whether the effects of CHX on the ILF pathway were mediated by TOR-signaling, we pretreated isolated vacuolar lysosomes with rapamycin, a TOR kinase inhibitor (7 μM for 15 minutes; Michaillat et al., 2012), with the expectation of abolishing CHX-mediated degradation of polytopic proteins by the ILF pathway. As expected, rapamycin blocked CHX-mediated sorting (**Figure 5F**), internalization (**Figure S2**) and degradation (**Figure 5G**) of Fet5-GFP, a polytopic protein that is degraded by the ILF pathway upon cycloheximide treatment but otherwise spared. Rapamycin alone or DMSO had no effect on Fet5-GFP sorting or degradation (**Figure S2**) and has no measurable effect on the membrane fusion reaction (Michaillat et al., 2012). Furthermore, rapamycin did not affect sorting of Fth1-GFP which does not require cycloheximide for degradation as it is constitutively sorted into the ILF pathway (**Figure S2**). Together these findings suggest that TOR-signaling mediates polytopic protein degradation by the ILF pathway in response to cycloheximide.

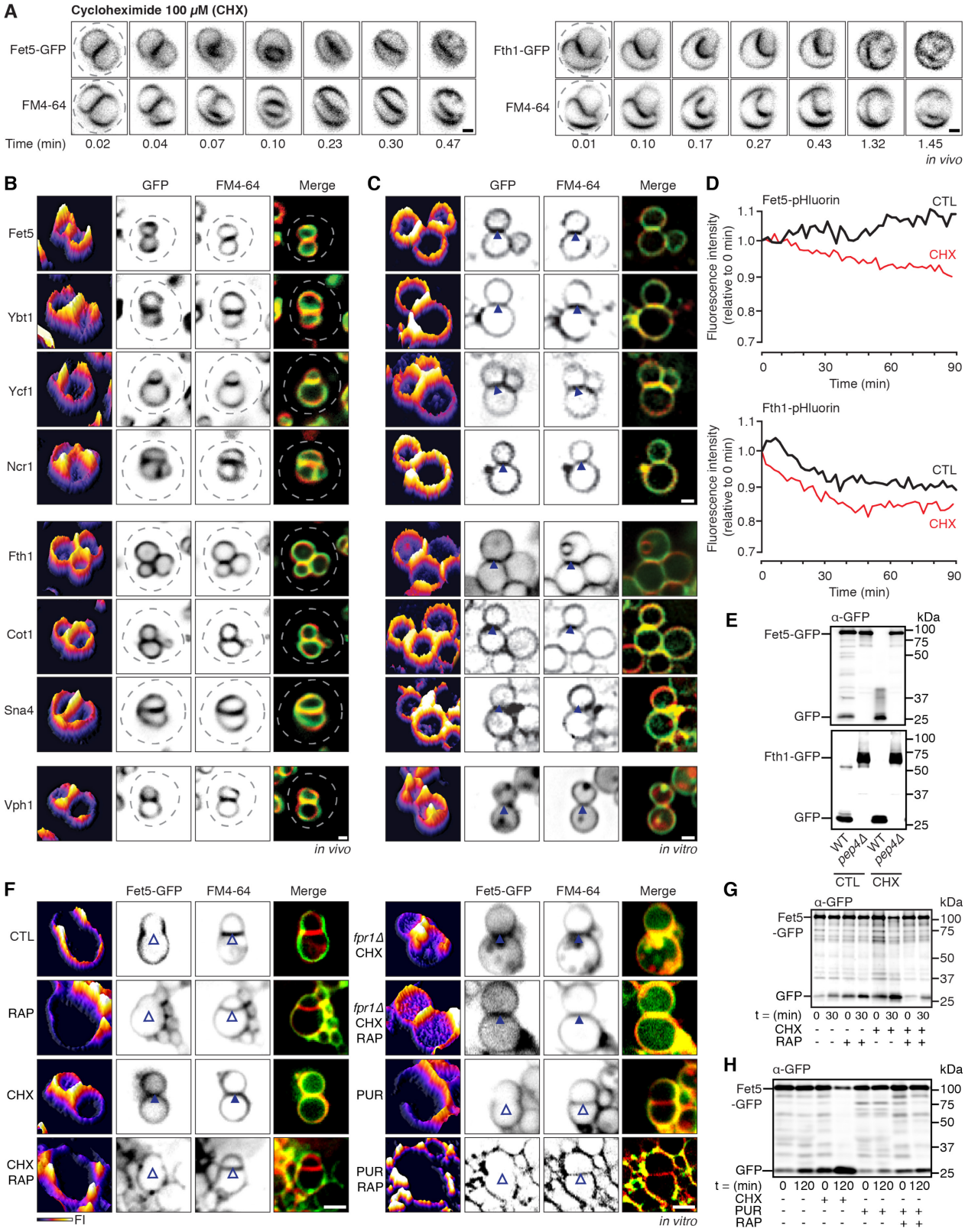
A
Cycloheximide 100 μM (CHX)
Fet5-GFP
FM4-64
Time (min)
0.02
0.04
0.07
0.10
0.23
0.30
0.47
Fth1-GFP
FM4-64
0.01
0.10
0.17
0.27
0.43
1.32
1.45
in vivo
B
GFP
FM4-64
Merge
Fet5
Ybt1
Ycf1
Ncr1
Fth1
Cot1
Sna4
Vph1
in vivo
C
GFP
FM4-64
Merge
in vitro
D
Fet5-pHluorin
CTL
CHX
Fluorescence intensity (relative to 0 min)
Time (min)
Fth1-pHluorin
CTL
CHX
Fluorescence intensity (relative to 0 min)
Time (min)
E
α-GFP
kDa
Fet5-GFP
GFP
Fth1-GFP
GFP
WT
pep4Δ
WT
pep4Δ
CTL
CHX
F
Fet5-GFP
FM4-64
Merge
CTL
RAP
CHX
CHX RAP
FI
fpr1Δ CHX
fpr1Δ CHX RAP
PUR
PUR RAP
in vitro
G
α-GFP
kDa
Fet5 -GFP
GFP
t = (min)
CHX
RAP
H
α-GFP
kDa
Fet5 -GFP
GFP
t = (min)
CHX
PUR
RAP

Figure 5. The ILF pathway degrades proteins in response to TOR signaling triggered by cycloheximide

(A) Images from time-lapse videos of vacuole fusion events within yeast cells expressing Fet5-GFP or Fth1-GFP after incubation with cycloheximide (CHX). Micrographs of docked vacuoles expressing different polytopic proteins tagged with GFP after CHX treatment imaged within cells **(B)** or *in vitro* **(C)**. **(D)** Relative fluorescence of isolated vacuoles expressing Fet5-pHluroin or Fth1-pHluorin during the *in vitro* fusion reaction under control conditions (CTL) or after CHX treatment. **(E)** Western blot analysis of Fet5-GFP or Fth1-GFP degradation after vacuole isolated from WT or *pep4*Δ*prb1*Δ cells were permitted to fuse for 120 minutes under CTL or CHX treatment. **(F)** Micrographs of docked vacuoles expressing Fet5-GFP or Fet5-GFP:*fpr1Δ* in the absence or presence of rapamycin (RAP), CHX or puromycin (PUR). **(G)** Western blot analysis of Fet5-GFP degradation under RAP, CHX or **(H)** PUR treatment. Scale bars, 1 μm (*in vivo*) or 2 μm (*in vitro*). See also **Figure S1, S2** and **movies S6** and **S7**.

2.4.4 pH regulates V-ATPase degradation by the ILF pathway

Surface levels of transporters and receptors must be tightly regulated for cellular physiological processes, from regulating nutrient uptake for metabolic homeostasis to properly detecting external hormonal or environmental cues (Van Belle and André, 2001). Often, substrate or ligand concentrations determine polytopic protein surface levels. For example, surface transporters Mup1, Fur4 and Can1 are downregulated and degraded by the MVB pathway upon substrate withdrawal (MacDonald et al., 2012; Keener and Babst, 2013; Ghaddar et al., 2014). Similarly, Ypq1 a lysosomal lysine transporter is downregulated and degraded through the MVB pathway upon lysine withdrawal (Li et al., 2015a). Thus, we reasoned that the ILF pathway may control the levels of lysosomal membrane proteins in a similar manner, possibly to mediate organellar contributions to cellular homeostasis, metabolism or signaling.

To test this hypothesis, we studied the effects of changing $[H^+]$ on Vph1-GFP turnover by the ILF pathway (**Figure 2B**; Wang et al., 2002). Vph1 is the stalk domain of the V-type H^+-ATPase pump complex that shunts H^+ from the cytoplasm to the lysosome lumen (Forgac, 2007). Besides providing the acid environment required for lysosomal hydrolase function, the V-ATPase is critical for cytoplasmic pH homeostasis (Diakov and Kane, 2010): The pump is inactivated when free cytoplasmic $[H^+]$ is low to prevent it from increasing pH to a level that is toxic to the cell. Conversely, it is activated to sequester H^+ within the vacuolar lumen when cytoplasmic $[H^+]$ is dangerously high. Thus, to mimic cytoplasmic pH acid or alkaline stress, we shifted the pH of the fusion reaction buffer from 6.80 to pH 6.38 or pH 7.32, respectively, and examined the effects on Vph1-GFP sorting (**Figures 6A** and **6B**), internalization (**Figure 6C**) and degradation (**Figure 6D**) by the ILF pathway *in vitro*. Under acid stress, when substrate levels are high, we find less Vph1-GFP in boundary membranes, less lumenal GFP fluorescence and less GFP-cleavage, demonstrating that Vph1 is spared under conditions that require V-ATPase activation for cell survival. In contrast, under alkali stress, we find enrichment of Vph1-GFP in the boundary membrane, an increase in lumenal GFP fluorescence and more GFP-cleavage, demonstrating that Vph1 is downregulated under conditions that promote V-ATPase inactivation.

But fusing GFP to Vph1 could change its lifetime or account for the observed changes in its turnover in response to acid or alkali stress. To eliminate these possibilities, we studied endogenous Vph1 degradation under pH stress by western blot analysis (**Figure 6E**) and found a similar pattern of degradation as observed for Vph1-GFP (**Figure 6D**) confirming that the

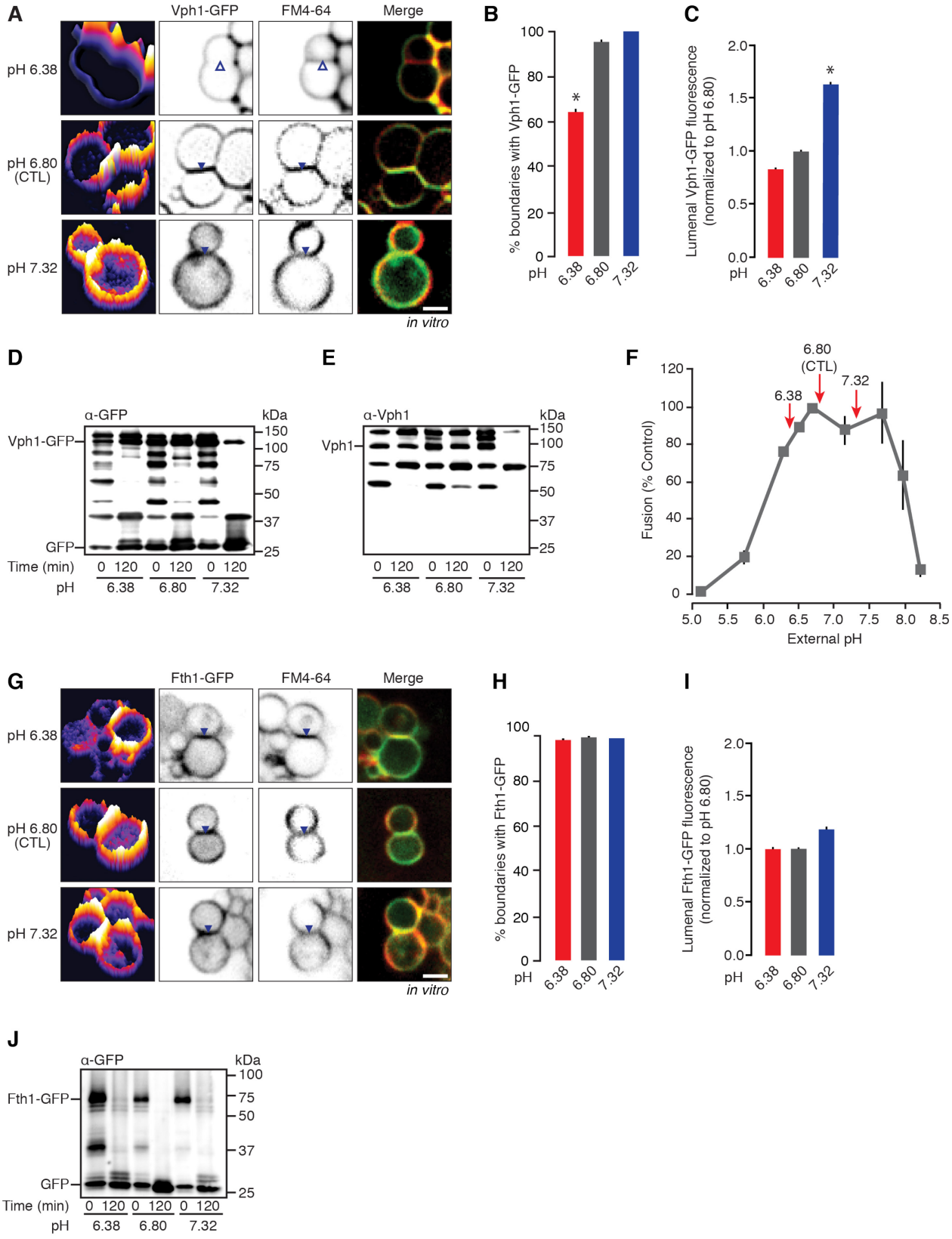
A
Vph1-GFP
FM4-64
Merge
pH 6.38
pH 6.80 (CTL)
pH 7.32
in vitro
B
% boundaries with Vph1-GFP
pH
6.38
6.80
7.32
C
Lumenal Vph1-GFP fluorescence (normalized to pH 6.80)
D
α-GFP
kDa
Vph1-GFP
GFP
Time (min)
pH
E
α-Vph1
Vph1
F
6.80 (CTL)
6.38
7.32
Fusion (% Control)
External pH
G
Fth1-GFP
H
% boundaries with Fth1-GFP
I
Lumenal Fth1-GFP fluorescence (normalized to pH 6.80)
J
Fth1-GFP

Figure 6. Changing pH affects degradation of Vph1-GFP by the ILF pathway

(A) Micrographs of docked vacuoles expressing Vph1-GFP imaged 60 minutes into the *in vitro* fusion reaction titrated to different pH values. **(B)** Percent of boundaries containing Vph1-GFP and **(C)** relative lumenal GFP fluorescence (normalized to pH 6.80; standard conditions) were calculated from micrographic data ($n \geq 308$). Western blots stained with antibodies against GFP **(D)** or Vph1 **(E)** indicating degradation kinetics of Vph1-GFP (a-Vph1 wasn't against Vph1-GFP) before and after fusion of isolated vacuoles at different pH values. **(F)** Homotypic vacuole fusion of isolated vacuoles was measured after reactions were titrated over a range of pH values. Arrows indicate experimental pH values used in other experiments shown ($n = 3$). **(G)** Micrographs of docked vacuoles expressing Fth1-GFP imaged at 60 minutes into the *in vitro* fusion reaction titrated to three pH values. **(H)** Percent of boundaries containing Fth1-GFP and **(I)** relative lumenal GFP fluorescence (normalized to pH 6.80) were calculated from micrographic data ($n \geq 91$). **(J)** Western blot kinetics of Fth1-GFP degradation before and after fusion of isolated vacuoles at different pH values. Scale bars, 2 μm (*in vitro*); *, $P < 0.05$. See also **Figure S3**.

epitope tag had no effect on Vph1 turnover. It is also possible that our observations were a consequence of simply altering the rates of organelle fusion. For example, acid stress could inhibit fusion accounting for the observed decrease in internalization and degradation of Vph1-GFP. To eliminate this possibility, we measured homotypic vacuole fusion using a content-mixing assay (**Figure 6F**) and confirmed that acid and alkali stress had no impact on organelle fusion *in vitro*. pH could also indiscriminately affect the machinery responsible for sorting within the ILF pathway. If so, then we expect that sorting of other polytopic proteins cleared by the ILF pathway should also be affected by acid and alkali stress. However, when we studied GFP-labeled Fth1 (**Figures 6G-J**), or Fet5 (**Figure S3**; neither translocate H^+), we found that sorting, internalization and degradation of both proteins were not affected by these stresses. Together, these results demonstrate that the ILF pathway selectively regulates membrane expression of Vph1, and presumably the activity of the V-ATPase, in response to changes in $[H^+]$ implicating a role in cellular pH homeostasis and confirming that it can mediate substrate-dependent degradation protein degradation.

2.4.5 Protein sorting in the ILF pathway does not require autophagy or ESCRT machinery

Findings presented thus far answer the first question posed earlier by demonstrating that the ILF pathway functions to control lysosome polytopic protein quality and quantity for organelle homeostasis and for membrane protein remodeling to accommodate cellular metabolism or ion homeostasis. But what are the mechanisms that underlie this process? Given that lysosomes contribute to autophagic and the MVB pathways, we first examined whether the ILF pathway may share underlying molecular machinery with these two major cellular protein degradation pathways. Although there is no evidence of autophagosomes or MVBs contributing to lysosomal polytopic protein sorting or internalization (**Figures 2-6**), it remains possible that mechanisms responsible for protein sorting in these pathways may also function in the ILF pathway, as they have been implicated in degradation of lysosome transporters and can be found on lysosome membranes (Li et al., 2015a,b). To eliminate this possibility, we deleted genes encoding essential components for autophagy, *ATG1* and *ATG7,* or for the MVB pathway, *VPS27* (ESCRT-0), *VPS23* (ESCRT-I) and *VPS36* (ESCRT-II), and examined effects on GFP-tagged polytopic protein distribution during homotypic vacuole fusion events (**Figures S4 and S5**). Deleting any of these genes had no affect on protein sorting *in vivo* (**Figures S4A** and **S4B**) or *in vitro*

(**Figures S5A** and **S5B**) or degradation (**Figure S4D**) even under conditions that induced protein clearance by the ILF pathway (**Figures S4C, S4D** and **S5C, S5D**). Thus, we are confident that the ILF pathway uses separate machinery from the autophagic and MVB pathways, representing a novel mechanism for cellular protein degradation.

2.4.6 The docking machinery sorts polytopic proteins for degradation

From the micrographic evidence presented, it is apparent that protein sorting occurs during the docking stage of the homotypic vacuolar lysosome fusion reaction when the boundary membrane is formed (Wang et al., 2002; Wickner, 2010). During docking, fusogenic lipids and proteins accumulate at the initial site of contact between organelles where they arrange into an expanding ring at the vertex between apposing membranes. This vertex ring represents the border between outer and boundary areas of the lysosome membrane where polytopic proteins are sorted to be spared or degraded. Thus, we hypothesized that the machinery assembled at the vertex ring may contribute to polytopic protein sorting, as well as driving membrane fusion. To test this hypothesis, we took a biochemical approach by blocking stages of the *in vitro* fusion reaction with protein or chemical inhibitors (Mayer and Wickner, 1997; Wickner and Haas, 2000; Wang et al., 2002) and monitored affects on the membrane distribution of Fet5-GFP or Fth1-GFP (**Figure 7**). First we targeted the lysosomal Rab GTPase Ypt7 that, when activated, orchestrates recruitment and assembly of the fusion machinery at the vertex ring (Brett et al., 2008). We reasoned that inactivating Ypt7 by adding rGyp1-46 (purified recombinant active domain of the Rab-GAP protein Gyp1; Rak et al., 2000) and rGdi1 (the Rab chaperone protein that extracts Ypt7 from vacuole membrane; e.g. Brett et al., 2008) or rGdi1 alone to fusion reactions should disrupt protein sorting (Eitzen et al., 2000). We found that these Ypt7 inhibitors prevent sorting of Fet5-GFP or Fth1-GFP into the boundary membrane (**Figures 7A** and **7B**), even when protein clearance was triggered with heat stress (**Figures 7C** and **7D**) or cycloheximide (**Figures S6A** and **S6B**), suggesting that active Ypt7 is important for selective entry, but not exclusion, of polytopic proteins into the boundary membrane during organelle fusion. Likewise, internalization (**Figures 7E** and **S6C**) and degradation (**Figure 7F**) of both polytopic proteins were blocked by Ypt7 inhibitors, illustrating the importance of the fusion machinery for lipid bilayer merger required to internalize polytopic proteins for degradation by the ILF pathway.

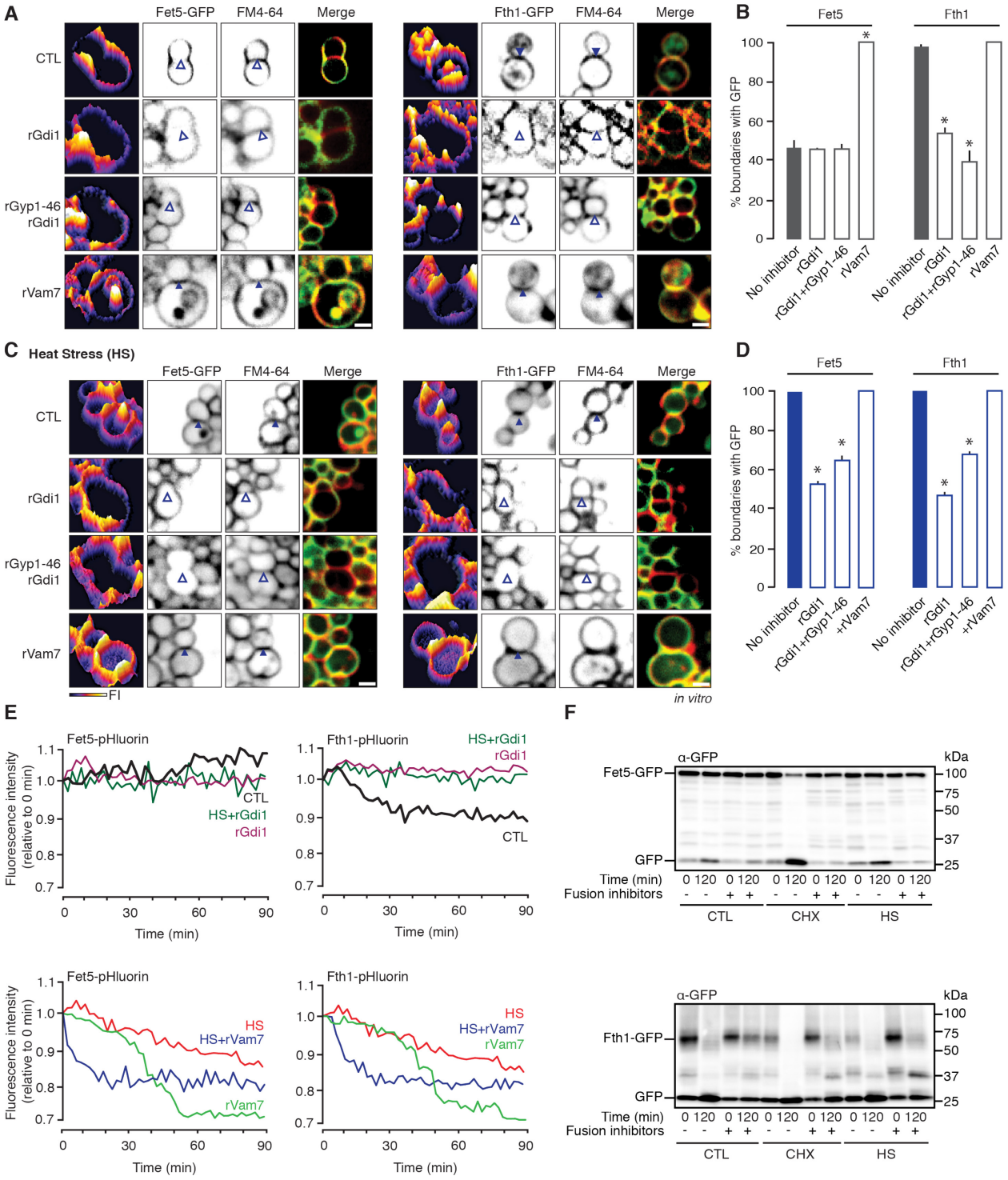
A
Fet5-GFP
FM4-64
Merge
Fth1-GFP
FM4-64
Merge
CTL
rGdi1
rGyp1-46
rGdi1
rVam7
B
Fet5
Fth1
% boundaries with GFP
No inhibitor
rGdi1
rGdi1+rGyp1-46
rVam7
C
Heat Stress (HS)
Fet5-GFP
FM4-64
Merge
Fth1-GFP
FM4-64
Merge
CTL
rGdi1
rGyp1-46
rGdi1
rVam7
FI
in vitro
D
Fet5
Fth1
% boundaries with GFP
No inhibitor
rGdi1
rGdi1+rGyp1-46
+rVam7
E
Fet5-pHluorin
Fth1-pHluorin
Fluorescence intensity (relative to 0 min)
Time (min)
CTL
HS+rGdi1
rGdi1
HS
HS+rVam7
rVam7
F
α-GFP
kDa
Fet5-GFP
Fth1-GFP
GFP
Time (min)
Fusion inhibitors
CTL
CHX
HS

Figure 7. Lysosomal polytopic protein sorting and internalization requires the membrane fusion machinery

(A) Micrographs of docked vacuoles expressing Fet5-GFP or Fth1-GFP during the *in vitro* fusion reaction in the absence (CTL) or presence of 4 μM rGdi, 4 μM rGdi and 3.2 μM rGyp1-46, or 100 nM rVam7. **(B)** Percent of boundaries containing Fet5-GFP or Fth1-GFP under these conditions calculated from micrographic data ($n \geq 103$). **(C)** Micrographs of docked vacuoles expressing Fet5-GFP or Fth1-GFP *in vitro* after heat stress (HS). **(D)** Percent of boundaries containing Fet5-GFP or Fth1-GFP calculated from micrographic analysis ($n \geq 242$.). **(E)** Relative fluorescence of isolated vacuoles expressing Fet5-pHluroin or Fth1-pHluorin during *in vitro* fusion reactions incubated with rGdi or rVam7 in CTL and HS treatment. **(F)** Western blot analysis of Fet5-GFP and Fth1-GFP degradation before and after fusion of isolated vacuoles under CTL, CHX or HS conditions. Scale bars, 2 μm (*in vitro*); *, $P < 0.05$. See also **Figures S4, S5** and **S6**.

Although this result implies a role for the docking machinery in protein sorting, an alternative interpretation is that blocking the membrane fusion reaction indirectly impairs protein sorting into the ILF pathway. Thus, we sought an approach to disrupt Ypt7 function without blocking membrane fusion to better understand its role in protein sorting. This involved using the recombinant soluble Q-SNARE protein Vam7 (rVam7) to drive the lysosome fusion reaction, as it bypasses the need for Rab activity (Thorngren et al., 2004). In the presence of rVam7, both Fet5-GFP and Fth1-GFP are present in the boundary membrane (**Figures 7A** and **7B**) and internalized (**Figure 7E**) in the absence or presence of heat stress (**Figures 7C-E**) or cycloheximide (**Figure S6**). Thus, bypassing Ypt7 activity blocks exclusion, but not inclusion, of polytopic proteins into the boundary membrane during fusion. Together, these results suggest that active Rab must be engaged to selectively sort polytopic proteins into the ILF pathway.

2.4.7 Protein sorting occurs during vertex ring expansion

All things considered, it seems that the docking machinery contributes to polytopic protein sorting at the vertex ring that surrounds the boundary membrane during lysosome fusion. If so, this machinery could function by employing a protein sieving mechanism that sorts polytopic proteins encountered within the lysosome membrane as the vertex ring expands. Alternatively, it could recognize and actively move polytopic proteins marked for degradation across the vertex ring into the boundary after it has assembled at the vertex ring (**Figure 8A**). To test these models, we first examined the membrane distribution of Fet5-GFP at early time points after membrane fusion was triggered *in vitro* when docking occurs (Jun et al., 2006). To accurately study early docking events, it is important to consider that some docked interfaces observed at early time points could be mature because organelle interactions can occur prior to triggering fusion – either within yeast cells (which contain 2-3 vacuoles), prior to isolation or during the organelle isolation process. Thus, to distinguish newly formed organelle interactions from existing, mature contact sites, we mixed vacuolar lysosomes isolated separately from two different yeast strains, one expressing Fet5-GFP and the other lacking a GFP tag, stained their membranes with FM4-64 to visualize contact sites, and analyzed only boundary membrane between Fet5-GFP-labeled and GFP-free organelles (**Figure 8B**). To assess vertex ring assembly at these early time points, we also monitored the membrane distribution of Vps33-GFP using the same approach (**Figure 8C**). We selected Vps33 because it is one of six subunits that comprise the HOPS tethering

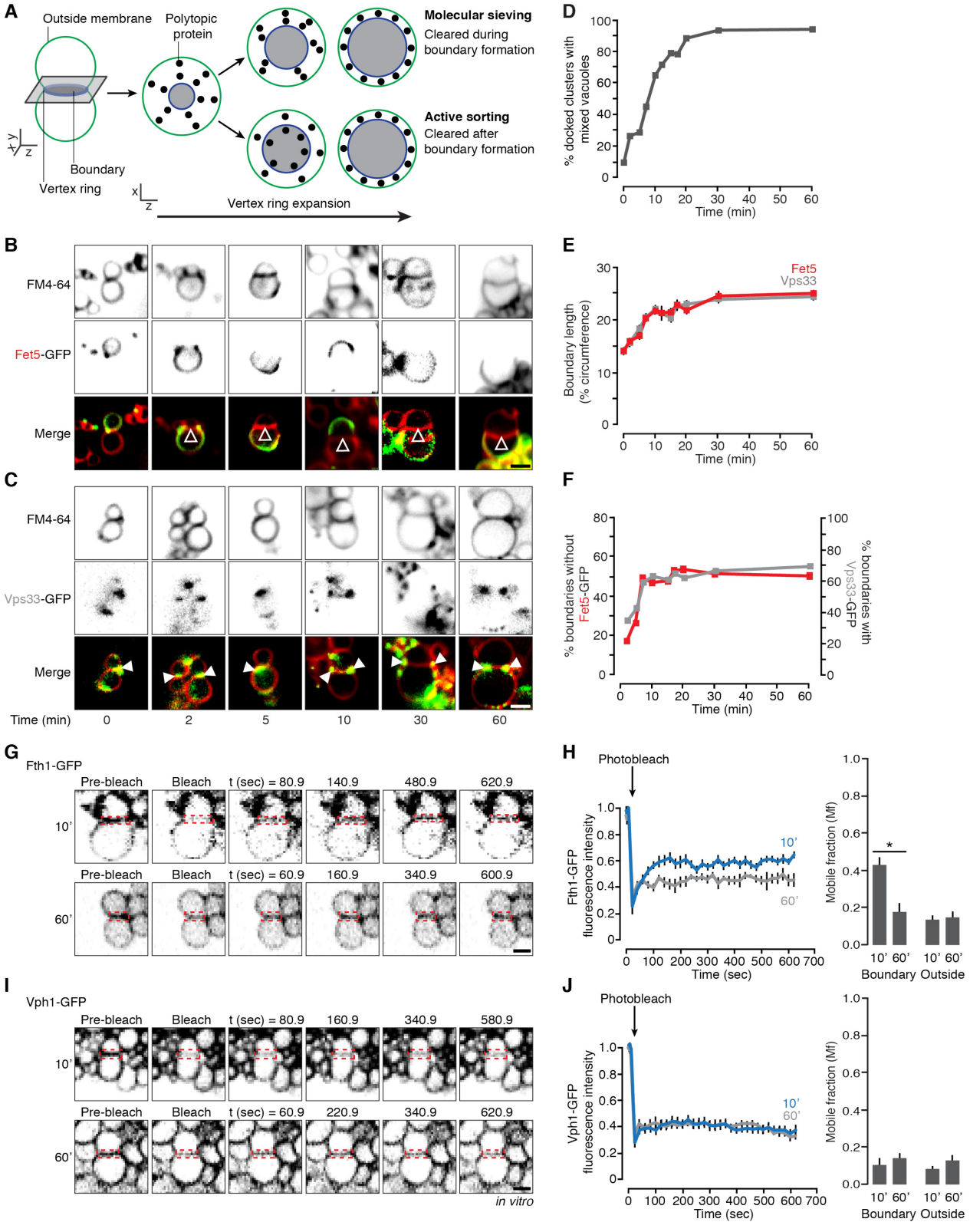
A
Outside membrane
Polytopic protein
Boundary
Vertex ring
Vertex ring expansion
Molecular sieving
Cleared during boundary formation
Active sorting
Cleared after boundary formation
B
FM4-64
Fet5-GFP
Merge
C
FM4-64
Vps33-GFP
Merge
Time (min) 0 2 5 10 30 60
D
% docked clusters with mixed vacuoles
Time (min)
E
Fet5
Vps33
Boundary length (% circumference)
Time (min)
F
% boundaries without Fet5-GFP
% boundaries with Vps33-GFP
Time (min)
G
Fth1-GFP
Pre-bleach Bleach t (sec) = 80.9 140.9 480.9 620.9
10'
Pre-bleach Bleach t (sec) = 60.9 160.9 340.9 600.9
60'
H
Photobleach
Fth1-GFP fluorescence intensity
Time (sec)
Mobile fraction (Mf)
Boundary Outside
I
Vph1-GFP
Pre-bleach Bleach t (sec) = 80.9 160.9 340.9 580.9
10'
Pre-bleach Bleach t (sec) = 60.9 220.9 340.9 620.9
60'
in vitro
J
Photobleach
Vph1-GFP fluorescence intensity
Time (sec)
Mobile fraction (Mf)
Boundary Outside

Figure 8. Protein sorting occurs during vertex ring expansion

(A) Working model demonstrating two hypotheses of polytopic protein sorting from the boundary membrane either through a molecular sieving mechanism or through active sorting. **(B)** Micrographs of docked vacuoles between Fet5-GFP and GFP-free organelles or between **(C)** Vps33-GFP and GFP-free organelles acquired at different times during the *in vitro* fusion reaction. **(D)** Percent of docked clusters that were mixed between Fet5-GFP and GFP-free organelles. 2179 docked vacuole clusters were observed. **(E)** Micrographic data were used to calculate the boundary membrane length between apposed vacuoles as a percentage of the circumference **(F)** and the percent of boundaries either without Fet5-GFP or with Vps33-GFP ($n \geq 108$). **(G)** Micrographs of fluorescence recovery after photobleaching (FRAP) analysis of the boundary membrane between docked vacuoles expressing Fth1-GFP 10 and 60 minutes after vacuoles were permitted to fuse. **(H)** GFP fluorescence intensity in the boundary was measured over the course of the experiment and the mobile fraction (Mf) was calculated for ROIs photobleached in the boundary or outside membranes of docked vacuoles ($n \geq 11$). **(I)** FRAP analysis of the boundary membrane between docked vacuoles expressing Vph1-GFP 10 and 60 minutes into the *in vitro* fusion reaction. **(J)** GFP fluorescence intensity in the boundary was measured and Mf values for ROIs photobleached in the boundary and outside membranes were calculated from micrographic analysis ($n \geq 13$). The red dotted box outlines ROIs subjected to photobleaching. Scale bars, 2 μm (*in vitro*); *, $P < 0.05$. See also **Figure S7**.

holocomplex, a key component of the fusion machinery that is recruited to the vertex ring by active Ytp7 as part of the docking subreaction (Wang et al., 2002). Hence, enrichment of Vps33-GFP at the edges of the boundary membrane between GFP-labeled and GFP-free vacuoles labels fusion machinery assemblies at the vertex ring triggered by ATP *in vitro*. By measuring lengths over time, we confirmed that boundary expansion occurred at the same rate and terminated at the same time (30 minutes) in both samples (**Figure 8E**), consistent with previous reports (e.g. Wang et al., 2002). Importantly, Fet5-GFP exclusion from boundaries occurred at the same rate as vertex ring assembly, assessed by monitoring Vps33-GFP enrichment at organelle vertices over time (**Figure 8F**). Notably, the half times of boundary expansion, Vps33-GFP enrichment and Fet5-GFP were similar, strongly suggesting that polytopic protein exclusion from the boundary membrane occurs during vertex ring expansion.

But does the same model also describe sorting of proteins into the boundary membrane for degradation? To address this question, we studied the lateral mobility of Fth1-GFP (an enriched protein) within the vacuole membrane using a fluorescence recovery after photo-bleaching (FRAP) during early and late stages of the docking subreaction *in vitro*. We hypothesized that if sorting occurred during vertex ring expansion, then Fth1-GFP should be mobilized into the boundary early (10 minutes) but not late into the reaction (60 minutes) after the fusion machinery is stabilized and no further increase in the boundary length is observed (**Figure 8E**). As predicted, Fth1-GFP fluorescence recovered to significantly higher level after photo-bleaching within the boundary membrane at 10 minutes (42.9%) as compared to 60 minutes (17.9%; **Figures 8G** and **8H**). Fth1-GFP mobility on the outer area of the vacuole membrane did not change over the course of the fusion reaction, and values were similar to those obtained when studying the boundary membrane at 60 minutes. These values were also similar to Vph1-GFP mobility on the outer and boundary membranes at early and late times (**Figures 8I** and **8J**). Because Vph1-GFP is uniformly distributed on the vacuole membrane (**Figures 2, 3,** and **6**; Wang et al., 2002), we speculate that these values (mobile fractions between 10.8 and 14%) represent a good measure of polytopic protein lateral mobility within the vacuolar lysosome membrane. We also assessed lipid mobility by recording FM4-64 fluorescence recovery (**Figure S7**). As expected, the mobile fraction of FM4-64 within the lipid bilayer was much higher (80%; as previously reported in Dhonukshe et al., 2006) than the polytopic proteins studied, lending confidence to our assessment of Fth1-GFP movement during vacuole fusion. All things

considered, the lateral mobility of Fth1-GFP is highest within the boundary membrane during the early stage of docking, lending support to a molecular sieving model of protein sorting into the ILF pathway that occurs during vertex expansion.

2.5 Discussion

2.5.1 The ILF pathway is a new mechanism responsible for organelle polytopic protein degradation within cells

Lysosomal polytopic proteins are critical for cellular nutrient recycling, signaling and ion homeostasis. Thus, it is important that we understand how they are regulated or degraded. Herein, we describe a new pathway responsible for turnover of transporters and membrane proteins on lysosomes: Using fluorescence microscopy we show that GFP-tagged polytopic proteins are selectively sorted into the boundary area of apposing membranes that is internalized into the lumen upon lipid bilayer fusion within living cells (**Figures 2, 4, 5** and **S4**). We confirmed our original observations by monitoring protein internalization using a pHluorin-based fluorescence assay and show that internalized proteins are degraded by lumenal hydrolases by western blot (**Figures 3-7** and **S6**). Of the eight studied, four proteins were spared and four were internalized by this pathway under normal growth conditions, indicating that lysosomal polytopic proteins have different lifetimes and that the protein content of the lysosomal membrane can change with every homotypic fusion event. Although it is not clear why the cell would want to rapidly turnover some proteins (e.g. Fth1) and not others (Fet5), this observation is consistent with reports of surface membrane proteins that are also constitutively degraded, e.g. the G-protein coupled receptor Ste3 is constitutively internalized and degraded by the MVB pathway (Davis et al, 1993). Because some proteins were spared, it was possible that they utilized an alternative mechanism for degradation, such as the vReD pathway (Li et al., 2015a,b). However, we found that all proteins were shunted to the ILF pathway after misfolding was induced by heat stress (**Figure 4**), confirming that all proteins studied can be degraded by this new pathway. Furthermore, by piggybacking membrane fusion, the ILF pathway seems like a more efficient alternative for lysosomes to turnover their membrane proteins as compared to the vReD pathway, which requires additional trafficking steps to deliver lysosomal proteins to the MVB for packaging and back to the lysosome for degradation (Li et al., 2015a). Although lysosomes frequently undergo homotypic fusion (Wickner, 2002), they require heterotypic fusion events

between MVBs or autophagosomes for delivery of incoming biomaterials to be recycled (Davies et al., 2009; Carlsson and Simonsen, 2015). As similar fusion machinery mediates these events (Luzio et al., 2009; Jiang et al., 2014), it is possible that intralumenal membrane fragments also form. Current advances in light and electron microscopy will allow us to test this hypothesis in the near future. In the mean time, it is tempting to speculate that the ILF pathway could allow these dynamic organelles to remodel the protein content within their membranes while they receive biomaterials for recycling.

But how are intralumenal fragments degraded? To prevent lysosome rupture, membrane lipids and proteins facing the lumen are resistant to attack by hydrolases (see Kolter and Sandhoff, 2005). However, when a portion of this membrane is internalized through the ILF pathway, the membrane conserves its orientation (*i.e*. the lumenal face remains lumenal) but becomes susceptible to degradation. Although many factors may be at play (*e.g*. perhaps selective lipid sorting into the boundary membrane promotes rupture or susceptibility to hydrolases; see Fratti et al., 2004), we speculate that this may be an outcome of lipid bilayer merger driven by asymmetrically aligned SNARE complexes (D'Agostino et al., 2016): SNARE-domains of *trans*-complexes extend into the cytoplasm around the vertex ring, where they interact with the fusion machinery (e.g. HOPS; Wickner, 2010). Upon zippering, they form *cis*-complexes that exclusively reside in the limiting membrane of the fusion product, not within the intralumenal fragment. As transmembrane domains of SNARE-complexes seem to stabilize the lipid bilayer during merger, the absence of these complexes within the fragment may destabilize the bilayer exposing the inner leaflet to lumenal hydrolases to initiate degradation. We have begun to characterize intermediates of this lipid bilayer fusion reaction in context to intralumenal fragment formation (Mattie et al., 2017) and plan to test this hypothesis in the near future.

2.5.2 A molecular sieving mechanism may be responsible for protein sorting in the ILF pathway

Upon the discovery of this new protein degradation pathway, we immediately sought to better understand the molecular basis of how it works. We present many lines of evidence to support a molecular sieving model of protein sorting that occurs during the docking stage of the fusion reaction when the machinery assembles at an expanding vertex ring between apposing organelles prior to lipid bilayer merger: (1) We find that polytopic proteins are selectively sorted into or out of the boundary area of membrane formed between apposing organelles during

docking (**Figures 3, 8** and **S7**). (2) When we block or bypass the activity of Ypt7, an important mediator of docking, protein sorting is disrupted (**Figures 7** and **S6**). (3) Using FRAP and time-lapse microscopy, we demonstrate that protein sorting occurs during expansion of the vertex ring that encircles the boundary between apposing lysosomes (**Figure 8**). Topologically, this mechanism is analogous to polytopic protein sorting into budding intralumenal vesicles on the outer membrane of immature MVBs, where the ESCRT machinery assembles into a ring at the neck of the budding vesicle (Nickerson et al., 2007). However, we demonstrate that the ESCRT machinery, as well as the autophagy machinery, does not contribute to the ILF pathway (**Figures S4** and **S5**). Furthermore, other cytoplasmic factors (e.g. components of the proteasome machinery) likely do not play a role because similar results were obtained from experiments conducted *in vivo* and *in vitro* (**Figure 3**). So what is the molecular basis of protein sorting in the ILF pathway?

Although we implicate molecular sieving in this process, we did not uncover the basis of protein selection. We are however confident that it is not simply protein size, for example, as it does not correlate with the observed sorting phenotypes. Rather, we speculate that the ILF pathway uses a ubiquitin-based mechanism similar to the other protein degradation pathways in the cell based on the following observations: Proteomic screens reveal that most of the lysosomal polytopic proteins studied can be ubiquitylated (Peng et al., 2003). Protein ubiquitylation machinery, such as adaptor proteins (e.g. Ssh4) and E3-ligases (Rsp5), are found on vacuole membranes (Pokrzywa et al., 2009; Li et al., 2015a). This includes a paralog of Sna3, an important adapter protein in the MVB pathway, called Sna4 that exclusively resides on vacuole lysosome membranes. At MVBs, Sna3 binds internalized surface polytopic proteins to accommodate ubiquitylation by Rsp5 and sorting into ILVs, and by doing so it too is internalized and degraded by the MVB pathway (MacDonald et al., 2012). Like Sna3, we show that Sna4 is sorted into the boundary of docked lysosomes and is internalized upon fusion (**Figures 2** and **3**), suggesting that perhaps Sna4 performs a similar function in the ILF pathway.

If ubiquitylation mediates degradation, then labeled proteins must be recognized at the vertex ring for sorting into the ILF pathway. Of the proteins that concentrate at this site, three contain partial potential ubiquitin binding domains (UBDs): Vps11, Vps18 and Vps39 (Nickerson et al., 2009). Together with 3 other subunits, these proteins form HOPS, the lysosomal multisubunit tethering complex important for MVB-lysosome and homotypic vacuolar lysosome fusion

(Balderhaar and Ungermann, 2013). Although speculative, these three partial domains may form a UBD when in complex that recognizes and sorts ubiquitinated lysosomal polytopic proteins into the boundary, similar to how the multiple UBDs of the ESCRT machinery sort surface proteins in the MVB pathway (Shields and Piper, 2012). Using the comprehensive set of approaches to study the ILF pathway presented herein, we have begun to test this model and it will be interesting to determine whether the ILF pathway shares protein labeling machinery but has unique sorting machinery as compared to other protein degradation pathways.

2.5.3 Importance of the ILF pathway to cell physiology

What is the purpose of the ILF pathway? Herein, we show that it performs at least three important functions: First, it mediates lysosomal polytopic protein degradation upon misfolding by heat stress (**Figure 4**). The ERAD pathway performs this function to clear damaged or unfolded proteins at the endoplasmic reticulum (Vembar and Brodsky, 2008), the proteasome for cytoplasmic proteins (Fang et al., 2014) and the MVB for surface polytopic proteins (Keener and Babst, 2013). Thus, we propose that the ILF pathway is an equally important contributor to cellular protein quality control. Second, the ILF pathway responds to changes in substrate levels to selectively regulate cognate transporter levels, as increasing pH promotes degradation of Vph1 by the ILF pathway (**Figure 6**) consistent with reports of how the V-ATPase regulates cellular pH homeostasis (Tarsio et al., 2011). Similar mechanisms are in place at the plasma membrane to regulate cellular nutrient uptake, receptor signaling and osmotic homeostasis (Keener and Babst, 2013). We speculate that ILF pathway performs an analogous function on lysosomes to potentially regulate Ca^{2+} signaling or nutrient export, for example, which are important contributors to cellular physiology and metabolism.

Lastly, the ILF pathway degrades proteins in response to TOR activation induced by the protein translation inhibitor cycloheximide (**Figure 5**). Lysosomes are an important source of cellular amino acids needed to feed the protein translation machinery. Thus, the activities of these two fundamental processes are tightly regulated through extensive metabolic signaling circuitry including the TOR pathway (Efeyan et al., 2012; Settembre et al., 2013). For example, when cellular amino acid pools are depleted, translation stops, TOR is activated and lysosome activity is enhanced to increase amino acid levels, closing a negative feedback loop. Blocking protein translation with puromycin or cycloheximide triggers protein degradation by the ILF pathway

within live cells (**Figure 5A** and **B; Figure S2**) lending support to this model. However, only cycloheximide elicits this response when added to purified organelle preparations devoid of ribosomal components, which is abolished by rapamycin, a TOR-signaling inhibitor, suggesting that it may also have a second target present on lysosome membranes that activates TOR signaling and triggers degradation of lysosomal polytopic proteins to increase cellular amino acid levels. In any case, our findings clearly demonstrate a role for the ILF pathway in cellular amino acid metabolism. Maintenance of amino acid levels through sustained or enhanced lysosome function is critical for survival as cells age (Aris et al., 2012). As such, impaired lysosome activity correlates with many age-related disorders such as Alzheimer's disease (Settembre et al., 2013). The transcriptional regulator TFEB plays a critical role in this process by increasing lysosome biogenesis (Settembre et al., 2013). By remodeling existing lysosomes to accommodate changes in cell physiology as they age, we argue that the ILF pathway may play a complementary and equally important role in cellular longevity.

Chapter 3. ESCRT-independent Surface Receptor and Transporter Protein Degradation by the ILF Pathway

3.1 Abstract

Surface receptor and transporter protein down-regulation drives cell signaling, quality control and metabolism underlying diverse physiology. After endocytosis, proteins are delivered to endosomes where ESCRTs package them into intralumenal vesicles, which are degraded by acid hydrolases upon fusion with lysosomes. However, reports of ESCRT-independent surface protein degradation are emerging suggesting that alternative, non-canonical pathways exist. Using *Saccharomyces cerevisiae* as a model, here we show that in response to substrates, protein misfolding or TOR signaling, some internalized surface transporters (Hxt3, Itr1, Aqr1) bypass ESCRTs en route to the lysosome membrane where they are sorted into an area that is internalized as an intralumenal fragment (ILF) and degraded upon organelle fusion. This ILF pathway also degrades typical ESCRT client proteins (Mup1, Can1, Ste3) when ESCRT function is impaired. As the underlying machinery is conserved, we speculate that the ILF pathway is an important contributor to receptor and transporter down-regulation in all eukaryotes.

3.2 Introduction

Surface polytopic proteins including receptors, transporters and channels are internalized and sent to the lysosome for degradation (Katzmann et al., 2002; Babst 2011; Henne et al., 2011). Precise control of their surface levels underlies diverse physiology, including endocrine function, wound healing, tissue development, nutrient absorption and synaptic plasticity (Katzmann et al., 2002; Palacios et al., 2005; Rodahl et al., 2009; Lobert and Stenmark, 2011; Zhou et al., 2010; Hislop and von Zastrow, 2011; Koumanov et al., 2012; Chassefeyre et al., 2015). Damaged surface proteins are also cleared by this mechanism to prevent proteotoxicity (Wang et al., 2011; Keener and Babst, 2013; Zhao et al., 2013). To trigger this process, surface proteins are labeled with ubiquitin – in response to changing substrate levels, heat stress to induce protein misfolding or cellular signaling for example – and then selectively internalized by the process of endocytosis (Blondel et al., 2004; Lewis and Pelham, 2009; MacGurn et al., 2011; Jones et al., 2012; MacDonald et al., 2012; Keener and Babst, 2013; Babst, 2014). Within the cell, they are sent to endosomes where they encounter ESCRTs (Endosomal Sorting Complexes Required for

Transport). These five protein complexes (ESCRT-0, ESCRT-I, ESCRT-II, ESCRT-III and the Vps4 complex) sort and package these internalized surface proteins into IntraLumenal Vesicles (ILVs; Henne et al., 2011). After many rounds, ILVs accumulate creating a mature MultiVesicular Body (MVB; Nickerson et al., 2010; Hanson and Cashikar, 2012). The MVB then fuses with lysosomes to expose protein laden ILVs to lumenal hydrolases for catabolism (Katzmann et al., 2002). Although many examples of ESCRT-mediated protein degradation have been published (see Babst, 2014), reports of ESCRT-independent degradation of surface proteins are emerging (e.g. Bowers et al., 2006; Theos et al., 2006; Leung et al., 2008; Silverman et al., 2013; Parkinson et al., 2015). Furthermore, ILVs can be formed independent of ESCRT function and proteins recognized by ESCRTs continue to be degraded when ESCRTs are impaired (Trajkovic et al., 2008; Blanc et al., 2009; Stuffers et al., 2009b; Edgar et al., 2014). These realizations have led to one of the most prominent open questions in our field: What accounts for ESCRT-independent ILV formation and surface polytopic protein degradation?

Around the time when ESCRTs were discovered (Katzmann et al., 2001), Wickner, Merz and colleagues reported that an ILV-like structure called an IntraLumenal Fragment (ILF) is formed as a byproduct of homotypic lysosome fusion in the model organism *Saccharomyces cerevisiae* (Wang et al., 2002). Prior to lipid bilayer merger, fusogenic proteins and lipids concentrate within a ring at the vertex between apposing lysosomal membranes (Wang et al., 2003b; Fratti et al., 2004). Upon SNARE-mediated membrane fusion at the vertex ring, the encircled area of membrane, called the boundary, is excised and internalized within the lumen of the fusion product where it encounters lysosomal hydrolases (Mattie et al., 2017). We recently discovered that lysosomal polytopic proteins, e.g. ion and nutrient transporters, are selectively sorted into the boundary membrane for degradation in response to substrate levels, misfolding by heat stress or TOR (Target Of Rapamycin) signaling (McNally et al., 2017). Named the ILF pathway, this process functions independently of ESCRTs and instead relies on the fusion protein machinery for transporter sorting and ILF formation. Thus, this process performs similar functions as ESCRTs, except the mechanisms underlying protein sorting and packaging and their cellular locations are distinct. The possibility exists that surface polytopic proteins may also be degraded by the ILF pathway if they can be delivered to the lysosome membrane after internalization.

Can internalized surface proteins be delivered to lysosome membranes? To our knowledge, this hypothesis has not been formally tested. However, this proposition seems reasonable when considering the consequence of bypassing ESCRT function in the canonical MVB pathway (**Figure 9A**): In theory, any internalized surface polytopic protein that is not packaged into ILVs by ESCRTs (or returned to the surface) remains embedded within the outer membrane of the mature MVB. When this membrane merges with the lysosome membrane upon heterotypic fusion, these proteins are then exposed to the ILF machinery, which may package them for degradation. Thus, by simply avoiding recognition by ESCRTs, internalized surface proteins are––by default—delivered to lysosome membranes and the ILF pathway. Upon reexamination of micrographs presented in earlier reports on receptor and transporter down-regulation, we found that some internalized surface polytopic proteins appear on lysosome membranes en route to the lumen for degradation, e.g. the high affinity tryptophan permease Tat2 (Beck et al., 1999), glucose transporters Hxt1 and Hxt3 (O'Donnell et al., 2015), peptide transporter Ptr2 (Kawai et al., 2014), and myo-inositol transporter Itr1 (Nikko and Pelham, 2009). We also noticed that most of these published studies do not directly assess whether ESCRTs are required for protein degradation. However, when the dependence on MVB formation was assessed, internalized surface proteins often accumulated on lysosome membranes when ESCRT function was disrupted, e.g. the general amino acid permease Gap1 (Nikko et al., 2003), ATP-binding cassette transporter Ste6 (Krsmanovic et al., 2005), and G-protein coupled receptor Ste3 (Yeo et al., 2003; Shields et al., 2009; Prosser et al. 2010). Thus, given that internalized surface transporters and receptors can appear on lysosome membranes, we decided to test the hypothesis that the ILF pathway represents an alternative, ESCRT-independent mechanism for degradation of surface polytopic proteins and may compensate for the loss of ESCRT function (**Figure 9A**).

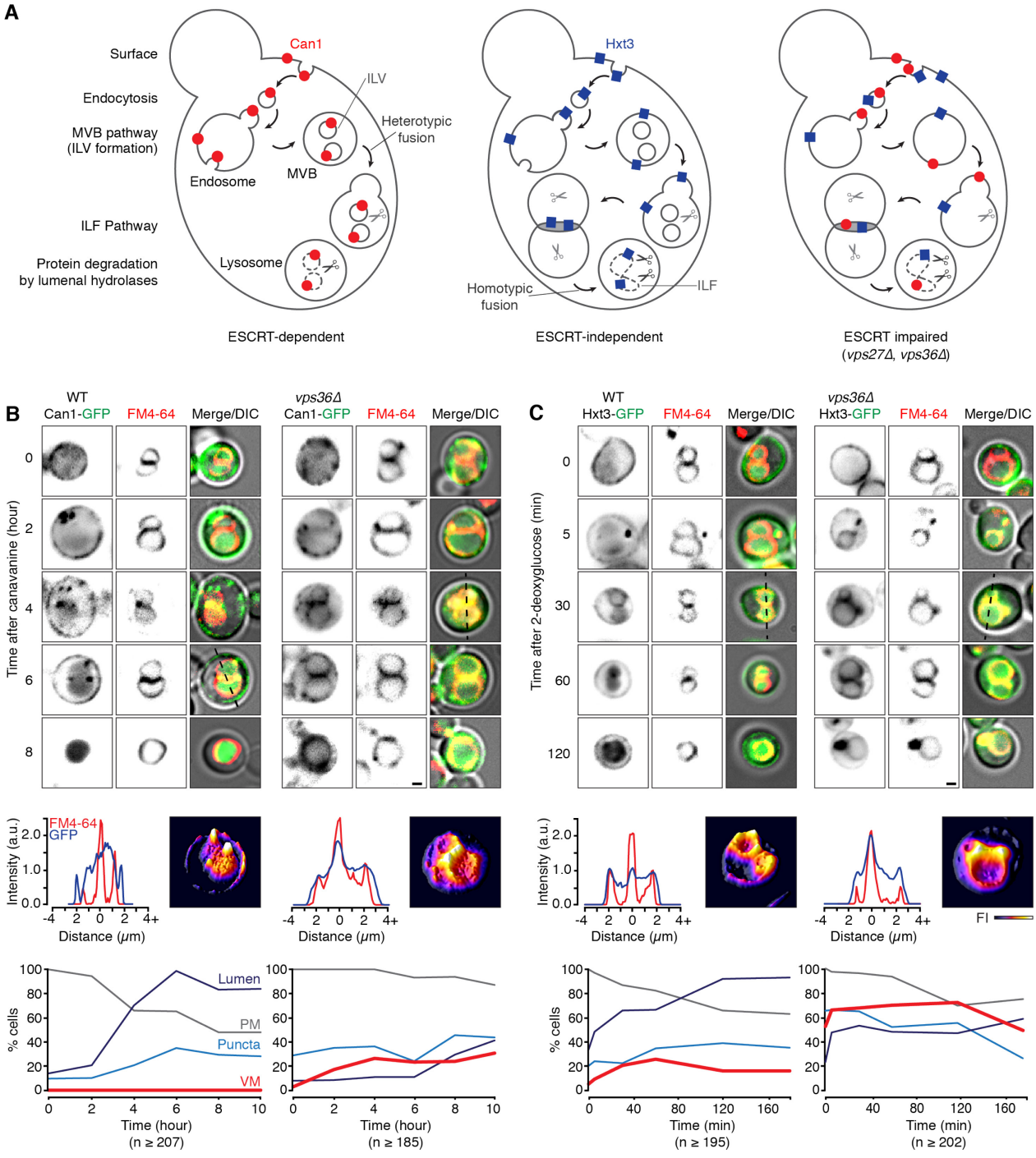
A
Surface
Endocytosis
MVB pathway
(ILV formation)
ILF Pathway
Protein degradation
by lumenal hydrolases
Can1
ILV
Heterotypic
fusion
Endosome
MVB
Lysosome
Hxt3
Homotypic
fusion
ILF
ESCRT-dependent
ESCRT-independent
ESCRT impaired
(vps27Δ, vps36Δ)
B
WT
Can1-GFP
FM4-64
Merge/DIC
vps36Δ
Can1-GFP
FM4-64
Merge/DIC
Time after canavanine (hour)
0
2
4
6
8
FM4-64
GFP
Intensity (a.u.)
Distance (μm)
% cells
Lumen
PM
Puncta
VM
Time (hour)
(n ≥ 207)
Time (hour)
(n ≥ 185)
C
WT
Hxt3-GFP
FM4-64
Merge/DIC
vps36Δ
Hxt3-GFP
FM4-64
Merge/DIC
Time after 2-deoxyglucose (min)
0
5
30
60
120
FI
Time (min)
(n ≥ 195)
Time (min)
(n ≥ 202)

Figure 9. Internalized surface proteins take two routes to the lysosomal lumen for degradation

(A) Cartoon illustrating how surface membrane proteins can be sorted for degradation by the canonical ESCRT-dependent or ILF pathways. Fluorescence and DIC micrographs showing routes taken by Can1-GFP **(B)** or Hxt3-GFP **(C)** from the surface to the lysosome lumen in response to 37 μM canavanine or 200 μM 2-deoxyglucose over time in live wild type or *vps36*Δ cells treated with FM4-64 to label vacuole membranes. Scale bars, 1 μm (*in vivo*). Middle panels include 3-dimensional GFP fluorescence intensity plots (right) and line plots (left) of GFP (blue) or FM4-64 (red) fluorescence intensity for micrographs where lines are indicated. Bottom panels indicate the proportion of the cell population that show GFP fluorescence on the plasma membrane (PM), intracellular puncta (Puncta), vacuolar lysosome membrane (VM) or lysosomal lumen (Lumen) over time after treatment with a toxic substrate.

3.3 Methods and Materials

3.3.1 Yeast strains and materials

All *Saccharomyces cerevisiae* strains used in this study are listed in **Table 3**. Biochemical and yeast growth reagents were purchased from either Sigma-Aldrich, Invitrogen or BioShop Canada Inc. Proteins used include recombinant Gdi1 purified from bacterial cells using a calmodulin-binding peptide intein fusion system (Brett and Merz, 2008) and recombinant Gyp1-46 (the catalytic domain of the Rab-GTPase activating protein Gyp1) purified as previously described (Eitzen et al. 2000). Reagents used in fusion reactions were prepared in 20 mM Pipes-KOH, pH 6.8, and 200 mM sorbitol (Pipes Sorbitol buffer, PS).

3.3.2 Fluorescence Microscopy

Images were acquired with a Nikon Eclipse TiE inverted microscope equipped with a motorized laser TIRF illumination unit, Photometrics Evolve 512 EM-CCD camera, CFI ApoTIRF 1.49 NA 100x objective lens, and 488 nm or 561 nm (50 mW) solid-state lasers operated with Nikon Elements software. Cross sectional images were recorded 1 μm into the sample and resulting micrographs and processed using ImageJ software (National Institutes of Health) and Adobe Photoshop CC. Images shown were adjusted for brightness and contrast, inverted and sharpened with an unsharp masking filter. Fluorescence intensity profiles of GFP fluorescence were generated using ImageJ software.

3.3.3 Live cell microscopy

Live yeast cells were stained with FM4-64 to label vacuole membranes and prepared for imaging using a pulse-chase method as previously described (Brett et al., 2008). For examining vacuolar localization of plasma membrane proteins, cells were incubated at 37 °C for 15 minutes for heat stress (**Figure 10A**) after FM4-64 staining. For other stress treatments yeast cells were incubated at 37°C for 30 minutes (**Figure 11A**) and incubated with 100 μM cycloheximide for 90 minutes at 30 °C (**Figure 12A**). Time-lapse videos were acquired at 30°C using a Chamlide TC-N incubator (Live Cell Instruments) with cells plated on coverslips coated with concavalin-A (1 mg/ml in 50 mM HEPES, pH 7.5, 20 mM calcium acetate, 1 mM $MnSO_4$). Yeast cells expressing Mup1-GFP were back diluted in Synthetic Complete (SC) media lacking methionine (Takara Bio USA, Inc.) for live cell microscopy. To assess surface protein degradation in response to

substrate addition, yeast cells expressing Can1-GFP or Hxt3-GFP wild type and when VPS36 is deleted were stained with FM4-64 for one hour at 30 °C in SC media. After two washes, cells were resuspended in fresh SC media with addition of either 37 μM canavinine (Sigma-Aldrich) for 2, 4, 6 or 8 hours (Can1) or with 500 μM 2-Deoxy-D-glucose (Sigma-Aldrich) for 5, 30, 60 or 120 minutes (Hxt3 and Fet5). After incubation, cells were washed and resuspended in SC media prior to imaging.

3.3.4 Vacuole isolation and homotypic vacuole fusion

Vacuoles were isolated from GFP derivative yeast cells as previously described (Haas, 1995) and fusion reactions were prepared using 6 μg of isolated vacuoles in standard fusion reaction buffer with 0.125 M KCl, 5 mM $MgCl_2$, 1 mM ATP and 10 μM CoA. Vacuolar membranes were stained with FM4-64 by treating vacuoles with 3 μM FM4-64 for 10 minutes at 27 °C. Reactions were incubated at 27 °C for 60 minutes, unless otherwise noted, and placed on ice prior to visualization by microscopy. Where indicated, vacuoles were incubated in the absence or presence of 3.2 μM Gyp1-46 and 4 μM rGdi. For heat stress treatment, vacuoles were pretreated for 5 minutes at 37 °C before addition to the fusion reaction and incubation for 30 minutes at 27°C. Where indicated, vacuoles were pretreated with 100 μM cycloheximide for 15 minutes at 27°C and incubated for an additional 15 minutes with the fusion reaction.

3.3.5 pHluorin-based assay to detect transporter internalization

Ecleptic pHluorin was cytoplasmically tagged to lysosomal membrane proteins (see Prosser et al., 2010). Fusion reactions (15 μl) were prepared using 6 μg of isolated vacuoles in standard reaction buffer, pH 6.80. Reactions were then transferred to black 96-well conical-bottom microtiter plates with 15 μl of titrated reaction buffer for a final buffer pH of 7.40. pHluorin fluorescence (λ_{ex} = 480 nm; λ_{em} = 515 nm) was recorded every two minutes for 90 minutes using a BioTek Synergy H1 plate reading flourometer. Data shown are representative traces with values normalized to time zero, n≥4.

3.3.6 Western blot analysis

Fusion reactions (60 μl) were prepared using 6 μg of isolated vacuoles in standard fusion reaction buffer with 0.125 M KCl, 5 mM $MgCl_2$, 1 mM ATP and 10 μM CoA from yeast strains

expressing GFP-tagged Mup1 or Hxt3 in wild type or when VPS27 or VPS36 is deleted. Where indicated, reactions were pretreated for 5 minutes at 37 °C for heat stress or for 15 minutes with 100 μM cycloheximide at 27 °C in the absence (CTL) or presence of 3.2 μM Gyp1-46 and 4 μM rGdi (GDI) prior to addition to the fusion reaction. Reactions were incubated at 27 °C followed by addition of protease inhibitors (6.7 μM leupeptin, 33 μM pepstatin, 1 mM PMSF and 10.7 mM AEBSF), 1% DDM and 5X laemmli sample buffer. Membrane proteins were solubilized by incubating reactions at 27 °C for 10 minutes prior to running on an SDS-Page gel and probing for α-GFP (Abcam, Cambridge, UK: ab290). Samples were repeated a minimum of three times. Gels were imaged using GE Amersham Imager 600 by chemiluminescence and edited and prepared using Adobe Photoshop and Illustrator CC software.

3.3.7 Data analysis and preparation

Cumulative probability measurements were calculated using isolated vacuole micrographs of docked vacuoles only. GFP fluorescence intensities were measured using ROI 4x4 pixels in diameter and acquiring a fluorescence value on the outer membrane, within the lumen and on the boundary membrane of docked vacuoles using ImageJ software. For assessing GFP fluorescence in the boundary membrane, micrographs taken 60 minutes into the fusion reaction were assessed. For lumenal GFP fluorescence, micrographs were assessed at 0 (ice), 30, 60, 90 and 120 minutes into the fusion reaction and correlated to individual vacuole size (boundary length, surface area and circumference). Data are reported as mean ± SEM. Acquired data was plotted using Synergy KaleidaGraph 4.0 software and figures were prepared using Adobe Illustrator CC software.

Table 3. Yeast strains used in Chapter 3

Strain	Genotype	Source
SEY6210	*MATα*, *leu1-3, 112 ura3-52 his3-200, trp1-901 lys2-801 suc2-D9*	Huh et al., 2003
BY4741	*MATα his3-Δ1 leu2-Δ0 met15-Δ0 ura3-Δ0*	Huh et al., 2003
Fet5-GFP	BY4741, *Fet5-GFP::HIS3MX*	Huh et al., 2003
Mup1-GFP	SEY6210, *Mup1-GFP::KanMX*	Prosser et al., 2011
Mup1-GFP:*vps27Δ*	SEY6210, *Mup1-GFP::KanMX, vps27Δ:HIS3MX*	This study
Mup1-GFP:*vps36Δ*	SEY6210, *Mup1-GFP::KanMX, vps36Δ:HIS3MX*	This study
Mup1-pHluorin	SEY6210, *Mup1-pHluorin::KanMX*	Prosser et al., 2011
Mup1-pHluorin:*vps27Δ*	SEY6210, *Mup1-pHluorin::KanMX, vps27Δ:HIS3MX*	This study
Mup1-pHluorin:*vps36Δ*	SEY6210, *Mup1-pHluorin::KanMX, vps36Δ:HIS3MX*	This study
Ste3-GFP	SEY6210, *Ste3-GFP::KanMX*	Prosser et al., 2011
Ste3-GFP:*vps27Δ*	SEY6210, *Ste3-GFP::KanMX , vps27Δ:HIS3MX*	This study
Can1-GFP	BY4741, *Can1-GFP::HIS3MX*	Huh et al., 2003
Can1-GFP:*vps36Δ*	BY4741, *Can1-GFP::HIS3MX , vps36Δ:KanMX*	This study
Hxt3-GFP	BY4741, *Hxt3-GFP::His3MX*	Huh et al., 2003
Hxt3-GFP:*vps36Δ*	BY4741, *Hxt3-GFP::His3MX, vps36Δ:KanMX*	This study
Hxt3-GFP:*vps27*Δ	BY4741, *Hxt3-GFP::His3MX, vps27Δ:KanMX*	This study
Itr1-GFP	BY4741, *Itr1-GFP::His3MX*	Huh et al., 2003
Itr1-GFP:*vps27*Δ	BY4741, *Itr1-GFP::His3MX, vps27Δ:KanMX*	This study
Aqr1-GFP	BY4741, *Aqr1-GFP::His3MX*	Huh et al., 2003
Aqr1-GFP:*vps27*Δ	BY4741, *Aqr1-GFP::His3MX, vps27Δ:KanMX*	This study

3.4 Results

3.4.1 Internalized surface proteins appear on lysosome membranes en route to the lumen for degradation

To test this hypothesis, we first confirmed that conventional ESCRT client proteins accumulate on vacuolar lysosome membranes when internalized into live cells that are missing components of the ESCRT machinery. To do so, we monitored cellular distribution of GFP-tagged transporters over time in populations of live *S. cerevisiae* cells using fluorescence microscopy and quantified their intracellular distribution (**Figure 9B**). GFP-tagged Can1, an arginine permease, is found on the plasma membrane prior to treatment with canavinine, a toxic arginine analog that triggers internalization and degradation of Can1 to prevent canavinine import and subsequent cell death (MacGurn et al., 2011). After treatment, Can1-GFP first appears on intracellular punctae and then later within the lysosomal lumen, but is never observed on the lysosome membrane. However when VPS36 (a subunit of ESCRT-II; Babst et al., 2002) is deleted, Can1-GFP continues to be internalized after canavanine treatment where it accumulates on large punctae (reminiscent of vps class E compartments; Raymond et al., 1992) as well as on lysosome membranes, and eventually some fluorescence is observed in the lumen. We also found GFP-tagged Hxt3, a low-affinity, high capacity glucose transporter, accumulated on lysosome membranes en route to the lysosomal lumen after being internalized in response to 2-deoxyglucose, a toxic glucose analog (O'Donnell et al., 2015***;*** **Figure 9C**). Importantly, this occurred in wild type cells and knocking out VPS36 did not prevent it from accumulating on lysosome membranes or within the lumen suggesting that Hxt3-GFP is processed for degradation by an ESCRT-independent mechanism. Because these surface polytopic proteins appear on the lysosome membrane after being internalized, we hypothesized that the ILF pathway may deliver them to the lysosome lumen for degradation.

3.4.2 Surface transporters are sorted and packaged for degradation by the ILF pathway

To test this hypothesis, we first studied the lysosome membrane distribution of Hxt3-GFP, which does not seem to require ESCRTs for lysosomal degradation and is present in boundary membranes of docked lysosomes within live cells after treatment with 2-deoxyglucose (**Figures 9C** and **S8**). It is worth noting that the resident lysosomal polytopic protein Fet5-GFP was

excluded from boundaries when cells were treated with 2-deoxyglucose (**Figure S8**), confirming that Hxt3-GFP sorting into the boundary is selective. Treating cells with heat stress to induce protein misfolding also caused Hxt3-GFP to appear in boundary membranes, similar to proteins that are degraded by the ILF pathway (**Figures 10A**; McNally et al., 2017). This discovery was not limited to Hxt3-GFP: we found that GFP-tagged Itr1 (a myo-inositol transporter; Nikko and Pelham, 2009) as well as Aqr1 (a major facilitator superfamily-type transporter that excretes amino acids; Velasco et al., 2004) take a similar route from the surface to the lysosomal lumen when live wild type cells were treated with heat stress (**Figure 10A**). Importantly, knocking out VPS36 did not affect sorting of these proteins into the boundary of docked lysosomes, confirming that they are sorted by an ESCRT-independent mechanism. We also found that Hxt3-GFP within the boundary was internalized during lysosome fusion events within live *vps36*Δ cells (**Figure 10B; Movie S8**), suggesting that ESCRT function is not necessary for protein delivery to the lumen for degradation.

Because the ILF machinery co-purifies with vacuolar lysosomes, we were able to develop cell-free assays to assess protein sorting, internalization and degradation by the ILF pathway (McNally et al., 2017). Thus, to further study how surface proteins may use this mechanism for degradation, we next isolated lysosomes from Hxt3-GFP expressing cells and imaged them 60 minutes after adding ATP to stimulate fusion *in vitro* (**Figure 10C**). Similar to findings made *in vivo*, Hxt3-GFP was sorted into the boundary during organelle fusion *in vitro.* Treating lysosomes with heat stress increased the amount of Hxt3-GFP sorted into the boundary (**Figure 10C** and **D**), suggesting that the machinery necessary to enhance Hxt3 degradation is present on lysosomes. Because the Rab GTPase Ypt7 is important for protein sorting into the ILF pathway (McNally et al., 2017), we next added the Rab inhibitors rGdi1 (a Rab-GTPase chaperone protein) and rGyp1-46 (the catalytic domain of the Rab GTPase activating protein Gyp1; Brett et al., 2008) to fusion reactions and found that Hxt3-GFP was no longer included in boundary membranes (**Figure 10C, 10D** and **S9**). Hxt3-GFP membrane distribution was not affected by deletion of VPS36, suggesting that sorting of Hxt3-GFP into the boundary requires Ypt7 and the fusion protein machinery, not ESCRTs.

To confirm that Hxt3 was internalized into the lumen upon lysosome fusion, we imaged lysosomes over the course of the fusion reaction *in vitro* (**Figure 10E**) and measured the GFP intensity within the lumen (**Figure 10F, 10G** and **S9**). As expected, Hxt3-GFP accumulated

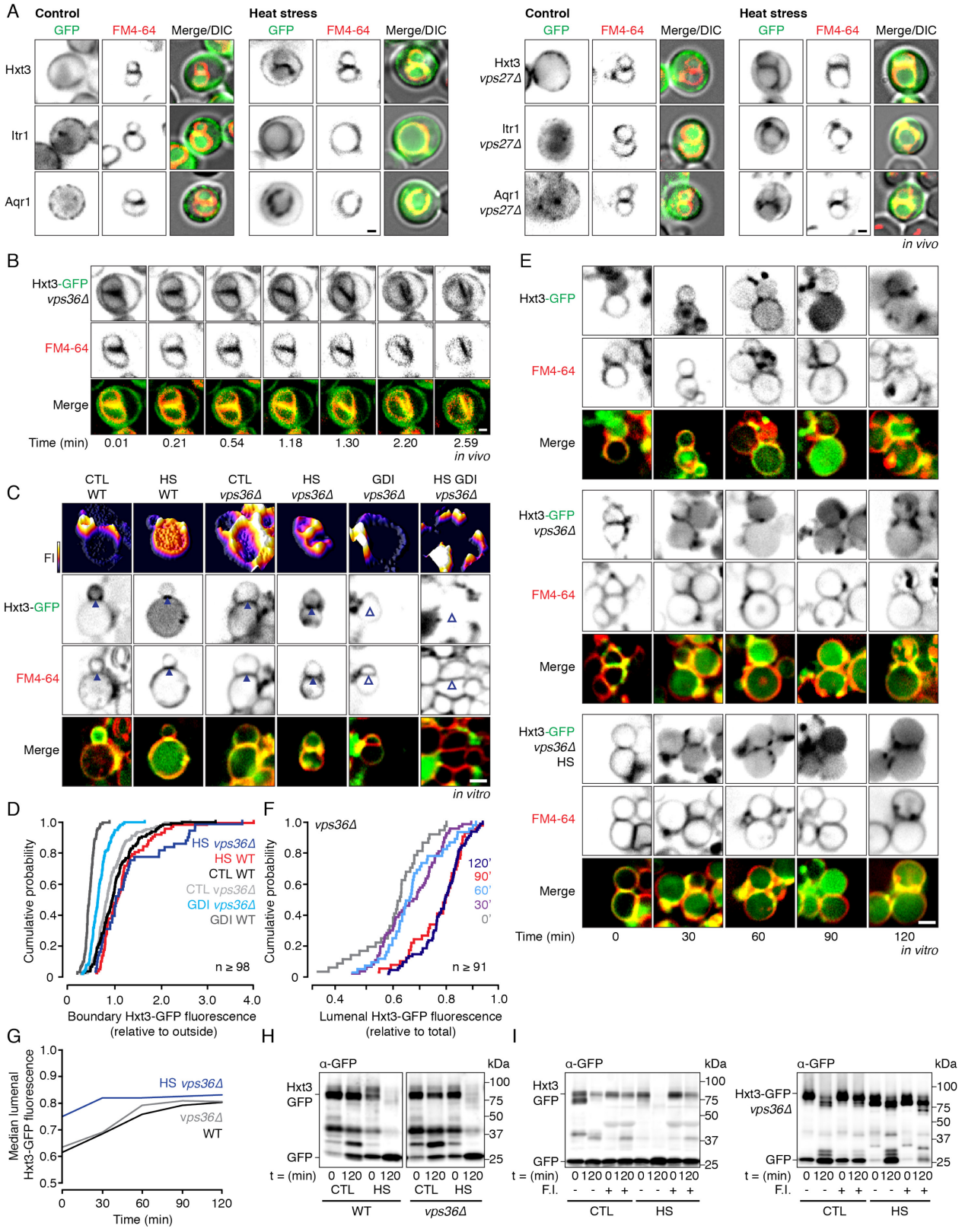
A
Control
Heat stress
GFP
FM4-64
Merge/DIC
Hxt3
Itr1
Aqr1
Hxt3 vps27Δ
Itr1 vps27Δ
Aqr1 vps27Δ
in vivo
B
Hxt3-GFP vps36Δ
FM4-64
Merge
Time (min) 0.01 0.21 0.54 1.18 1.30 2.20 2.59
in vivo
C
CTL WT
HS WT
CTL vps36Δ
HS vps36Δ
GDI vps36Δ
HS GDI vps36Δ
FI
Hxt3-GFP
FM4-64
Merge
in vitro
D
Cumulative probability
HS vps36Δ
HS WT
CTL WT
CTL vps36Δ
GDI vps36Δ
GDI WT
n ≥ 98
Boundary Hxt3-GFP fluorescence (relative to outside)
E
Hxt3-GFP
FM4-64
Merge
Hxt3-GFP vps36Δ
Hxt3-GFP vps36Δ HS
Time (min) 0 30 60 90 120
in vitro
F
vps36Δ
120'
90'
60'
30'
0'
n ≥ 91
Lumenal Hxt3-GFP fluorescence (relative to total)
G
Median lumenal Hxt3-GFP fluorescence
HS vps36Δ
vps36Δ
WT
Time (min)
H
α-GFP
kDa
Hxt3 GFP
GFP
t = (min) 0 120 0 120 0 120 0 120
CTL HS CTL HS
WT
vps36Δ
I
α-GFP
kDa
Hxt3 GFP
GFP
t = (min) 0 120 0 120 0 120 0 120 0 120
F.I. - - + + - - + +
CTL HS
Hxt3-GFP vps36Δ

Figure 10. Some surface proteins are sorted for degradation by the ILF pathway

(A) Fluorescence and DIC micrographs of live wild type (left) or *vps27*Δ (right) cells expressing GFP-tagged Hxt3, Itr1 or Aqr1 before (control) and after heat stress for 15 minutes. **(B)** Images from time-lapse video showing homotypic lysosome fusion within live *vps36*Δ cells expressing Hxt3-GFP. See **movie S8**. **(C)** Fluorescence micrographs of lysosomes isolated from wild type (WT) or *vps36*Δ cells after 30 minutes of fusion in the absence or presence of heat stress (HS) or rGdi1 and rGyp1-46 (GDI). 3-dimensional fluorescence intensity (FI) plots of Hxt3-GFP are shown. Arrowheads indicate Hxt3-GFP enrichment (closed) or exclusion (open) within the boundary membrane. Also see **Figure S9 A**. **(D)** Cumulative probability plot of Hxt3-GFP fluorescence measured at boundaries between lysosomes isolated from wild type (WT) or *vps36*Δ cells after fusion in the presence or absence of heat stress (HS) or fusion inhibitors (rGdi1), as shown in **C**. Also see **Figure S9 B**. **(E)** Fluorescence micrographs of lysosomes isolated from wild type or *vps36*Δ cells expressing Hxt3-GFP acquired over the course of the fusion reaction in the absence or presence of heat stress (HS). **(F)** Cumulative probability plot of Hxt3-GFP fluorescence measured within the lumen of lysosomes isolated from *vps36*Δ cells after 0, 30, 60, 90 or 120 minutes of fusion, as shown in **E**. Also see **Figure S9 C**. **(G)** Median values of lumenal GFP fluorescence observed over time for three conditions studied ($n \geq 105$). **(H and I)** Western blot analysis of Hxt3-GFP degradation before or after lysosomes isolated from wild type (WT) or *vps36*Δ cells underwent fusion for 120 minutes in the absence (CTL) or presence of heat stress (HS; **H**), or after fusion in the presence or absence of the fusion inhibitors (F.I.) rGdi1 and rGyp1-46 (**I**). Cells or isolated organelles were stained with FM4-64 to label vacuolar membranes. Scale bars, 1 μm (*in vivo*) or 2 μm (*in vitro*).

within the lumen over time after lysosome fusion was stimulated with ATP. Heat stress increased the rate and amount of lumenal GFP accumulation over time. Importantly, Hxt3-GFP internalization did not require VPS36, confirming that delivery to the lumen did not require ESCRT function. Once delivered to the lumen of lysosomes, polytopic proteins embedded within ILFs are degraded by acid hydrolases (McNally et al., 2017). To assess proteolysis, we conducted western blot analysis to detect cleavage of GFP from Hxt3-GFP (**Figure 10H**) and found that more GFP was cleaved after lysosome fusion was stimulated *in vitro*. More Hxt3-GFP cleavage was further stimulated when lysosomes were treated with heat stress, consistent with sorting and internalization phenotypes observed. Furthermore, cleavage was unaffected by deleting VPS36 (**Figure 10H**) but was blocked by the fusion inhibitors rGdi1 and rGyp1-46 (**Figure 10I**), confirming that the fusion machinery, not ESCRTs, was responsible for Hxt3-GFP degradation. Together, these findings indicate that in response to substrates or protein misfolding the surface transporter Hxt3-GFP is internalized and delivered to lysosome membranes where it utilizes the ILF pathway, and not ESCRTs, for degradation.

3.4.3 The ILF pathway degrades ESCRT client proteins when MVB formation is impaired

When ESCRT function is disrupted cells survive and surface proteins that are typically sorted and packaged by ESCRTs continue to be degraded although less efficiently (e.g. the manganese transporter Smf1; Jensen et al., 2009). In **Figure 9B** we show that Can1-GFP accumulates on lysosome membranes when VPS36 is deleted, suggesting that the ILF pathway may account for degradation. We confirmed that a similar distribution is observed for other ESCRT client proteins including GFP-tagged Ste3, a G-protein coupled receptor (Shields et al., 2009), and Mup1, a methionine permease (MacDonald et al., 2012; **Figure 11A**). Importantly, all three are present on boundary membranes formed between docked lysosomes within cells missing either VPS36 or VPS27 (a subunit of ESCRT-0; Katzmann et al., 2003*;* **Figure 11A** and **S10**), suggesting that disrupting function of ESCRT–0 or –1 results in the same outcome. As expected, all three surface proteins also accumulate in boundaries upon treatment with heat stress to induce protein misfolding (**Figure 11A**) when components of ESCRTs are deleted. Using Mup1-GFP as an example, we next monitored live *vps27*Δ cells and found that it is present within ILFs that form during organelle fusion (**Figure 11B; Movie S9**), suggesting that Mup1-GFP is sorted and packaged for degradation by the ILF pathway.

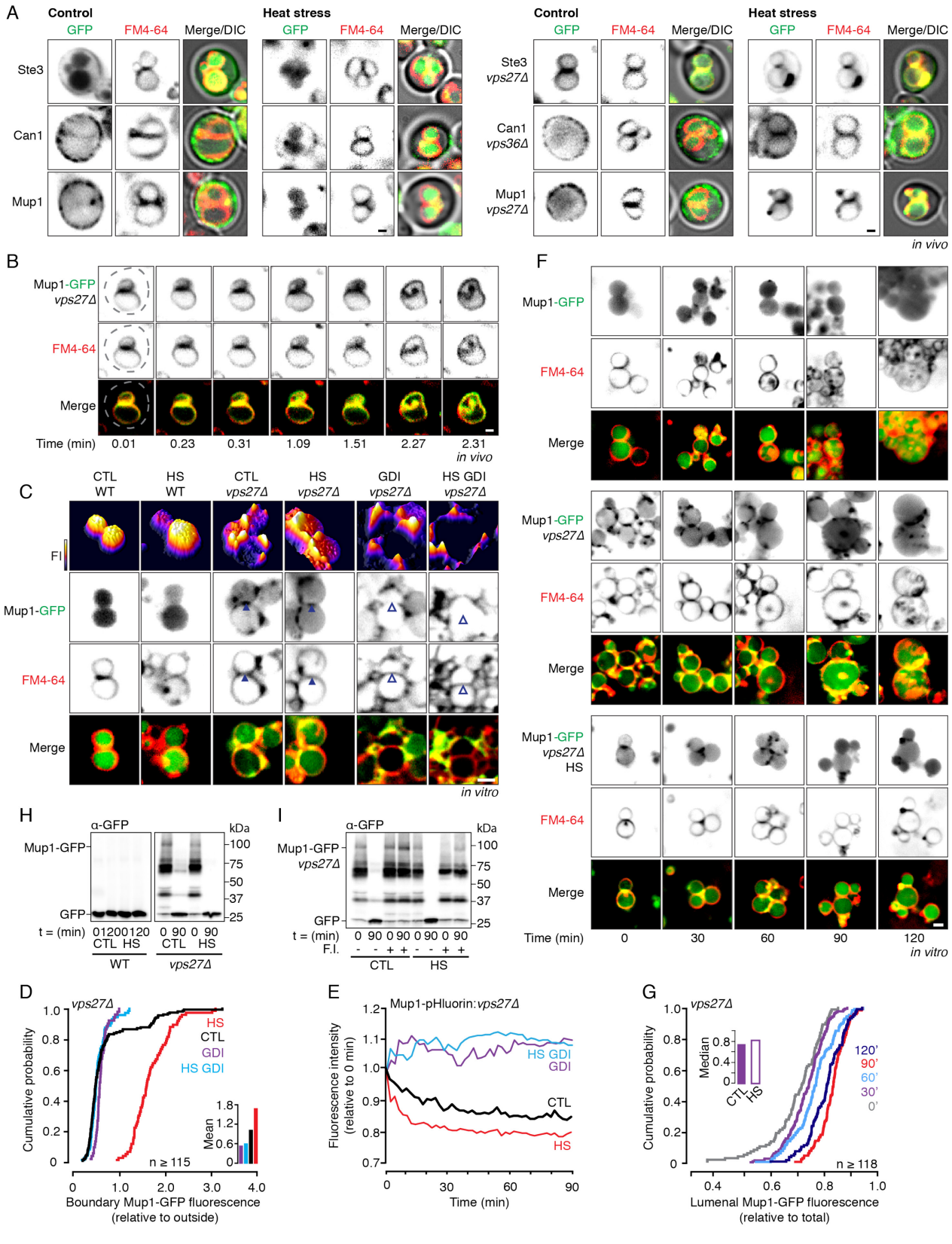
A
Control
Heat stress
GFP
FM4-64
Merge/DIC
Ste3
Can1
Mup1
Ste3 vps27Δ
Can1 vps36Δ
Mup1 vps27Δ
in vivo
B
Mup1-GFP vps27Δ
FM4-64
Merge
Time (min) 0.01 0.23 0.31 1.09 1.51 2.27 2.31
in vivo
C
CTL WT
HS WT
CTL vps27Δ
HS vps27Δ
GDI vps27Δ
HS GDI vps27Δ
FI
Mup1-GFP
FM4-64
Merge
in vitro
F
Mup1-GFP
FM4-64
Merge
Mup1-GFP vps27Δ
Mup1-GFP vps27Δ HS
Time (min) 0 30 60 90 120
in vitro
H
α-GFP
kDa
Mup1-GFP
GFP
100
75
50
37
25
t = (min) 0 1 2 0 1 2 0 0 90 0 90
CTL HS CTL HS
WT
vps27Δ
I
α-GFP
kDa
Mup1-GFP vps27Δ
GFP
t = (min) 0 90 0 90 0 90 0 90
F.I. - - + + - - + +
CTL HS
D
vps27Δ
Cumulative probability
HS
CTL
GDI
HS GDI
Mean
n ≥ 115
Boundary Mup1-GFP fluorescence (relative to outside)
E
Mup1-pHluorin:vps27Δ
Fluorescence intensity (relative to 0 min)
HS GDI
GDI
CTL
HS
Time (min)
G
vps27Δ
Cumulative probability
Median
CTL HS
120'
90'
60'
30'
0'
n ≥ 118
Lumenal Mup1-GFP fluorescence (relative to total)

Figure 11. The ILF pathway compensates for ESCRTs when VPS27 is deleted

(A) Fluorescence and DIC micrographs of live wild type (left) and *vps27*Δ or *vps36*Δ (right) cells expressing GFP-tagged Ste3, Can1 or Mup1 before (control) and after heat stress for 30 minutes. Also see **Figure S10 A**. **(B)** Images from time-lapse video showing homotypic lysosome fusion within live *vps27*Δ cells expressing Mup1-GFP. See **movie S9**. **(C)** Fluorescence micrographs of lysosomes isolated from wild type (WT) or *vps27*Δ cells after 30 minutes of fusion in the absence or presence of heat stress (HS) or rGdi1 and rGyp1-46 (GDI). 3-dimensional fluorescence intensity (FI) plots of Mup1-GFP are shown. Arrowheads indicate Mup1-GFP enrichment (closed) or exclusion (open) within the boundary membrane. **(D)** Cumulative probability plot of Mup1-GFP fluorescence measured at boundaries between lysosomes isolated from *vps27*Δ cells after 30 minutes of fusion in the absence (CTL) or presence of heat stress (HS) or fusion inhibitors (GDI), as shown in (C), Inset shows mean values ($n \geq 115$). **(E)** Fluorescence of lysosomes isolated from *vps27*Δ cells expressing Mup1-pHluorin during the *in vitro* fusion reaction under control conditions (CTL) or after heat stress (HS) in presence or absence of rGdi1 and rGyp1-46 (GDI). Also see **Figure S10 B**. **(F)** Fluorescence micrographs of lysosomes isolated from wild type or *vps27*Δ cells expressing Mup1-GFP acquired over the course of the fusion reaction in the absence or presence of heat stress (HS). **(G)** Cumulative probability plot of Mup1-GFP fluorescence measured within the lumen of lysosomes isolated from *vps27*Δ cells after 0, 30, 60, 90 or 120 minutes of fusion, as shown in **(F)**. Inset shows median values at 30 minutes for lysosomes from *vps27*Δ cells in the presence or absence of heat stress ($n \geq 118$). Also see **Figure S10 C. (H and I)** Western blot analysis of Hxt3-GFP degradation before or after lysosomes isolated from wild type (WT) or *vps36*Δ cells underwent fusion for 120 minutes in the absence (CTL) or presence of heat stress (HS; **H**), or after fusion in the presence or absence of the fusion inhibitors (F.I.) rGdi1 and rGyp1-46 (**I**). Cells or isolated organelles were stained with FM4-64 to label vacuolar membranes. Scale bars, 1 μm (*in vivo*) or 2 μm (*in vitro*).

We confirmed this finding by isolating lysosomes from Mup1-GFP expressing cells and studying its membrane distribution during homotypic fusion *in vitro* (**Figure 11C**). Again, Mup1-GFP only appears on lysosomal membranes when VPS27 is deleted, where it is present in boundary membranes of docked lysosomes. Inducing protein misfolding with heat stress promotes sorting of Mup1-GFP into the boundary (**Figure 11C** and **D**), confirming that isolated lysosomes possess the molecular machinery required to process Mup1-GFP for degradation. Furthermore, addition of the Ypt7 inhibitors rGdi1 and rGyp1-46 prevents Mup1-GFP entry into the boundary, confirming that this process is dependent on the fusion machinery and not ESCRT function.

We next demonstrated that Mup1 was internalized into the lumen by tagging its cytoplasmic C-terminus with pHluorin, a pH-sensitive variant of GFP, and monitoring fluorescence over the course of the fusion reaction *in vitro* (**Figure 11E**). As expected, in the absence of VPS27, Mup1-pHluorin fluorescence decreases over the course of the fusion reaction, indicative of exposure to the acid lumen of the lysosome, in the presence or absence of heat stress. No change in Mup1-pHuorin was observed when lysosomes isolated from wild type cells were studied (**Figure S10**), as Mup1-GFP is exclusively found in the lumen (see **Figure 11C**). Addition of Ypt7 inhibitors prevented internalization (**Figure 11E**) confirming that the fusion machinery was required for Mup1-pHluorin internalization. To confirm this result, we imaged isolated lysosomes at different time points over the course of the fusion reaction in vitro (**Figure 11F**) and measured GFP intensity within the lumen (**Figures 11G and S10**). As Mup1-GFP is exclusively found within the lumen of lysosomes isolated from wild type cells, lumenal GFP intensity does not change over time. However, in the absence of VPS27, Mup1-GFP is initially present on lysosome membranes and accumulates within the lumen over time. Heat stress increases lumenal Mup1-GFP, consistent with an increase of Mup1-GFP observed in the boundary (**Figure 11D**) and increased Mup1-pHluorin internalization upon organelle fusion (**Figure 11E**) in the ESCRT deficient background.

Once inside the lumen, Mup1-GFP should be degraded by acid hydrolases. To confirm, we conducted western blot analysis to detect cleavage of GFP from Mup1 before or 120 minutes after the homotypic lysosome fusion was stimulated with ATP *in vitro* (**Figure 11H**). Organelles isolated from wild type cells only contained cleaved GFP, confirming that Mup1-GFP was being sent to lysosomes for degradation prior to isolation. However, intact Mup1-GFP is detected on

lysosome preparations from *vps27*Δ cells and is cleaved after fusion is stimulated. As predicted, treating lysosomes isolated from *vps27*Δ cells with heat stress increases GFP cleavage (**Figure 11H**) and the fusion inhibitors rGdi1 and rGyp1-46 blocks GFP cleavage (**Figure 11I**), consistent with effects on Mup1-GFP sorting and internalization (**Figure 11C–G**). Together these findings indicate that when ESCRT function is impaired, internalized surface polytopic proteins that are typically degraded by the ESCRT pathway are instead shunted to lysosome membranes where they are sorted and packaged for degradation by the ILF pathway.

3.4.4 The ILF pathway degrades surface proteins in response to TOR signaling

Thus far we have shown that the ILF pathway degrades internalized surface transporters and receptors in response to toxic substrates for cell survival, or in response to protein misfolding for cellular quality control. Another important stimulus of protein degradation is TOR signaling (Laplante and Sabatini, 2012): TOR kinase is thought to be activated by high cytoplasmic amino acid levels or ribosome inactivity to promote degradation of soluble cytosolic proteins by the proteasome (Rousseau and Bertolotti, 2016), surface polytopic proteins by ESCRTs (MacGurn et al., 2011) and lysosomal polytopic proteins by the ILF pathway (McNally et al., 2017), which in turn raises free amino acid levels and closes a negative feedback loop (Settembre et al., 2013). Given the newfound role of the ILF pathway in surface polytopic protein degradation, we next sought to determine if this process also responds to TOR using cycloheximide (CHX) to trigger TOR signaling (see MacGurn et al., 2011; McNally et al., 2017). As predicted, we found that surface Hxt3-GFP was internalized and appeared on membranes and in the lumen of lysosomes in live cells in response to CHX, in the presence or absence of VPS36 (**Figure 12A**), suggesting that CHX-mediated down-regulation of Hxt3-GFP does not require ESCRTs. Similar observations were made for Mup1-GFP in cells lacking VPS27 (**Figure 12A**) as well as other ESCRT client proteins (**Figure S11**), suggesting that CHX triggers degradation of these surface proteins by the ILF pathway when ESCRT function is impaired. To confirm these observations, we recorded lysosome fusion events within live *vps27*Δ or wild type cells and observed boundary-localized Mup1-GFP or Hxt3-GFP, respectively, being internalized into the lumen upon fusion (**Figure 12B; movies S10** and **S11**). Together, these results suggest that TOR signaling also induces surface protein degradation by the ILF pathway.

We next confirmed these findings in vitro using cell-free assays to further validate our hypothesis (**Figures 12C** and **S11**). We find that in the absence of VPS27, Mup1-GFP is enriched in boundary membranes upon treatment with CHX in vitro (**Figure 12D**), confirming that the TOR machinery that responds to CHX co-purifies with isolated lysosomes (McNally et al., 2017). We made similar findings for Hxt3-GFP in the absence or presence of VPS36 (**Figure 12D**), confirming that ESCRT function was not important for Hxt3-GFP sorting in response to CHX. By measuring the lumenal GFP fluorescence intensity, we found that CHX caused more Hxt3-GFP and Mup1-GFP to accumulate inside lysosomes after membrane fusion was stimulated for 60 minutes in vitro (**Figure 12E**). We verified this finding by monitoring Mup1-pHluorin fluorescence over the course of the lysosome fusion reaction in vitro (**Figure 12F**), confirming that CHX stimulated protein internalization during fusion. We next confirmed that CHX also triggered more Hxt3-GFP and Mup1-GFP protein degradation by examining GFP cleavage by Western blot analysis (**Figure 12G**). Importantly, the lysosome membrane fusion inhibitors rGdi1 and rGyp1-46 blocked Hxt3-GFP and Mup1-GFP protein sorting (**Figure 12C** and **D**), internalization (**Figure 12E** and **F**) and degradation (**Figure 12G**). Furthermore, these events occurred in the absence of key components of the ESCRT machinery (VPS27 or VPS36; **Figures 12C–G** and **S11**). Thus, we conclude that the ILF pathway is responsible for degradation of some surface proteins (e.g. Hxt3-GFP) and degrades others (Mup1-GFP) to compensate for ESCRT impairment in response to TOR activation by CHX.

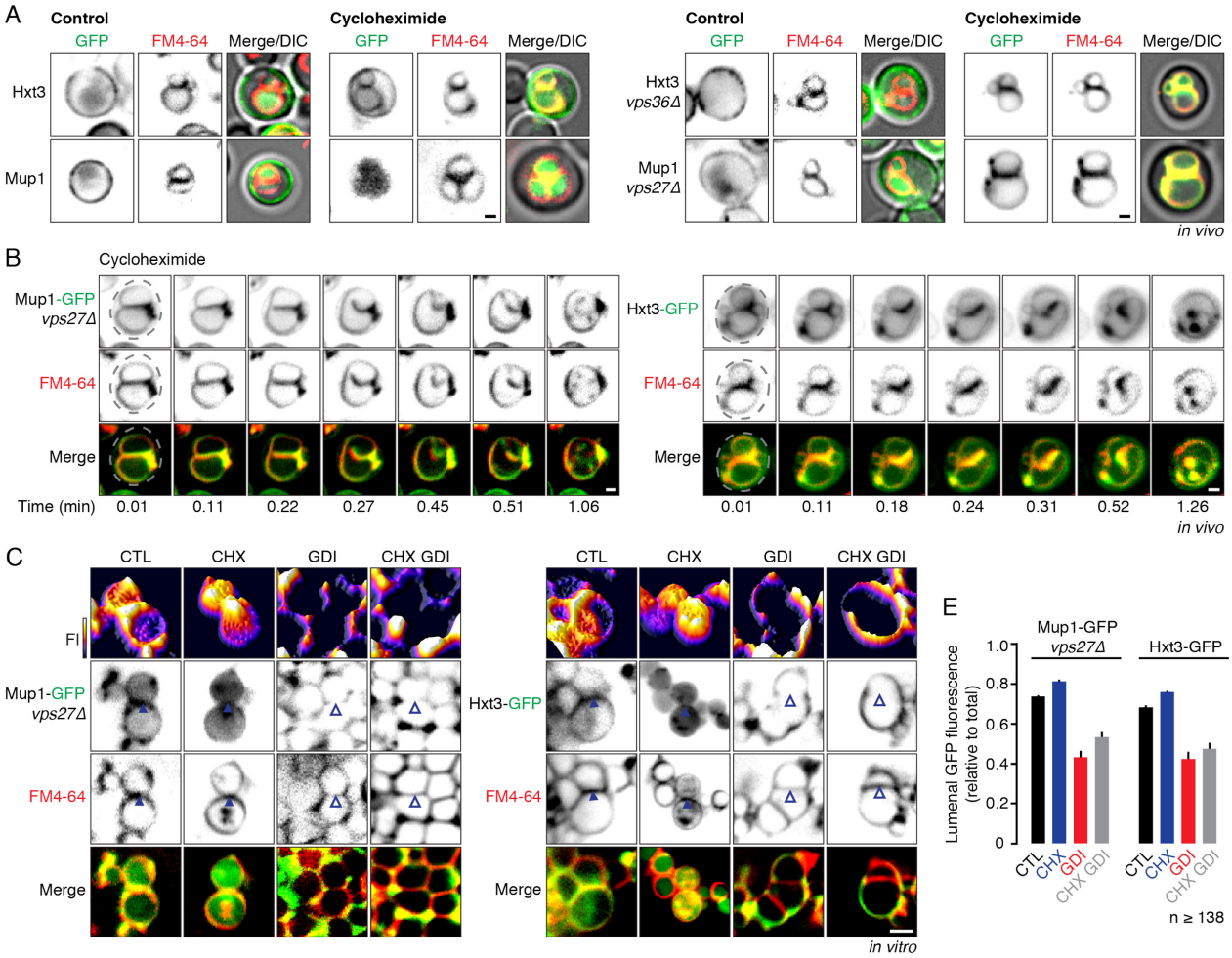
A
Control
Cycloheximide
GFP
FM4-64
Merge/DIC
Hxt3
Mup1
Hxt3 vps36Δ
Mup1 vps27Δ
in vivo
B
Cycloheximide
Mup1-GFP vps27Δ
Hxt3-GFP
FM4-64
Merge
Time (min)
0.01 0.11 0.22 0.27 0.45 0.51 1.06
0.01 0.11 0.18 0.24 0.31 0.52 1.26
in vivo
C
CTL CHX GDI CHX GDI
FI
Mup1-GFP vps27Δ
Hxt3-GFP
FM4-64
Merge
in vitro
E
Mup1-GFP vps27Δ
Hxt3-GFP
Lumenal GFP fluorescence (relative to total)
CTL CHX GDI CHX GDI
n ≥ 138
D
vps27Δ
CHX
CTL
CHX GDI
GDI
Cumulative probability
Mean
n ≥ 110
Boundary Mup1-GFP fluorescence (relative to outside)
CHX vps36Δ
CHX WT
CTL WT
CTL vps36Δ
CHX GDI vps36Δ
CHX GDI WT
Boundary Hxt3-GFP fluorescence (relative to outside)
F
Mup1-pHluorin:vps27Δ
CHX GDI
GDI
CTL
CHX
Fluorescence intensity (relative to 0 min)
Time (min)
G
α-GFP
kDa
Hxt3-GFP
Hxt3-GFP vps36Δ
Mup1-GFP
Mup1-GFP vps27Δ
GFP
t = (min) 0 120 0120 0120
F.I. - - - - + +
CTL CHX
WT vps27Δ

Figure 12. The ILF pathway degrades surface proteins in response to TOR activation

(A) Fluorescence and DIC micrographs of live wild type (left) or ESCRT impaired (*vps27*Δ or vps36Δ; right) cells expressing GFP-tagged Hxt3 or Mup1 before (control) and after treatment with 100 μM cycloheximide (CHX) for 30 minutes. Also see **Figure S11 A**. **(B)** Images from time-lapse video showing homotypic lysosome fusion within live *vps27*Δ cells expressing Mup1-GFP (see **movie S10**) or wild type cells expressing Hxt3-GFP (see **movie S11**) after CHX treatment. **(C)** Fluorescence micrographs of lysosomes isolated from cells expressing Mup1-GFP in wild type or *vps27*Δ background or from cells expressing Hxt3-GFP after 30 minutes of fusion in the absence or presence of CHX or rGdi1 and rGyp1-46 (GDI). 3-dimensional fluorescence intensity (FI) plots of Mup1-GFP or Hxt3-GFP are shown. Arrowheads indicate GFP enrichment (closed) or exclusion (open) within the boundary membrane. Also see **Figure S11 B** and **C**. **(D)** Cumulative probability plots of GFP fluorescence measured at boundaries between docked lysosomes isolated from yeast cells expressing Mup1-GFP or Hxt3-GFP in wild type or ESCRT deficient cells (*vps27*Δ or *vps36*Δ) after fusion in the presence or absence of CHX or fusion inhibitors (GDI), as shown in (**C**; $n \geq 110$). **(E)** Mean lumenal GFP fluorescence from micrographs as shown in **C.** Mean ± SEM. **(F)** Fluorescence of lysosomes isolated from *vps27*Δ cells expressing Mup1-pHluorin during the *in vitro* fusion reaction under control conditions (CTL) or after cycloheximide treatment (CHX) in presence or absence of rGdi1 and rGyp1-46 (GDI). Also see **Figure S11 D**. **(G)** Western blot analysis of Mup1-GFP or Hxt3-GFP degradation before or after lysosomes isolated from wild type (WT) or ESCRT impaired (*vps27*Δ or *vps36*Δ) cells underwent fusion for 120 minutes in the absence (CTL) or presence of CHX, or after fusion in the presence or absence of the fusion inhibitors (F.I.) rGdi1 and rGyp1-46. Cells or isolated organelles were stained with FM4-64 to label vacuolar membranes. Scale bars, 1 μm (*in vivo*) or 2 μm (*in vitro*).

3.5 Discussion

3.5.1 The ILF pathway degrades surface proteins without ESCRTs

Here we demonstrate that some internalized surface polytopic proteins are delivered to the vacuolar lysosome membrane where they are sorted into ILFs for degradation upon organelle fusion independent of ESCRT function (**Figures 9C, 10** and **12**). Previous reports of surface protein degradation often only include micrographs indicating the surface distribution of a protein before internalization, and its presence in the lumen of lysosomes afterwards (e.g. Berkower et al., 1994; Egner et al., 1995; Shields et al., 2009; Keener and Babst, 2013; Zhao et al., 2013; Ghaddar et al., 2014; O'Donnell et al., 2015); and many important papers originally describing degradation of surface receptors or transporters do not include any micrographs (e.g. Hicke and Reizman, 1996). Because the outcomes of both ESCRT and ILF pathways are equal, evidence showing the intracellular route of luminal delivery now seems important. For the ESCRT pathway, this requires imaging fixed and stained samples by electron microscopy to visualize proteins on small ILVs within endosomes (Haigler et al., 1979; Futter et al., 1996; Klumperman and Raposo, 2014) as current methods of light microscopy cannot distinguish whether proteins are present on ILVs or limiting membranes of endosomes. However for the ILF pathway, here we show surface transporters being delivered to the lumen during homotypic lysosome fusion in real time within live cells using HILO microscopy (e.g. **Figures 10B** and **12B, movies S9** and **S11**). These include sugar transporter Hxt3, as well as the peptide transporter Aqr1 and myo-inositol transporter Itr1, but re-examination of micrographs in previous reports reveal the presence of other internalized surface transporters on lysosome membranes as well (e.g. Tat2; Beck et al., 1999), suggesting that ILF-dependent degradation of surface proteins may be widespread in *S. cerevisiae*. These transporters and the underlying fusion machinery responsible for the ILF pathway (Nickerson et al., 2009; Spang, 2016) are evolutionarily conserved, suggesting that a similar process may regulate surface glucose (Hxt/GLUT gene family) or myo-inositol (Itr/HMIT) transporters levels important for cellular metabolism or nutrient (re-) absorption in human epithelial cells within the ileum or kidney for example (Smith et al., 2013; Chen et al., 2015; Schneider, 2015). Given that the mechanism of degradation has been elucidated for only a handful of an estimated ~5,500 polytopic proteins encoded by the human genome (Fagerberg et al., 2010), we speculate that the ILF pathway could be equally important as the ESCRT pathway for determining surface protein lifetimes and thus may underlie diverse physiology.

We also show that the ILF pathway sorts and packages internalized surface proteins that are typically processed for degradation by ESCRTs when MVB formation is impaired (**Figures 9B, 11** and **12**). Unlike protein sorting into the ESCRT pathway, we were able to visualize their internalization by the ILF pathway in real time within live cells (**Figures 11B and 12B; movies S9** and **S10**). These include the ESCRT client proteins Mup1, Ste3 and Can1 that have been extensively used to characterize this pathway in *S. cerevisiae* (e.g. Lin et al., 2008). This may not be limited to internalized surface proteins, as biosynthetic cargo such as lysosomal acid hydrolases (e.g. the carboxypeptidase Cps1 and polyphosphatase Phm5) also utilize the MVB pathway for delivery to the lysosomal lumen, and deleting components of ESCRTs redistributes it on the lysosome membrane (a classic phenotype used to discover and characterize the ESCRT pathway; e.g. McNatt et al., 2007). We speculate that compensation by the ILF pathway may mediate residual surface protein degradation previously observed when ESCRTs are impaired (Jensen et al., 2009), thus permitting cell survival when the primary process for sorting and packaging membrane proteins for degradation is dysfunctional. Loss-of-function mutations in human orthologs of ESCRT components are linked to cancers and neurodegenerative disorders for example and etiology is thought to involve improper cargo degradation (Saksena and Emr, 2009; Stuffers et al., 2009a; Alfred and Viccari, 2016). Thus, assuming the ILF pathway also functions in human cells, it is tempting to speculate that up-regulating the ILF pathway by increasing lysosome numbers and activity through TFEB (Transcription Factor EB) signaling for example (Ferguson, 2015; Napolitano and Ballabio, 2016), may offer a therapeutic strategy to treat ESCRT-related diseases.

3.5.2 Coordination of cellular protein degradation pathways for survival and physiology

What determines whether a surface protein uses the ESCRT or ILF pathways for degradation? Here we show that protein sorting into the ILF pathway is triggered by the same stimuli that mediate entry into the ESCRT pathway: changes in substrate levels (e.g. Nikko and Pelham, 2009*;* **Figure 9**), protein misfolding by heat stress (Keener and Babst, 2013*;* **Figures 10 and 11**), or TOR signaling (MacGurn et al., 2011; Jones et al., 2012*;* **Figure 12**). In the ESCRT pathway, this is mediated by cargo protein recognition by adapter proteins (e.g. arrestins; Lin et al., 2008; Nikko and Pelham, 2009) and ubiquitylation by E3-ligases (e.g. Rsp5; MacDonald et al., 2012) at surface or endosomal membranes. Although the mechanism responsible for protein

sorting by the ILF pathway has not been elucidated, we have preliminary evidence suggesting that adapter proteins and E3-ligases are required for protein sorting into the ILF pathway (*data not shown*), suggesting that both pathways recognize ubiquitylated proteins, which my explain why the ILF pathway can degrade proteins that are typically substrates for the ESCRT pathway. Furthermore, the same labeling machinery is present at the plasma membrane, endosomes and lysosomal membranes (e.g. Li et al., 2015a; Li et al., 2015b), suggesting that proteins are ubiquitylated in a similar manner at these sites and thus different patterns of protein ubiquitylation are unlikely. The presence of similar labeling machinery on the plasma and lysosome membranes may also explain why more Mup1-GFP is sorted into the ILF pathway and degraded when isolated lysosomes are treated with CHX or heat stress in vitro (**Figures 11** and **12**).

The underlying mechanism may also be ubiquitin-independent. This is because ubiquitylation is not required for sorting of all protein cargoes into the ESCRT pathway: some proteins bind to chaperones such as Sna3 to mediate degradation (Reggiori and Pelham, 2001; McNatt et al., 2007; MacDonald et al., 2012). Sna3 has a paralog called Sna4 that is exclusively found on lysosome membranes (Pokyrzwa et al., 2009) and is sorted into the ILF pathway (McNally et al., 2017). Thus, we hypothesize that perhaps chaperone binding specificity may determine which pathway is used by surface polytopic proteins for degradation. For example, Hxt3 may preferentially interact with Sna4 instead of Sna3. If so, internalized Hxt3 avoids Sna3-mediated incorporation into ILVs by ESCRTs at the endosome and remains on the limiting membrane. Upon MVB-lysosome fusion, Hxt3 is delivered to lysosome membranes where it can encounter Sna4 and be degraded by the ILF pathway. We are currently testing this hypothesis and anticipated results will help reveal unique and shared mechanisms that underlie these different cellular protein degradation pathways, giving us a better understanding of how they orchestrate global changes in protein turn over that occur during cell differentiation, the cell cycle or cellular aging for example.

3.5.3 The ILF pathway as an alternative for other ESCRT-related cellular physiology

Could the ILF pathway also be responsible for ESCRT-independent ILV formation? Like ESCRTs, the ILF machinery selectively sorts and packages proteins into what are essentially large intralumenal vesicles. Thus, we speculate that homotypic fusion likely contributes to

generating intralumenal vesicles observed within lysosomes that are needed for proper lipid catabolism (Kallunki et al., 2013). However, the underlying machinery is also responsible for heterotypic lysosome membrane fusion events between autophagosomes (Jiang et al., 2014) and MVBs (Luzio et al., 2009; Epp et al., 2011). Moreover, paralogous machinery underlies endosome membrane fusion required for earlier trafficking events during endocytosis (Balderhaar and Ungermann, 2013; Spang, 2016; Chou et al., 2016*)*. Thus we speculate that ILF formation during organelle fusion may occur at other sites in the cell, including during homo- or heterotypic endosome fusion, which may account for ILVs within endosomes observed when ESCRTs are depleted (Trajkovic et al., 2008; Blanc et al., 2009; Stuffers et al., 2009b; Edgar et al., 2014) or for observed ILVs that are much larger than those derived by ESCRTs (e.g. Fairn et al., 2011). Although incredibly speculative, this ESCRT-independent mechanism may also account for exosome formation when lysosomes or lysosome-related organelles containing ILVs fuse with the plasma membrane (Reddy et al., 2001; Jaiswal et al., 2002; Blott and Griffiths, 2002). New methods of super-resolution fluorescence microscopy or electron microscopy are necessary to test this hypothesis as these organelles, ILVs and exosomes are expected to be smaller (e.g. 25-50 nm in diameter; see Palay and Palade, 1955; Hanson and Cashikar, 2012; Edgar et al., 2014) than those observed during homotypic vacuolar lysosome fusion (up to 1 μm in diameter based on boundary membrane lengths observed; Mattie et al., 2017; McNally et al., 2017). If true, these findings will confirm that the ILF pathway is as important as the ESCRT pathway for cellular physiology.

Chapter 4. ILF and vReD pathways both control individual lysosomal transporter protein lifetimes

4.1 Abstract

Lysosomal nutrient transporter proteins move lumenal products of biomaterial catabolism to the cytoplasm for reuse by the cell. Two mechanisms control their lifetimes: the ILF (IntraLumenal Fragment) and vReD (Vacuole REcycling and Degradation) pathways. But it is not clear if they function independently. Using *S. cerevisiae* as a model, here we show that the ILF pathway mediates constitutive turnover of the lysine transporter Ypq1 and zinc transporter Cot1 – known vReD client proteins – *in vivo* and *in vitro*. In contrast, the vReD pathway mediates constitutive degradation of the amino acid transporter Vba4. Activation of TOR with cycloheximide enhances their degradation by these pathways. However, misfolding by heat stress shunts all three into the ILF pathway. Thus, both pathways control individual transporter lifetimes, although only the ILF pathway mediates protein quality control. The pathway chosen depends on protein fate: degradation is imminent by the ILF pathway, whereas the vReD pathway permits reuse.

4.2 Introduction

Lysosomes are tasked with recycling biomaterials within all eukaryotic cells (Perera and Zoncu, 2016). In addition to being an important source of cellular nutrients, their activity is required to clear toxic aggregates or damaged proteins and organelles to prevent cell death. To function, lysosomes must perform three fundamental functions (de Duve and Wattiaux, 1966; Luzio et al., 2007): first they must fuse with membrane-encapsulated compartments containing biomaterials, which exposes them to lumenal acid hydrolases for catabolism–the second essential function of lysosomes. Finally, the products of degradation (lipids, sugars, amino acids, and other nutrients) are translocated across the lysosomal membrane by nutrient transporter proteins to the cytoplasm where they are re-used by the cell. In addition to acting as important stores for nutrients, lysosomes also store metals and other ions, and controlled release (or uptake) by lysosomal transporter proteins is critical for metabolism, signaling and programmed cell death (Kroemer and Jäättelä, 2005; Xu and Ren, 2015; Lim and Zoncu, 2016). Thus, lysosomal

transporter proteins expression and activity is critical for lysosome function, yet we know little about their lifetimes or how they are regulated.

Recently two mechanisms have been discovered that control polytopic protein lifetimes on the vacuolar lysosome (or vacuole) in the model organism *Saccharomyces cerevisiae*: The first, termed the vReD (Vacuole membrane REcycling and Degradation) pathway, is essentially a mechanism to feed vacuolar polytopic proteins to the canonical MultiVesicular Body (MVB) pathway, which is responsible for surface transporter and receptor protein down-regulation (Davies et al., 2009*;* **Figure 13A**): In response to changes in substrate levels, the vacuolar amino acid transporter Ypq1 (Li et al., 2015a) or zinc transporter Cot1 (Li et al., 2015a) are ubiquitylated and sorted into areas of the vacuole membrane that form vesicles, which then supposedly fuse with endosomal compartments. Here they are thought to encounter ESCRTs (Endosomal Sorting Complexes Required for Transport) that sort and package them into intralumenal vesicle (ILVs) forming a MVB, which when mature fuses with the vacuole to expose protein-laden ILVs to lumenal acid hydrolases for catabolism. Although the evidence presented confirms the existence of the vReD pathway, widespread use by vacuolar polytopic proteins has not been confirmed and its contributions to vacuole membrane homeostasis or remodeling remain elusive.

The second, termed the IntraLumenal Fragment (ILF) pathway, is an ESCRT-independent mechanism that relies on vacuole membrane fusion machinery for protein sorting and internalization (McNally et al., 2017; **Figure 13A**): In response to substrates, protein misfolding or TOR-signaling, vacuolar polytopic proteins such as the V-ATPase (Vph1), metal transporters (Fth1, Fet5), ABC transporters (Ybt1, Ycf1) and the lipid transporter Ncr1 are selectively sorted into an area of membrane, called the boundary, encircled by the fusion machinery that assembles into a ring at contact sites between apposing organelles prior to homotypic fusion. Upon lipid bilayer scission at the ring, the boundary membranes merge and are internalized within the lumen of single organelle as a protein-laden ILF that is catabolized by hydrolases. The ILF pathway is thus intrinsic to organelle membrane fusion, utilizing the fusion protein machinery – including the Rab GTPase Ypt7, the HOmotypic fusion and Protein Sorting (HOPS) tethering complex and soluble NSF attachment protein receptor (SNARE) proteins – for efficient cargo protein degradation. While this pathway has been shown to be crucial for remodeling the vacuolar membrane proteome, protein sorting and degradation by this pathway remains relatively elusive.

Although these pathways seem mutually exclusive, the outcome is equal: To topologically accommodate degradation by lumenal hydrolases, vacuolar membrane proteins are either sorted and packaged into ILVs by ESCRTs at endosomes for the vReD pathway, or into ILFs – which are essentially large ILVs – by the fusion machinery on vacuoles for the ILF pathway (**Figure 13A**). But it is unclear why lysosomal membrane proteins take different routes. Furthermore, Emr and colleagues reported that they were unable to visualize entry of some ILF client proteins into the vReD pathway (e.g. Vph1, Fth1; Li et al., 2015a), suggesting that protein degradation by these pathways is mutually exclusive and possibly dependent on protein identity. However, we found that the ZnT family zinc transporter and vReD client protein Cot1 is also degraded by the ILF pathway (Li et al., 2015b; McNally et al. 2017). This preliminary work raises many important questions that must be answered to comprehensively understand vacuole transporter regulation and its contribution to cell biology: Can both pathways degrade the same client proteins? What determines which degradation pathway is selected? Does each contribute to vacuole membrane homeostasis or protein quality control? Does each mediate vacuolar lysosome membrane remodeling in response to signaling responsible for cellular metabolism or aging?

4.3 Methods and Materials

4.3.1 Yeast strains and reagents

All *Saccharomyces cerevisiae* strains used in this study are listed in **Table 4**. Biochemical and yeast growth reagents were purchased from either Sigma-Aldrich, Invitrogen or BioShop Canada Inc. Proteins used include recombinant Gdi1 purified from bacterial cells using a calmodulin-binding peptide intein fusion system (Brett and Merz, 2008) and recombinant Gyp1-46 (the catalytic domain of the Rab-GTPase activating protein Gyp1) purified as previously described (Eitzen et al., 2000). Reagents used in fusion reactions were prepared in 20 mM Pipes-KOH, pH 6.8, and 200 mM sorbitol (Pipes Sorbitol buffer, PS).

4.3.2 Fluorescence microscopy

Images were acquired with a Nikon Eclipse TiE inverted microscope equipped with a motorized laser TIRF illumination unit, Photometrics Evolve 512 EM-CCD camera, CFI ApoTIRF 1.49 NA 100x objective lens, and 488 nm or 561 nm (50 mW) solid-state lasers operated with Nikon Elements software. Cross sectional images were recorded 1 μm into the

sample and resulting micrographs were processed using ImageJ software (National Institutes of Health) and Adobe Photoshop CC. Images shown were adjusted for brightness and contrast, inverted and sharpened with an unsharp masking filter. Fluorescence intensity profiles of GFP fluorescence were generated using ImageJ software.

4.3.3 Live cell microscopy

Live yeast cells were stained with FM4-64 to label vacuole membranes and prepared for imaging using a pulse-chase method as previously described (Brett et al., 2008). Where indicated, cells were incubated at 37 °C for 30 minutes for heat stress, with 100 μM cycloheximide for 90 minutes at 30 °C, or with 7 μM rapamycin for 90 minutes at 30 °C after FM4-64 staining. Time-lapse videos were acquired at 30°C using a Chamlide TC-N incubator (Live Cell Instruments) with cells plated on coverslips coated with concavalin-A (1 mg/ml in 50 mM HEPES, pH 7.5, 20 mM calcium acetate, 1 mM $MnSO_4$).

To assess how changing substrate levels affect polytopic protein sorting, yeast cells expressing Ypq1-GFP were incubated over night at 30 °C in YPD media supplemented with 125 μM lysine. Cells were back diluted in fresh YPD media supplemented with lysine and stained with FM4-64 for one hour at 30 °C. After two washes, cells were resuspended in SC media lacking lysine for 6 hours before collection and imaging.

Yeast cells expressing Cot1-GFP were incubated over night at 30 °C in SC media. Cells were back diluted in fresh SC media for FM4-64 staining, one hour at 30 °C. After two washes, cells were resuspended in SC media supplemented with 2 mM $ZnCl_2$ and grown for two hours at 30 °C (Li et al., 2015b). Cells were washed twice prior to imaging.

4.3.4 Vacuole isolation and homotypic vacuole fusion

Vacuoles were isolated from yeast cells as previously described (Haas, 1995). Fusion reactions were prepared using 6 μg of vacuoles isolated from GFP derivative strains in standard fusion reaction buffer with 0.125 M KCl, 5 mM $MgCl_2$, 1 mM ATP and 10 μM CoA. Vacuolar membranes were stained with FM4-64 by treating vacuoles with 3 μM FM4-64 for 10 minutes at 27 °C. Reactions were incubated at 27 °C for 60 minutes, unless otherwise noted, and placed on ice prior to visualization by HILO microscopy.

For examining the contribution of the fusion machinery, vacuoles were incubated in the

absence (CTL) or presence of 3.2 μM rGyp1-46 or 4 μM rGdi1 (F.I.). For heat stress treatment, vacuoles were pretreated for 5 minutes at 37 °C before addition to the fusion reaction and incubation for 30 minutes at 27 °C. Where indicated, vacuoles were pretreated with 100 μM cycloheximide for 15 minutes at 27 °C and incubated for an additional 15 minutes with the fusion reaction. Vacuoles were pretreated for 15 minutes at 27 °C with 7 μM Rapamycin, followed by addition of cycloheximide (where indicated) and fusion reaction constituents for an additional 30 minute incubation. Vacuoles were pretreated for 5 minutes at 27 °C with 25 μM $ZnCl_2$ before addition to the fusion reaction and incubation for additional time points.

Vacuole content mixing was assessed using a complementary, split β-lactamase based assay as previously described (Jun and Wickner, 2007) with increasing concentrations of $ZnCl_2$. For all concentrations tested, isolated vacuoles were pretreated for 5 minutes at 27 °C prior to addition of the fusion reaction constituents and further incubation for 90 minutes at 27 °C. Data shown was normalized to values obtained at 90 minutes under standard fusion conditions (n = 2).

4.3.5 Western blot analysis

Samples were prepared from isolated vacuoles from yeast strains expressing a GFP-tagged vacuolar membrane protein. Fusion reactions were prepared as previously described. Where indicated, samples were pretreated with heat stress, cycloheximide, or rapamycin and with fusion inhibitors rGyp1-46 and rGdi1, as previously described. Samples were incubated for 0 (ice), 30, 60, 90, or 120 minutes at 27 °C. After incubation, protease inhibitors (6.7 μM leupeptin, 33 μM pepstatin, 1 mM PMSF and 10.7 mM AEBSF), 1% DDM and 5X laemmli sample buffer were added. To solubilize membrane proteins but avoid aggregation due to boiling, reactions were incubated at 27 °C for 10 minutes prior to running on an SDS-Page gel. Samples were probed for α-GFP (Abcam, Cambridge, UK). All samples were repeated at least three times. Gels were imaged using GE Amersham Imager 600 by chemiluminescence and edited and prepared using Adobe Photoshop and Illustrator CC software.

4.3.6 Data analysis and presentation

For quantitative analysis of isolated vacuole micrographs we calculated the relative boundary membrane or lumenal GFP fluorescence using only docked vacuoles by measuring the surface area, the length of the boundary. GFP fluorescence intensities were measured using a ROI 4x4

pixels in diameter and acquiring a fluorescence value on the outer vacuole membrane, within the lumen and on the boundary membrane using ImageJ software. Data are reported as mean ± SEM. Comparisons were calculated using Student two-tailed *t*-test, *P* values < 0.05 indicate significant differences (*). Quantitative data was acquired using ImageJ software and plotted using Prism GraphPad version 7.0 software. Figures were prepared using Adobe Illustrator CC software.

Table 4. Yeast strains used in Chapter 4

Strain	Genotype	Source
BY4741	*MATα his3-Δ1 leu2-Δ0 met15-Δ0 ura3-Δ0*	Huh et al., 2003
Ypq1-GFP	BY4741, *Ypq1-GFP::KanMX*	This study
Ypq1-GFP:*vps36Δ*	BY4741, *Ypq1-GFP::KanMX, vps36Δ:HIS3MX*	This study
Cot1-GFP	BY4741, *Cot1-GFP::HIS3MX*	Huh et al., 2003
Cot1-GFP:*vps27*Δ	BY4741, *Cot1-GFP::HIS3MX, vps27Δ:KanMX*	This study
Vph1-GFP	BY4741, *Vph1-GFP::HIS3MX*	Huh et al., 2003
Vba4-GFP	BY4741, *Vba4-GFP::HIS3MX*	Huh et al., 2003
Vba4-GPF:*vps27*Δ	BY4741, *Vba4-GFP::HIS3MX, vps27Δ:HIS3MX*	This study
Vba4-GPF:*vps36*Δ	BY4741, *Vba4-GFP::HIS3MX, vps36Δ:HIS3MX*	This study

4.4 Results

4.4.1 vReD client proteins Cot1 and Ypq1 are constitutively degraded by the ILF pathway

To better resolve how vReD and ILF pathways contribute to vacuole membrane protein turnover, we first determined if Ypq1, the only other known vReD client protein besides Cot1 (Li et al., 2015a), is also degraded by the ILF pathway. Recently, Emr and colleagues suggested that Ypq1 is exclusively degraded by the vReD pathway (Zhu et al., 2017). But they mostly present images of yeast cells containing a single vacuole, eliminating the possibility of detecting sorting and degradation of Ypq1 by the ILF pathway, as it requires two organelles. However, most cells within an actively growing yeast culture contain two or more vacuoles (Li and Kane, 2009). To resolve this issue, we simply studied cells with multiple vacuoles. Similar to Cot1, we find that GFP-tagged Ypq1 is present in the boundary membranes of docked organelles within live cells under standard growth conditions (**Figure 13B**). Using HILO microscopy, we then recorded homotypic vacuole fusion events in live cells and found that Ypq1-GFP embedded in the boundary membrane is internalized within the lumen upon the completion of fusion (**Figure 13C; Movie S12**). Closer examination of micrographs presented in the three publications describing the vReD pathways reveal that fluorescent protein-tagged Ypq1 and Cot1 also accumulate within the boundary membrane between docked vacuoles when images of untreated yeast cells containing two or more vacuolar lysosomes are shown (Li et al., 2015a Figures 2A, 2C and 4I; Li et al., 2015b Figures 5D, 6C and 7C; Zhu et al., 2017 Figures 1A). Thus, our results are consistent with these previous reports, and suggest that, like Cot1-GFP, Ypq1-GFP is constitutively sorted for degradation by the ILF pathway.

When degraded by the vReD pathway, Ypq1-GFP is recognized, sorted and packaged for degradation by the ESCRT machinery (Li et al., 2015a). Thus, it is possible that ESCRTs may sort Ypq1-GFP into the boundary as well. To test this hypothesis, we deleted VPS36, a gene encoding a subunit of ESCRT-I (Henne et al., 2011), to disable the ESCRT machinery and found that it had no effect on Ypq1-GFP sorting into the ILF pathway (**Figure 13B** and **C; Movie S13**). We made similar observations for Cot1-GFP when VPS27, a gene encoding a component of ESCRT-0 (Katzmann et al., 2003), was deleted (**Figure 13C; Movies S14-15**). This confirms our previous work suggesting that protein degradation by the ILF pathway is ESCRT-independent (McNally et al., 2017) and eliminating the possibility that the vReD pathway was responsible for the observed sorting phenotypes.

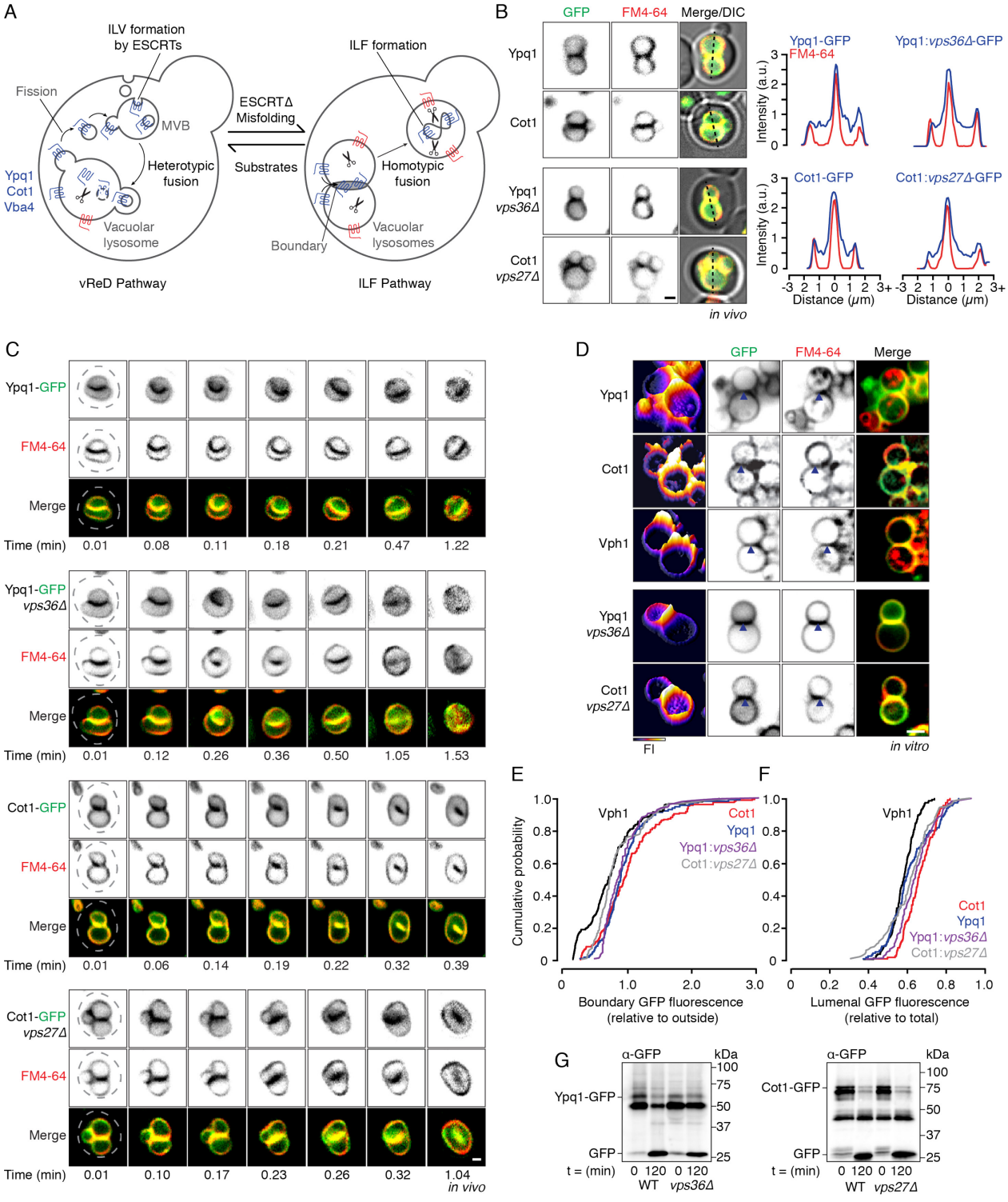
A
ILV formation by ESCRTs
Fission
MVB
Heterotypic fusion
Ypq1
Cot1
Vba4
Vacuolar lysosome
vReD Pathway
ESCRTΔ Misfolding
Substrates
ILF formation
Homotypic fusion
Boundary
Vacuolar lysosomes
ILF Pathway
B
GFP
FM4-64
Merge/DIC
Ypq1
Cot1
Ypq1 vps36Δ
Cot1 vps27Δ
in vivo
Ypq1-GFP FM4-64
Ypq1:vps36Δ-GFP
Cot1-GFP
Cot1:vps27Δ-GFP
Intensity (a.u.)
Distance (μm)
C
Ypq1-GFP
FM4-64
Merge
Time (min) 0.01 0.08 0.11 0.18 0.21 0.47 1.22
Ypq1-GFP vps36Δ
Time (min) 0.01 0.12 0.26 0.36 0.50 1.05 1.53
Cot1-GFP
Time (min) 0.01 0.06 0.14 0.19 0.22 0.32 0.39
Cot1-GFP vps27Δ
Time (min) 0.01 0.10 0.17 0.23 0.26 0.32 1.04
in vivo
D
GFP
FM4-64
Merge
Ypq1
Cot1
Vph1
Ypq1 vps36Δ
Cot1 vps27Δ
FI
in vitro
E
Vph1
Cot1
Ypq1
Ypq1:vps36Δ
Cot1:vps27Δ
Cumulative probability
Boundary GFP fluorescence (relative to outside)
F
Lumenal GFP fluorescence (relative to total)
G
α-GFP
kDa
100
75
50
37
25
Ypq1-GFP
GFP
t = (min) 0 120 0 120
WT vps36Δ
Cot1-GFP
WT vps27Δ

Figure 13. vReD client proteins, Ypq1 and Cot1, are constitutively degraded by the ILF pathway

(A) Working model describing how lysosomal membrane proteins can be selectively sorted for degradation by either the ILF or vReD pathways. **(B)** vReD client proteins, Ypq1 and Cot1, are constitutively degraded by the ILF pathway within wild type cells or when components of the ESCRT machinery are deleted. Line-scan analysis of Ypq1-GFP or Cot1-GFP in wild type and ESCRT deficient cells illustrating GFP (blue) or FM4-64 (red) fluorescence distribution along the dotted line. **(C)** Images from time-lapse videos of live yeast cells undergoing vacuole fusion expressing Ypq1-GFP or Cot1-GFP in wild type and ESCRT deficient cells. Cells were stained with FM4-64 to label with vacuolar membrane. Dotted lines outline each cell as observed in DIC. Scale bars, 1 μm (*in vivo*). **(D)** Micrographs of vacuoles isolated from cells expressing Ypq1-GFP or Cot1-GFP in wild type or ESCRT deficient backgrounds labeled with FM4-64 under standard fusion conditions. Isolated vacuoles from cells expressing Vph1-GFP demonstrating that Vph1-GFP is uniformly distributed around the vacuolar membrane. A closed arrowhead indicates boundary membranes containing GFP fluorescence. GFP fluorescence intensity profile plots (left panel). Scale bar, 2 μm (*in vitro*). Cumulative probability curves of GFP fluorescence intensity within the boundary **(E)** or vacuolar lumen **(F)** of micrographs presented in **D** ($n \geq 102$). Western blot analysis of Ypq1-GFP **(G)** and Cot1-GFP **(H)** degradation before and after fusion of isolated vacuoles in wild type (WT) and ESCRT deficient backgrounds. See also **Movies S12-15**.

The machinery necessary for protein degradation by the ILF pathway co-purifies with isolated organelles permitting study *in vitro* (McNally et al., 2017). Thus, we next confirmed that Ypq1-GFP sorting into the ILF pathway observed *in vivo* also persists *in vitro* (**Figure 13D**). We measured the GFP fluorescence at these boundary membranes and found that, like Cot1-GFP, Ypq1-GFP was enriched at these sites (**Figure 13E**), as compared to GFP-tagged Vph1, the stalk domain of the vacuolar V-type H^+-ATPase, that is uniformly distributed on vacuole membranes during fusion (Wang et al., 2002; McNally et al., 2017). Furthermore, protein sorting was unaffected by deleting components of the ESCRT machinery, confirming that entry of Ypq1 and Cot1 into the ILF pathway is independent of ESCRTs and as such, the vReD pathway. To confirm that Ypq1-GFP was internalized during the fusion reaction *in vitro*, we sought to determine if Ypq1-GFP appeared within the lumen over time (**Figure 13F**). As expected, we found that more Ypq1-GFP and Cot1-GFP accumulated within the lumen as compared to Vph1-GFP under fusogenic conditions. Here they should be exposed to acid hydrolases for degradation (Luzio et al., 2007). Thus, we next conducted western blot analysis to assess protein degradation and found that more GFP was cleaved from Ypq1 and Cot1 (**Figure 13G**) after lysosome fusion was stimulated *in vitro*. Importantly, observed protein degradation continued to occur in the absence of ESCRT activity. In all, these results reveal that both known vReD client proteins, Ypq1 and Cot1, are constitutively turned over by the ILF pathway.

4.4.2 Vba4, a vacuolar amino acid transporter, is constitutively degraded by the vReD pathway

At this point, it would seem that all vacuolar polytopic proteins rely on the ILF pathway for constitutive turnover. However, when conducting studies to identify additional ILF client proteins, we discovered that GFP-tagged Vba4, a vacuole amino acid transporter (Kawano-Kawada et al., 2015), was excluded from boundary membranes between docked vacuoles in living cells (**Figures 14A** and **B; Movie S16**). We quantified this phenotype using still images (**Figure 14C**) and confirmed that it is prevalent within the population of cells analyzed (**Figure 14D**). This sorting phenotype (boundary exclusion) is similar to other resident transporter proteins that were reported to avoid the ILF pathway and are spared during homotypic vacuole fusion (e.g. GFP-tagged Fet5, Ybt1, Ycf1 and Ncr1; McNally et al., 2017). However, unlike these other transporter proteins, Vba4-GFP also appeared on puncta adjacent to the vacuole membranes

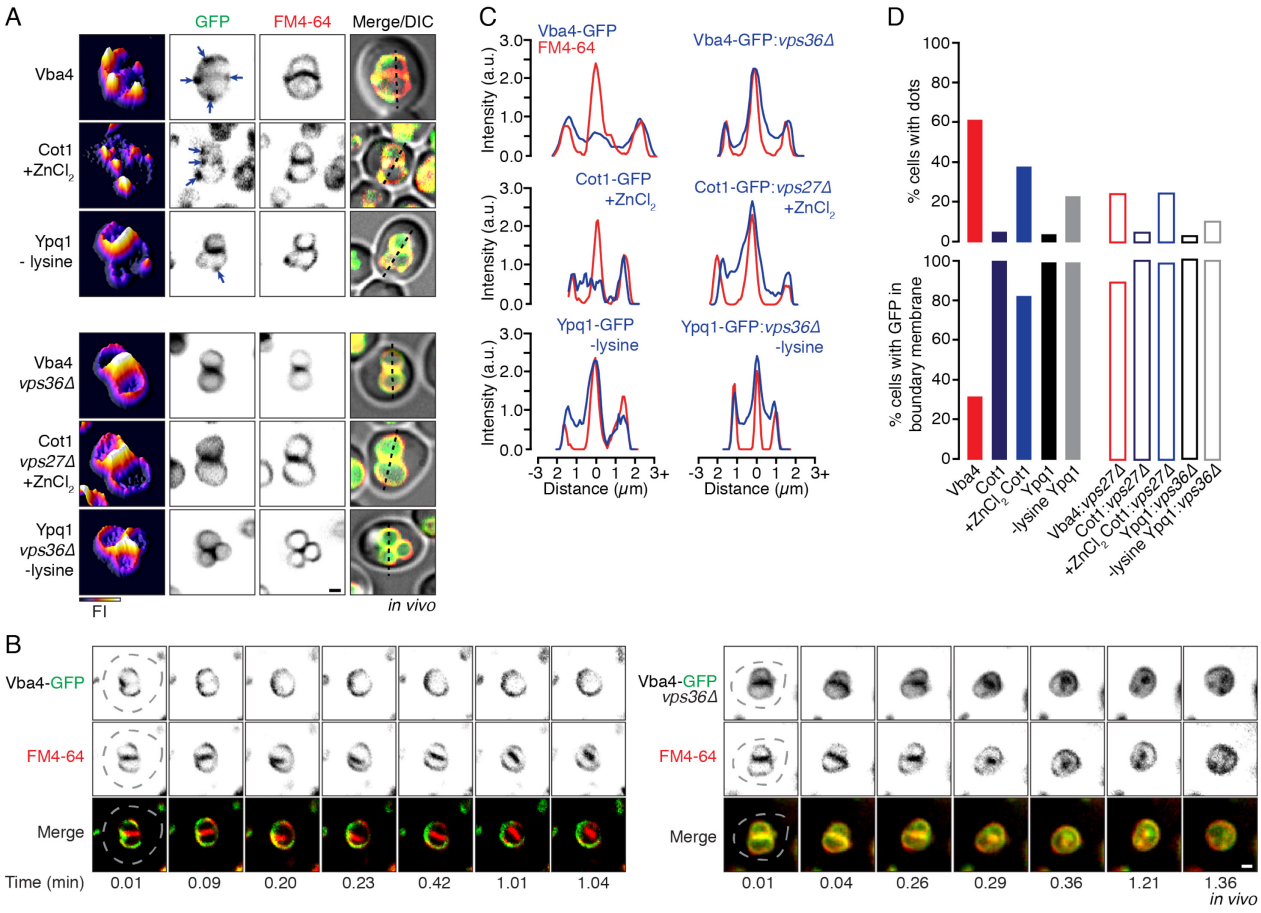

Figure 14. The vacuolar amino acid transporter, Vba4, is a new and constitutive vReD cargo within live cells

(A) Micrographs of docked vacuoles within cells expressing Vba4-GFP, Cot1-GFP, or Ypq1-GFP demonstrating their sorting by vReD and ILF pathways. Vba4-GFP is a constitutive vReD client protein, whereas Cot1-GFP and Ypq1-GFP are sorted by the vReD pathway when cognate substrate levels are manipulated: addition of 2 mM $ZnCl_2$ or lysine withdrawal, respectively. Arrows highlight puncta adjacent to the vacuolar membrane. **(B)** Images from time-lapse videos of live yeast cells undergoing vacuole fusion expressing Vba4-GFP in a wild type strain or when VPS36 is deleted. Cells were stained with FM4-64 to label the vacuolar membrane. Dotted lines outline each cell as observed in DIC. Scale bar, 1 μm (*in vivo*). **(C)** Line-scan analysis of images shown in **A** illustrating GFP (blue) or FM4-64 (red) fluorescence distribution along the dotted line. **(D)** Quantification of *in vivo* micrographs demonstrating the percent of cells with GFP fluorescence present within the boundary membrane and the percent of cells with dots (puncta) adjacent to the vacuolar membrane ($n \geq 155$). See also **Movies S16-17**.

(**Figure 14A**) within most cells analyzed (**Figure 14D**). Importantly, these puncta resembled Cot1-GFP or Ypq1-GFP -positive structures that form to mediate their degradation by the vReD pathway in response to changes in substrate levels (**Figures 14A** and **D**; Li et al., 2015a; Li et al., 2015b). Consistent with this interpretation, in the presence of $ZnCl_2$ Cot1-GFP was also excluded from boundary membranes and appeared on puncta adjacent to the vacuole membrane (**Figure 14A**), suggesting that it is redirected from the ILF pathway to the vReD pathway. However, despite the appearance of Ypq1-GFP on puncta, the GFP-tagged protein continued to be present in boundary membranes after lysine withdrawal (**Figures 14A** and **D**), suggesting that Ypq1-GFP substrate-induced degradation is not dependent on the vReD pathway exclusively. In any case, together these results show that Vba4 avoids the ILF pathway and rather is a bone fide vReD client protein, the first shown to be constitutively degraded by this pathway.

To further study protein degradation by these two pathways, we purified vacuoles from these strains and found that puncta form adjacent to isolated vacuoles when we monitored Vba4-GFP or Cot1-GFP (with $ZnCl_2$) under fusogenic conditions over time (**Figures 15A** and **B**). This suggests that the vReD machinery responsible for protein sorting and packaging also co-purifies with organelles permitting further study *in vitro*. Notably, Ypq1-GFP did not appear on puncta *in vitro* (**Figure 13D**) despite the absence of lysine from the reaction buffer, suggesting that the machinery responsible for sensing extracellular lysine withdrawal to signal Ypq1-GFP degradation by the vReD pathway may not co-purify with lysosomes. Thus, we focused on studying only Vba4-GFP and Cot1-GFP and found that both proteins continued to be excluded from boundaries between docked organelles (**Figure 15C**) and appeared on puncta (**Figure 15B**) over time, confirming that their sorting phenotypes were recapitulated *in vitro*. Importantly, the conditions used to stimulate Cot1-GFP sorting into the vReD pathway do not completely block the *in vitro* fusion reaction, suggesting the membrane fusion machinery is intact (**Figure S12**).

When counting GFP-positive puncta that formed over time *in vitro*, we noticed that this variably increased until a peak at 30 minutes for Vba4-GFP or 60 minutes for Cot1-GFP and then decreased afterwards, suggesting that these compartments were generated and then consumed during the reaction (**Figure 15B**). This result is consistent with Cot1-GFP and Vba4-GFP being first sent to endosomal compartments (represented as puncta in our micrographs) where they are packaged by the ESCRT machinery in to ILVs within MVBs which later fuse with vacuoles (consumption of puncta) to deliver these proteins to the lumen for degradation (Li et al., 2015a).

To test this hypothesis, we measured the fluorescence intensity of Vba4-GFP and Cot1-GFP (with $ZnCl_2$) within the lumen over time (**Figure 15D**). As expected, both GFP-tagged proteins accumulated within the lumen, signifying that they were exposed to acid hydrolases for degradation. To confirm this, we assessed GFP-cleavage from Vba4 or Cot1 (with $ZnCl_2$) by western blot (**Figures 15E and F**) and found that both proteins were indeed degraded over time *in vitro*. As Vba4-GFP is excluded from boundary membranes, but rather appears on vesicles that are consumed over time under standard fusion conditions, we conclude that Vba4-GFP is constitutively delivered to the vacuole for degradation by the vReD pathway, whereas Cot1-GFP degradation by the vReD pathway requires manipulating cognate substrate levels.

4.4.3 The ILF pathway compensates for loss of vReD function

The vReD pathway requires ESCRTs to recognize, sort and package proteins for degradation. To confirm that the vReD pathway is responsible for constitutive Vba4-GFP degradation, we deleted VPS36 to block ESCRT function and expected Vba4-GFP to accumulate in puncta (as this stage of the vReD pathway is supposedly ESCRT-independent) but it should not be delivered to the vacuole lumen, as ILV formation is ESCRT-dependent (Li et al., 2015a). However, we found that knocking out VPS36 caused Vba4-GFP to accumulate within the boundary membrane at the interface between docked vacuoles (**Figures 14A–C**) in nearly all cells examined (**Figure 14D**), and Vba4-GFP was internalized within an ILF upon homotypic vacuole fusion within living cells (**Figure 14B; Movie S17**). We made similar observations *in vitro* (**Figures 15A**) whereby the intensity of Vba4-GFP fluorescence within the boundary membrane increased over time (**Figure 15C**), suggesting that it was now sorted into the ILF pathway.

Moreover, Vba4-GFP–positive puncta did not efficiently form *in vivo* (**Figure 14D**) or *in vitro* (**Figure 15B**), although Vba4-GFP continued to accumulate in the lumen over time (**Figure 15D**). Consistent with this finding, Vba4-GFP continued to be degraded in the absence of VPS36 (**Figure 15E**). We made similar observations *in vitro* for Cot1-GFP, whereby $ZnCl_2$ normally triggers Cot1-GFP degradation by the vReD pathway, but when ESCRT function is disrupted, it resorts to the ILF pathway (**Figures 14** and **15**). All things considered, we conclude that vReD-mediated protein degradation is rerouted to the ILF pathway when ESCRT function is impaired.

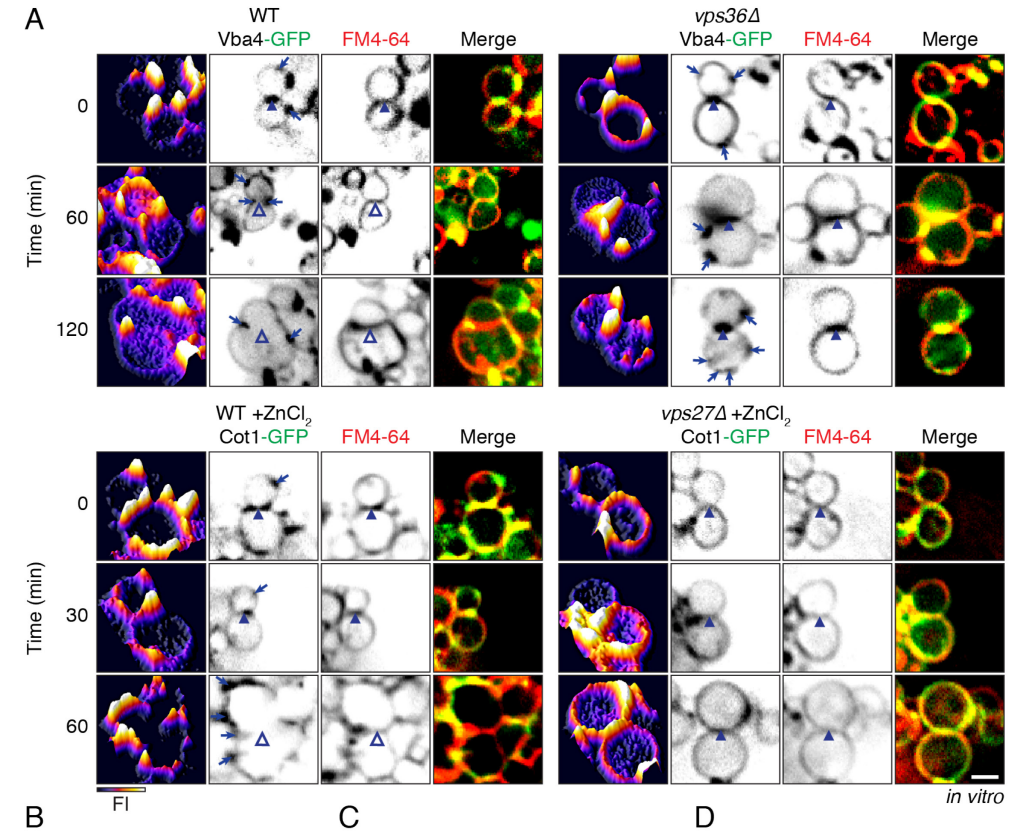
A
WT
Vba4-GFP
FM4-64
Merge
vps36Δ
Vba4-GFP
FM4-64
Merge
Time (min)
0
60
120
WT +ZnCl2
Cot1-GFP
FM4-64
Merge
vps27Δ +ZnCl2
Cot1-GFP
FM4-64
Merge
Time (min)
0
30
60
FI
in vitro

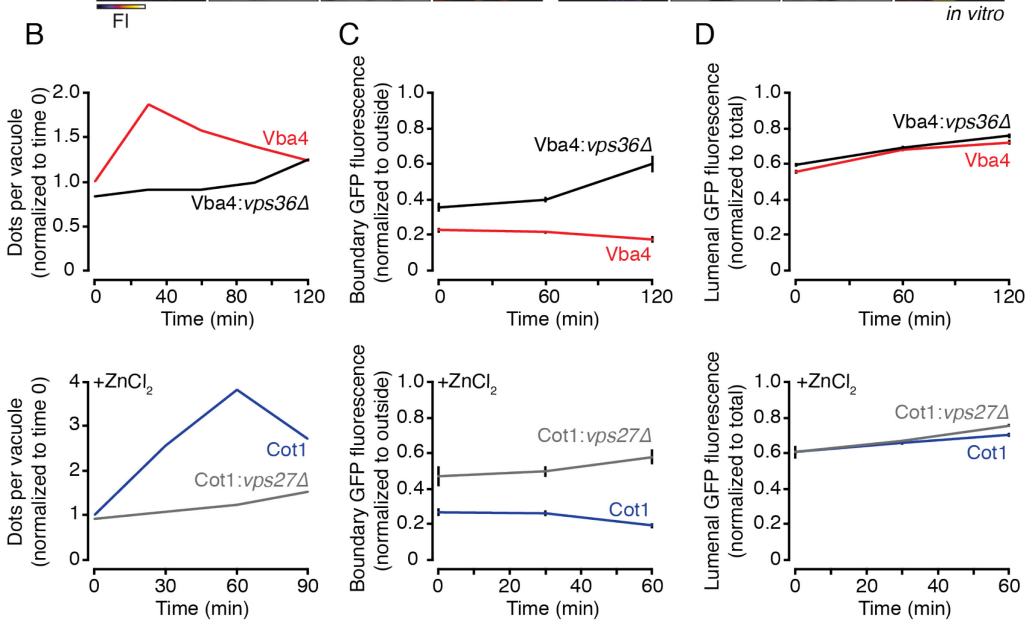
B
Dots per vacuole (normalized to time 0)
Vba4
Vba4:vps36Δ
Time (min)
C
Boundary GFP fluorescence (normalized to outside)
Vba4:vps36Δ
Vba4
Time (min)
D
Lumenal GFP fluorescence (normalized to total)
Vba4:vps36Δ
Vba4
Time (min)
Dots per vacuole (normalized to time 0)
+ZnCl2
Cot1
Cot1:vps27Δ
Time (min)
Boundary GFP fluorescence (normalized to outside)
+ZnCl2
Cot1:vps27Δ
Cot1
Time (min)
Lumenal GFP fluorescence (normalized to total)
+ZnCl2
Cot1:vps27Δ
Cot1
Time (min)

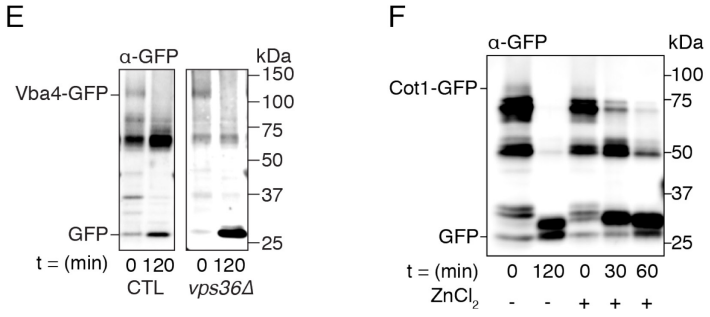
E
α-GFP
kDa
Vba4-GFP
GFP
t = (min)
0 120
0 120
CTL
vps36Δ
F
α-GFP
kDa
Cot1-GFP
GFP
t = (min)
0 120 0 30 60
ZnCl2
- - + + +

Figure 15. Vba4-GFP and Cot1-GFP are sorted by the vReD pathways on isolated vacuoles
(A) Fluorescence micrographs of docked vacuoles isolated from cells expressing either Vba4-GFP or Vba4-GFP:*vps36*Δ under standard fusion conditions, or from cells expressing Cot1-GFP or Cot1-GFP:*vps27*Δ after pre-treatment with 25 μM $ZnCl_2$ for 5 minutes over time. Arrows highlight puncta adjacent to the vacuolar membrane. Boundaries containing (closed) or lacking (open arrowheads) GFP fluorescence are indicated. GFP fluorescence intensity profile plots (left panel). Scale bar, 2 μm (*in vitro*). **(B)** Quantification of the number of dots (puncta) compared to the number of vacuoles (normalized to the wild type (WT) strain at time zero) from micrographs as shown in **A**. Average boundary membrane **(C)** or lumenal **(D)** GFP fluorescence intensity over time for micrographs as shown in **A**. Data presented are means ± SEM ($n \geq 123$). Western blot analysis of **(E)** Vba4-GFP and Vba4-GFP:*vps36*Δ degradation kinetics before and after fusion of isolated vacuoles under standard reaction conditions or **(F)** Cot1-GFP before and after fusion of isolated vacuoles in the absence or presence of $ZnCl_2$ treatment. See also **Figure S12**.

4.4.4 Protein degradation by the vReD pathway can be stimulated by TOR

TOR (target of rapamycin) is a critical signaling serine/threonine kinase important for a variety of cellular processes including cellular metabolism, regulating organismal growth and homeostasis, and for supplying the cell with nutrients under metabolic stress conditions (Dunlop and Tee, 2009; Laplante and Sabatini, 2012; Perera and Zoncu, 2016). To presumably increase cellular amino acid levels, both the ILF and MVB pathways degrade vacuolar or surface polytopic proteins, respectively, in response to activation of TOR signaling by the translation inhibitor cycloheximide (CHX; MacGurn et al., 2011; McNally et al., 2017). However, it is not known if vReD also mediates vacuolar transporter protein degradation in response to TOR signaling. Thus to test this, we treated cells with cycloheximide and examined the membrane distribution of Vba4-GFP, the only client protein that is constitutively degraded by the vReD pathway. We find that Vba4-GFP continues to be excluded from boundary membranes (**Figures 16A** and **B**) within the cell population (**Figure 16C**) but more puncta appear adjacent to vacuoles (**Figure 16C**) in the presence of CHX, indicating that sorting of Vba4-GFP into the vReD pathway is enhanced. In addition, Vba4-GFP is spared from internalization into the vacuolar lumen upon fusion, despite the presence of a lumenal membrane fragment, and instead accumulates on puncta (**Movie S18**). Importantly, treatment with rapamycin, a TOR signaling inhibitor, blocked this effect (**Figures 16A, 16B** and **16D**), confirming that TOR activation was required. We made similar observations *in vitro* (**Figures 16E–H**) and found that more Vba4-GFP accumulated in the vacuole lumen in the presence of CHX (**Figure 16G**). Consistent with this observation, GFP cleavage from Vba4 was enhanced in the presence of CHX (**Figure 16H**). Importantly, the observed increase in lumenal delivery (**Figure 16G**) and degradation (**Figure 16H**) of Vba4-GFP was blocked by pretreating isolated organelles with rapamycin. Thus, we conclude that Vba4-GFP degradation by the vReD pathway can be regulated by TOR signaling.

Can other proteins get shunted into the vReD pathway in response to TOR signaling? Although Ypq1-GFP and Cot1-GFP are constitutively degraded by the ILF pathway (see **Figure 13**), they are rerouted into the vReD pathway in response to changing substrate levels (**Figure 14**). Thus, it is possible that TOR activation by CHX may also drive Ypq1-GFP or Cot1-GFP into the vReD pathway for degradation. To answer this question, we treated cells expressing either protein with CHX and examined the effects on their cellular membrane distribution (**Figures 16A–C**). Both proteins continued to be present in boundary membranes in all cells, and neither

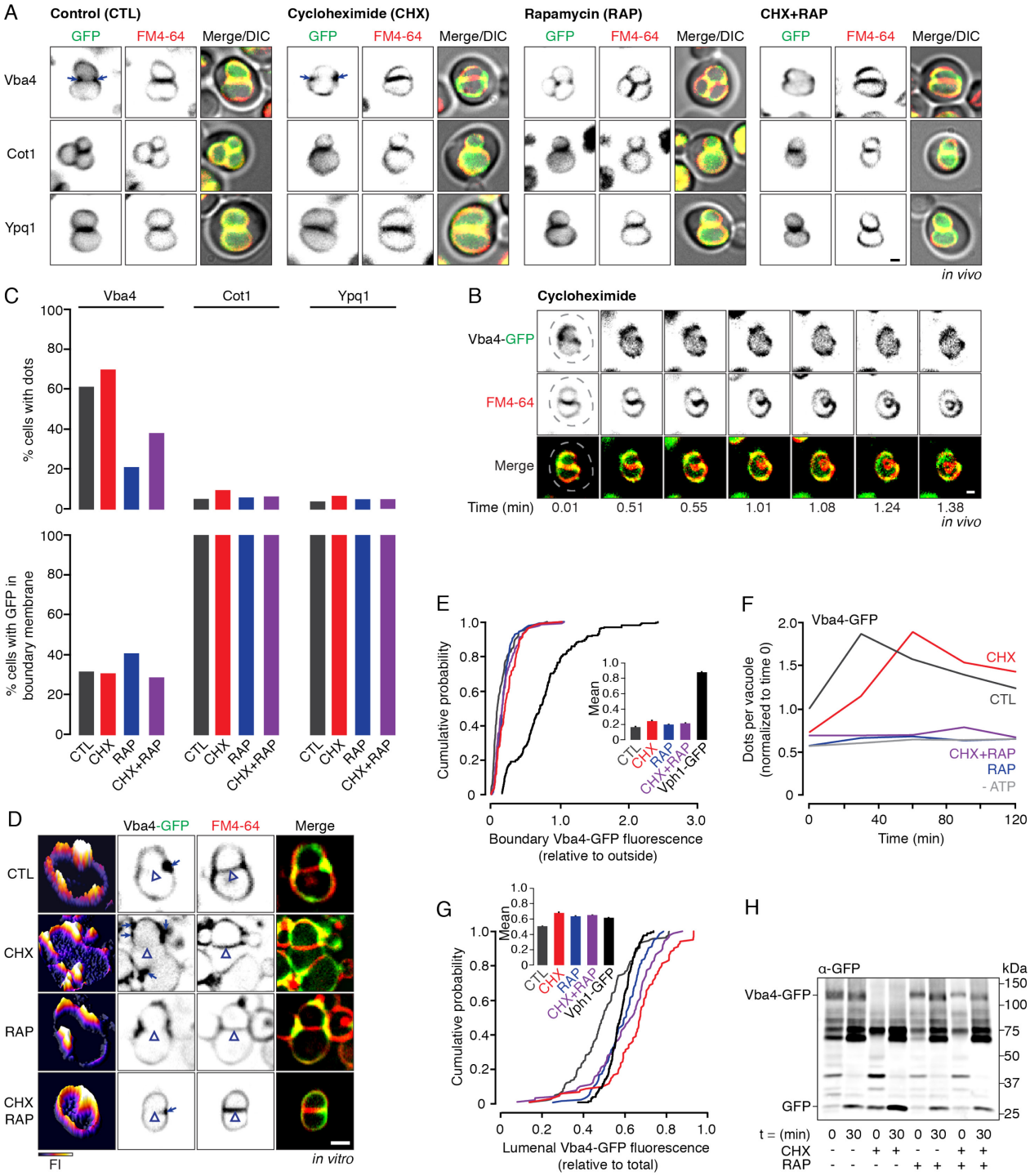
A
Control (CTL)
Cycloheximide (CHX)
Rapamycin (RAP)
CHX+RAP
GFP
FM4-64
Merge/DIC
Vba4
Cot1
Ypq1
in vivo
B
Cycloheximide
Vba4-GFP
FM4-64
Merge
Time (min)
0.01
0.51
0.55
1.01
1.08
1.24
1.38
in vivo
C
Vba4
Cot1
Ypq1
% cells with dots
% cells with GFP in boundary membrane
CTL
CHX
RAP
CHX+RAP
D
Vba4-GFP
FM4-64
Merge
CTL
CHX
RAP
CHX RAP
FI
in vitro
E
Cumulative probability
Boundary Vba4-GFP fluorescence (relative to outside)
Mean
Vph1-GFP
F
Vba4-GFP
Dots per vacuole (normalized to time 0)
Time (min)
CHX
CTL
CHX+RAP
RAP
- ATP
G
Cumulative probability
Lumenal Vba4-GFP fluorescence (relative to total)
Mean
Vph1-GFP
H
α-GFP
kDa
Vba4-GFP
GFP
150
100
75
50
37
25
t = (min)
0 30 0 30 0 30 0 30
CHX
RAP

Figure 16. Protein degradation by the vReD pathway is stimulated in response to TOR signaling

(A) Fluorescence micrographs of docked vacuoles within cells expressing Vba4-GFP, Cot1-GFP or Ypq1-GFP under standard conditions (CTL) or after incubation with cycloheximide (CHX), rapamycin (RAP), or both. Arrows highlight puncta adjacent to the vacuolar membrane. **(B)** Images from a time-lapse video of a vacuole fusion event within a yeast cell expressing Vba4-GFP after CHX treatment, stained with FM4-64 to label the vacuolar membrane. Dotted line outlines the yeast cell as observed in DIC. Scale bars, 1 μm (*in vivo*). **(C)** Quantification of *in vivo* micrographs demonstrating the percent of cells with GFP fluorescence present within the boundary membrane and the percent of cells with dots (puncta) adjacent to the vacuolar membrane ($n \geq 204$)**. (D)** Micrographs of vacuoles isolated from cells expressing Vba4-GFP under standard fusion conditions (CTL) or after treatment with CHX, RAP or both. Boundary membranes lacking GFP fluorescence are indicated by open arrowheads and GFP fluorescence profile are plotted (left panel). Arrows highlight puncta adjacent to the vacuolar membrane. Scale bar, 2 μm (*in vitro*). Cumulative probability curves of GFP fluorescence intensity within the boundary membrane **(E)** or vacuolar lumen **(G)** of micrographs presented in **D.** ($n \geq 104$). **(F)** Quantification of the number of dots (puncta) compared to the number of vacuoles (normalized to Vba4-GFP CTL at time zero) from micrographs as shown in **D**. ($n \geq 359$ vacuoles). **(H)** Western blot analysis of Vba4-GFP degradation before or after fusion has progressed for 30 minutes under standard fusion conditions or after treatment with CHX, RAP or both. See also **Figure S13** and **Movie S18.**

really appeared on puncta, suggesting that CHX did not reroute Ypq1-GFP or Cot1-GFP from the ILF pathway to the vReD pathway. These results were confirmed *in vitro* (**Figure S13A**), whereby CHX enhanced sorting into the boundary membrane (**Figure S13B**), increased lumenal delivery (**Figure S13C**) and increased degradation (**Figure S13D**) of Ypq1-GFP and Cot1-GFP. Furthermore, protein degradation was blocked by fusion inhibitors (**Figure S13E**), confirming that enhanced degradation of Ypq1-GFP and Cot1-GFP by TOR activation was mediated by the ILF pathway instead of the vReD pathway.

4.4.5 The ILF pathway exclusively mediates vacuolar polytopic protein quality control

To prevent cellular proteotoxicity and maintain proteostasis, misfolded or damaged proteins are selectively cleared by multiple degradation pathways, such as the proteasome or chaperone-mediate autophagy for cytoplasmic proteins (Cuervo and Dice, 2000b; Kaushik et al., 2011), the ESCRT pathway for some surface polytopic proteins (Babst, 2014), and the ILF pathway for vacuolar polytopic proteins including Cot1 (McNally et al., 2017). Although its contribution to protein quality control has not been assessed, the vReD pathway relies on similar ESCRT machinery that clears misfolded surface proteins (Raiborg and Stenmark, 2009; Li et al., 2015a*)*. Thus, it is possible that, like the ILF pathway, the vReD pathway may clear some misfolded vacuolar transporter proteins. To test this hypothesis, we subjected cells to heat stress to induce protein misfolding (Keener and Babst, 2013; McNally et al., 2017) and monitored changes in the membrane distributions of Vba4-GFP, Ypq1-GFP and Cot1-GFP within living cells (**Figures 17A** and **B**). We found that Ypq1-GFP and Vba4-GFP are both sorted into the boundary membrane between docked organelles in response to heat stress in nearly all cells analyzed (**Figure 17C**), similar to Cot1-GFP as previously reported (McNally et al., 2017). As Vba4-GFP is normally excluded from boundary membranes, we also used HILO microscopy to confirm that it was indeed internalized within an ILF upon homotypic lysosome fusion after heat stress within living cells (**Figure 17D; Movie S19**). We made similar observations when VPS36 or VPS27 were deleted, confirming that sorting of misfolded proteins into the boundary in response to heat stress was ESCRT-independent (**Figures 17A–C**).

To better characterize this process, we replicated these results *in vitro* (**Figure 18A**), whereby heat stress caused enrichment of all three proteins within the boundary membrane (**Figure 18B**) and enhanced accumulation within the vacuole lumen (**Figure 18C**). To confirm

that these misfolded proteins were degraded, we assessed GFP-cleavage by western blot and found that degradation of Vba4-GFP, Cot1-GFP and Ypq1-GFP was enhanced by heat stress (**Figure 18D**). Since the ILF pathway relies on the vacuole fusion machinery for protein sorting and internalization (McNally et al., 2017), we reasoned that blocking the membrane fusion reaction would also inhibit protein sorting into the boundary membrane. To test this, we added the vacuole fusion inhibitors rGdi1 and rGyp1-46 (to block Rab-GTPase activation; Brett et al., 2008). As expected, blocking Rab activity prevented protein sorting (**Figures 18A** and **B**), internalization (**Figure 18C**), and proteolysis (**Figure 18D**), confirming that membrane fusion machinery, not ESCRTs, are required for observed polytopic protein degradation. In sum, we conclude that the ILF pathway, not vReD, is responsible for clearing misfolded vacuolar polytopic proteins, and thus is an important contributor to cellular protein quality control.

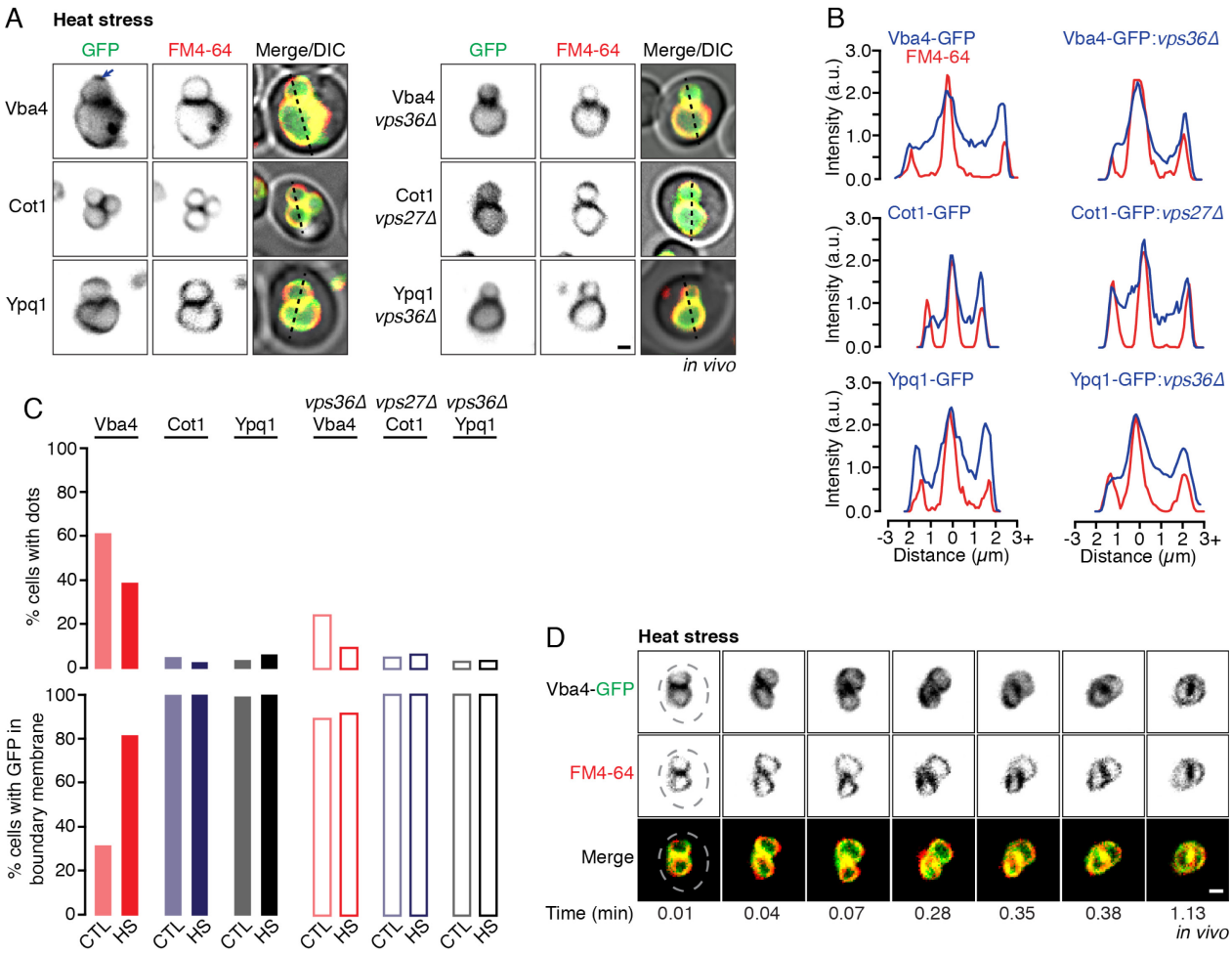

Figure 17. The ILF pathway degrades misfolded lysosomal polytopic proteins within live cells

(A) Fluorescence and DIC micrographs of docked vacuoles from cells expressing Vba4-GFP, Cot1-GFP or Ypq1-GFP in wild type or ESCRT deficient (*vps27*Δ or *vps36*Δ) strains after heat stress treatment. Arrow highlights puncta adjacent to the vacuolar membrane. **(B)** Line-scan analysis of *in vivo* images shown in **A** illustrating GFP (blue) or FM4-64 (red) fluorescence distribution along the dotted line. **(C)** Quantification of *in vivo* micrographs demonstrating the percent of cells with GFP fluorescence present within the boundary membrane and the percent of cells with dots (puncta) adjacent to the vacuolar membrane under standard fusion conditions (CTL) or when cells were treated with heat stress (HS). CTL bars are quantifications from Figure **14 D** and **E**. (n ≥ 148). **(D)** Images from a time-lapse video demonstrating a vacuole fusion event within a yeast cell expressing Vba4-GFP after heat stress (HS) treatment, stained with FM4-64 to label the vacuolar membrane. Dotted line outlines the yeast cell as observed in DIC. Scale bars, 1 μm (*in vivo*). See also **Movie S19**.

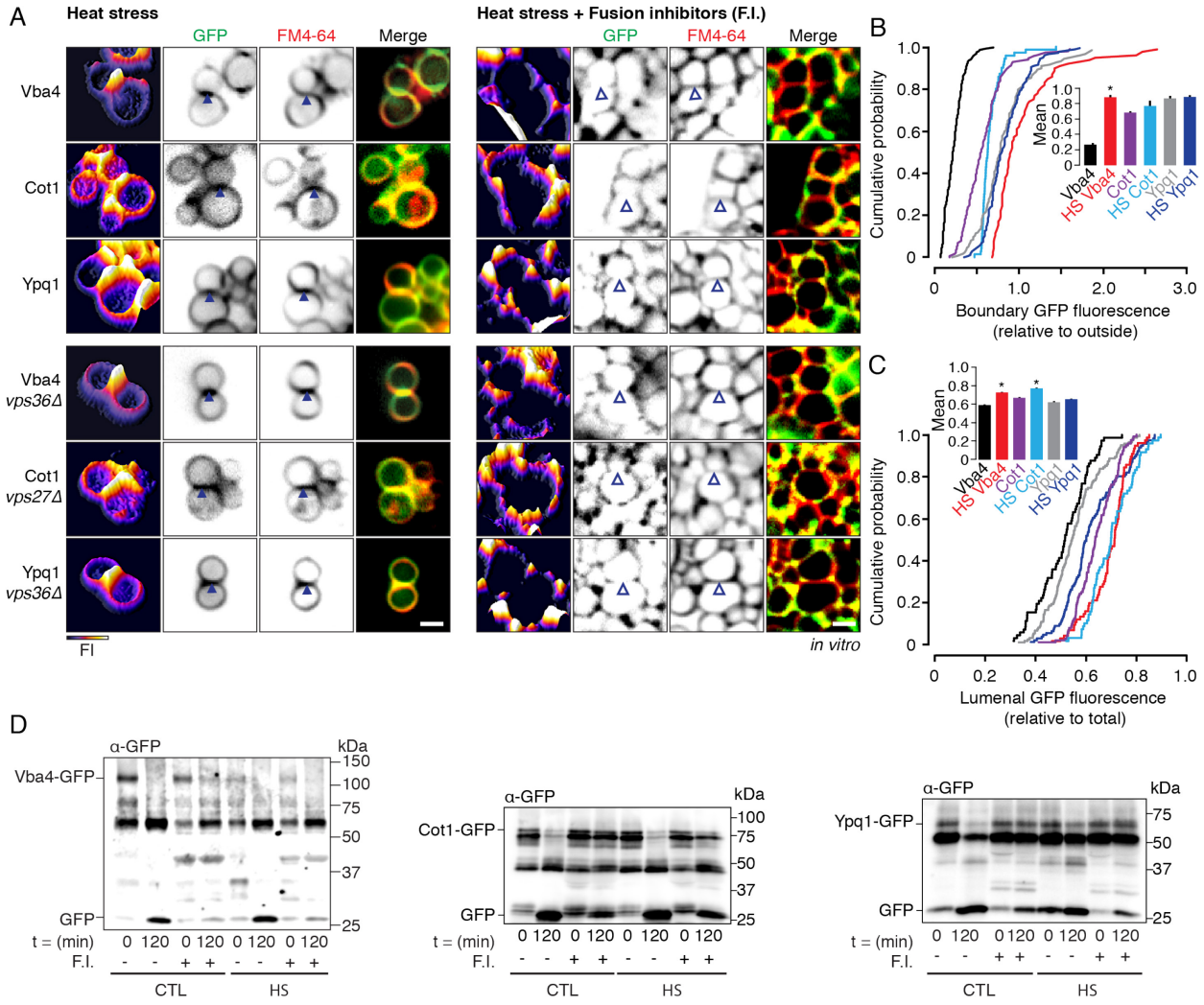

Figure 18. The ILF pathway degrades polytopic proteins when misfolded by heat stress on isolated vacuoles

(A) Fluorescence micrographs of vacuoles isolated from cells expressing Vba4-GFP, Cot1-GFP or Ypq1-GFP from wild type or ESCRT deficient strains after treatment with heat stress (HS) in the absence or presence of the fusion inhibitors rGdi1 and rGyp1-46 (F.I.). Boundary membranes containing (closed arrowhead) or lacking (open arrowhead) GFP fluorescence are indicated and GFP fluorescence profile are plotted (left panel). Scale bar, 2 µm (*in vitro*). Cumulative probability curves of GFP fluorescence intensity within the boundary **(B)** or vacuolar lumen **(C)** of micrographs presented in **A**. (n ≥ 102). **(D)** Western blots comparing Vba4-GFP, Cot1-GFP and Ypq1-GFP degradation kinetics before and after fusion under standard conditions (CTL) or when isolated vacuoles were subjected to heat stress (HS) in the absence or presence of fusion inhibitors rGdi1 and rGyp1-46 (F.I.).

4.5 Discussion

4.5.1 vReD and ILF pathways cooperate for lysosomal proteostasis

Despite being critical for lysosome physiology, it was unclear how lysosomal nutrient transporter proteins lifetimes were regulated until recently, when two processes were independently discovered: the ESCRT-dependent vReD pathway (Li et al., 2015a) and ESCRT-independent ILF pathway (McNally et al., 2017). However, if the two pathways function independently or cooperate to maintain or remodel the protein landscape on vacuolar lysosome membranes remained elusive. Herein, we find that they work together to control lysosomal proteostasis and begin to decipher their distinct contributions to this process: (1) Client proteins are shared by both pathways, as vReD client proteins Ypq1 and Cot1 are constitutively degraded by the ILF pathway (**Figure 13**). (2) Both pathways are responsible for constitutive turnover of vacuolar nutrient transporters, as we identified a new vReD client protein, Vba4, which is the first shown to be constitutively degraded by this pathway (**Figures 14** and **15**). (3) Similar to the ILF pathway, the vReD pathway responds to TOR activation suggesting that both may play a role in cellular metabolic homeostasis (**Figure 16**). (4) Only the ILF pathway appears to mediate quality control of lysosomal polytopic proteins, as all proteins studied are shunted into this pathway when misfolded upon heat stress (**Figures 17** and **18**). (5) The ILF pathway compensates for the loss of the vReD pathways when ESCRT function is impaired (**Figures 14** and **15**). Two questions immediately arise from these discoveries: *What allows one pathway to compensate for the other? Why two pathways?*

4.5.2 What allows one pathway to compensate for the other?

Here we show that when components of the ESCRT machinery are deleted, the vReD pathway is blocked and the ILF pathway compensates for this loss by degrading Vba4 for example (**Figure 14**). We have also shown that the ILF pathway degrades internalized surface proteins that are normally packaged into intralumenal vesicles at the endosome by ESCRTs when MVB formation is impaired (McNally and Brett, submitted). These results provide important insight into the underlying mechanisms that maybe shared. Fundamentally, both pathways require a mechanism to recognize and label client polytopic proteins, and selectively sort them into an area of membrane that is internalized into the organelle lumen for exposure to and degradation by acid hydrolases. These two pathways diverge at the sorting stage, as the sorting

machinery is different (i.e. ESCRT-dependent versus ESCRT-independent), as are the membrane locations where sorting occurs and the mechanisms used for membrane severing required for internalization. Thus, we argue that they share the same labeling machinery. Selective client protein sorting by the vReD pathway requires protein ubiquitylation by E3-ubiquitin ligases and E4-adapter proteins (Li et al., 2015a; Li et al., 2015b). It is not surprising that the E3-ligase Rsp5 implicated in the vReD pathway also ubiquitylates surface proteins sorted into the canonical MVB pathway, as both are ESCRT-dependent (Horák, 2003; MacDonald et al., 2012). This ligase is also important for mediating soluble protein labeling for degradation by the proteasome (Glickman and Ciechanover, 2002), highlighting that most degradation pathways share protein labeling machinery.

However, the basis of client protein labeling in the ILF pathway remains unknown. But given that it can degrade vReD client proteins in the absence of ESCRT function and all cellular degradation pathway seem to share protein labeling machinery, we speculate that the ILF pathway also recognizes and sorts client proteins ubiquitylated by E3-ligases and E4-adapter proteins. We have initiated studies to test this hypothesis and preliminary work indicates that the E4-adapter protein Ssh4, responsible for Ypq1 ubiquitylation for degradation by the vReD pathway (Li et al., 2015a), also mediates degradation of the copper-oxidase Fet5 by the ILF pathway (data not shown). Thus, because they share the same protein labeling machinery, it seems that the ILF and vReD pathways coordinate functions with other cellular protein degradation pathways to restructure the cellular proteome, e.g. for metabolic reprogramming which requires remodeling the proteomes of lysosomes, mitochondria, peroxisomes, lipid droplets, ER, and cytoplasm (Lemus and Goder, 2014; Tasset and Cuervo, 2016).

4.5.3 Why two pathways?

There are two important distinctions between these two pathway that may explain why they co-exist: First, the vReD pathway permits vacuole polytopic protein recycling, whereby after sorting and delivery to the endosomes client proteins could avoid being packaged into ILVs by the ESCRT machinery. If so, they would remain on the MVB perimeter membrane, and upon MVB-vacuole fusion, be returned to the vacuole membrane. This is akin to surface receptor protein recycling, whereby after internalization, receptors can be packaged into ILVs for degradation or returned to the surface (Maxfield and McGraw, 2004). Thus, we propose that the

vReD pathway acts in a similar manner, to regulate levels of nutrient transporter proteins on vacuolar lysosome membranes. On the other hand, sorting into the ILF pathway ensures client protein degradation, as they are immediately exposed to lumenal proteases. This is based on the assumption that ILF-vacuole membrane "back" fusion does not occur, as GFP accumulates within the lumen in a diffuse pattern, not on puncta, over the course of the fusion reaction (**Figures 13 - 18**), and ILFs fragment and seem to dissolve quickly after being formed within the lumen (**Movies S13** and **S17**; also see McNally et al., 2017). This explains why all misfolded proteins – which cannot be reused – are shunted into the ILF pathway for degradation (**Figures 17** and **18**).

It should be noted however, that the same group that published the first papers describing the vReD pathway now claim that an endosomal intermediate is not required (Zhu et al., 2017). Rather, the ESCRT machinery is recruited to the vacuole membrane where it drives ILV formation directly into the vacuole lumen. Why the authors would contradict their original claims and why this mechanism exists as an alternative to microautophagy, which produces similar products, is unclear. However, we find that GFP-positive puncta continue to form, albeit less efficiently, when components of the ESCRT machinery are deleted (**Figures 15A** and **B**). We argue that this phenotype supports the original hypothesis, whereby client proteins accumulate at an endosomal intermediate adjacent to the vacuole membrane, because they cannot be packaged into ILVs by ESCRTs. This result cannot explain the alternative, where we would expect sorting on the vacuole membrane to be entirely abolished, resulting in no observable puncta.

This alternative model also suggests that the vReD pathway does not require membrane fusion. This is based on two observations: (1) Applying heat shock to inhibit temperature-sensitive alleles of genes necessary for endosome and vacuole membrane fusion (Vps18 and Vam7) does not impair Ypq1-GFP degradation by the vReD pathway (Zhu et al., 2017). However, prolonged heat shock induces many cellular stress pathways, and here we show that it also stimulates protein misfolding and degradation by the ILF pathway. Using an alternative approach that does not require heat shock, we find that protein degradation by the vReD pathway is blocked in vitro by protein inhibitors that target both endosome and vacuole membrane fusion (e.g. Vba4-GFP; **Figure 18D**). Thus, we argue that perhaps other cellular mechanisms stimulated by heat stress could account for their observations. (2) ILVs are observed within vacuoles after triggering degradation of Ypq1-GFP using a "RapiDeg" method, whereby addition of rapamycin

induces binding of a Ypq1 fusion protein (Ypq1-GFP-2xFKBP) to FBR domain of human mTOR fused to ubiquitin (FRB-Ubx3), which mimics K63 ubiquitin linkage (Zhu et al., 2017). Only in the presence of rapamycin, these two inserted motifs rapidly heterodimerize to ubiquitinate Ypq1, without requiring its previously characterized E3 Ub-ligase (Rsp5) and E4-adaptor protein (Ssh4; Li et al., 2015a; Zhu et al., 2017). Once ubiquitinated, Ypq1 is sorted off of the vacuolar membrane and into the lumen where it is degraded. But the origin of these ILVs is unclear, as they do not show how they are formed – noting that herein we show formation of ILFs to demonstrate that they are a product of vacuole fusion (**Figures 13C, 14B, 16B and 17D; Movies S12 – S19**). Also, herein we show that addition of rapamycin affects protein degradation by the vReD pathway, suggesting that this method has off-target effects that interfere with the interpretation of the data. Importantly, these vesicles are only observed in an unusual mutant background (Zhu et al., 2017). Thus, given that the method of ubiquitylation to trigger degradation and the genetic background are not found in nature, it is not clear whether this process is physiologically relevant. Whereas, herein we show how these two pathways contribute to protein turnover in wild type cells under normal growth conditions. Thus, in all, our data support the original model describing the vReD pathway that requires an endosomal intermediate, possibly permitting lysosomal polytopic protein recycling, as it does for surface proteins.

The second distinction between the ILF and vReD pathways is organelle copy number: The vReD pathway can function when cells contain only a single vacuolar lysosome. However, because it requires merger of two organelle membranes, the ILF pathway functions only in cells with two or more vacuoles. Although this distinction seems trivial, it is worth noting that most micrographs presented in the reports by Emr and colleagues exclusively show cells containing single vacuoles (Li et al., 2015a; Li et al., 2015b; Zhu et al., 2017), which only permits analysis of the vReD pathway. Here we use an unbiased approach to study both pathways, by studying all cells in the population, i.e. those with single or multiple vacuoles. When conducting experiments, we did notice that GFP-positive puncta were more likely to be found in cells containing single vacuoles, suggesting that the vRed pathway may prevail in these cells, whereas the ILF pathway would only contribute to vacuolar lysosome protein turnover in cells with multiple organelles. When considering this idea, it is important to note that metazoan cells contain hundreds to thousands of lysosomes (Luzio et al., 2014). These organelles are particularly mobile and

frequently make contact often resulting in fusion (Wang et al., 2002; Luzio et al., 2007; Wickner, 2010). Each of these fusion events could accommodate protein turnover by the ILF pathway, which seems like a logical and efficient mechanism for maintaining organelle homeostasis or accommodating proteome remodeling. Whereas, the vReD pathway requires multiple membrane trafficking steps and seems to be most relevant when only a single vacuolar lysosome is present – something that never occurs in metazoan cells – questioning its relevance to human cell physiology.

4.5.4 Physiological relevance

What roles do these pathways potentially play in lysosome and cell physiology? All proteins have finite lifetimes. Lysosomal transporter proteins are proposed to have shorter than average lifetimes because their lumenal faces are exposed to acid hydrolases making them particularly susceptible to damage. In support of this idea, here we find that both the ILF and vReD pathways constitutively turnover (presumably defective) nutrient transporters from the vacuolar lysosome membrane. Without such mechanisms in place, these damaged proteins would accumulate, which is thought to permeabilize the lysosome membrane. This in turn facilitates release of lumenal hydrolases into the cytoplasm, which is catastrophic for the cell and implicated in cell death programs (Aits and Jäättelä, 2013; Donida et al., 2017). Here we find the ILF pathway clears and degrades misfolded lysosomal polytopic proteins and thus we speculate that its function is critical for preserving lysosome integrity necessary for cell survival or it may be inhibited during programmed cell death.

Beyond potential roles in organelle homeostasis, the protein landscape on the lysosome membrane defines organellar signaling properties (by possibly regulating levels of Ca^{2+} transporter or channels) and metabolic output (by changing the repertoire of nutrient transporters). This is akin to altering the expression profile of transporters or receptors on the plasma membrane in response to changes in nutrient levels or cellular signaling to mediate a myriad of physiological events. Here we show that the ILF and vReD pathways respond to similar stimuli to selectively down regulate some nutrient transporters and speculate that this alters organelle function for diverse cell physiology, including the cellular aging program that depends on changes in lysosome function (Carmona-Gutierrez et al., 2016). The machinery underlying both pathways and most client proteins are evolutionarily conserved, suggesting that

they contribute to lysosome physiology in all eukaryotic cells. However, currently neither pathway has been shown to function in metazoan cells. But we hypothesize that they also determine lysosomal polytopic protein lifetimes and contribute to lysosome physiology in a similar manner, whereby they may also contribute to human lysosomal disorders linked to mutations in lysosomal transporters, e.g. the cholesterol transporter Ncr1 and Niemann-Pick type C disease (Parenti et al., 2015).

Chapter 5. Discussion

5.1 Overview

We sought to investigate how eukaryotic cells control the expression levels of lysosomal polytopic proteins and combat ESCRT-impairment using *Saccharomyces cerevisiae* and its vacuolar lysosome as models. All proteins tested and their primary cellular functions are listed in **Table 5**. This work is represented as three publications, each an individual chapter with conclusions as follows:

In Chapter 2, we discovered a new cellular protein degradation pathway, that we named the IntraLumenal Fragment (ILF) pathway, which intrinsically accommodates the internalization and degradation of resident vacuolar lysosome polytopic proteins. Prior to this work, these proteins lacked a described mechanism of regulated turnover, despite their obvious importance to eukaryotic cell physiology. We found that resident nutrient transporters are selectively sorted, internalized, and degraded within the lysosomal (vacuolar) lumen upon homotypic organelle membrane fusion (**Figures 2** and **3**). Importantly, we show that this process is independent of the autophagy or ESCRT machinery (**Figure S4** and **S5**) and instead relies on the membrane fusion machinery, specifically the Rab GTPase Ypt7 for protein sorting and internalization (**Figures 7** and **S6**). These proteins have diverse lifetimes (**Figures 2** and **3**) that are regulated in response to protein quality control (**Figure 4**), changes in cognate substrate levels (**Figure 6**), and TOR activation induced by cycloheximide treatment (**Figures 5** and **S2**). We propose that the ILF pathway plays a critical role in lysosome remodeling and homeostasis by changing the lysosomal membrane protein landscape to accommodate changes in cell physiology, such as clearing misfolded proteins to retain organelle function or as cells age.

In Chapter 3, we demonstrate that plasma membrane polytopic proteins, such as surface receptors and transporter, can also be sorted for degradation by the ILF pathway when localized to the vacuolar membrane. This work illustrates how the ILF pathway can accommodate the degradation of known ESCRT client proteins by compensating for the MultiVesicular Body pathway when MVB formation is impaired (**Figures 9, 11, 12 S10** and **S12**), thus permitting cell survival. In addition, we show that some surface proteins can bypass ESCRT machinery for degradation by the ILF pathway, identifying the ILF pathway as an ESCRT-independent pathway for surface protein turnover (**Figures 10** and **S9**). In both cases, surface proteins that are internalized by endocytosis avoid packaging into intralumenal vesicles and upon fusion between

the endosome and the lysosome, proteins are redistributed to the lysosomal membrane where they can interact with and be sorted by the membrane fusion machinery for degradation (**Figures 10, 11, 12, S9** and **S11**). Surface protein sorting and degradation by the ILF pathway is in response to changes in substrate levels (**Figures 9** and **S8**), upon protein misfolding (**Figures 10, 11, S9** and **S10**) and in response to TOR activation (**Figures 12** and **S11**). Our data suggests that the ILF pathway is an important contributor to the overall regulation of not only lysosomal membrane proteins, but also of surface polytopic proteins. Thus, we propose that the ILF pathway can likely degrade other proteins within eukaryotic cells if they can localize to lysosomal membranes, such as soluble proteins known to function at lysosomal membranes.

In Chapter 4, we addressed the contributions of the ILF and vReD (Vacuole membrane REcycling and Degradation) pathways in remodeling the lysosomal polytopic protein landscape and found that the two pathways complement each other. Since the vReD pathway has only been shown to function in response to changes in substrate levels, we first concluded that the ILF pathway constitutively degrades both previously reported vReD cargoes, Ypq1 and Cot1, in the presence or absence of ESCRT proteins (**Figure 13**). We identified a new, constitutive vReD cargo, the amino acid permease Vba4, and confirmed that sorting by vReD requires the ESCRT-machinery (**Figures 14** and **15**). Similar to surface protein degradation, the ILF pathway compensates for ESCRT impairment (**Figures 14** and **15**). Lastly, we show that all lysosomal membrane proteins tested, including Vba4, are shunted into the boundary membrane for degradation upon heat stress (**Figures 17** and **18**). This key finding highlights the ILF pathway as a universal quality control mechanism for lysosomal polytopic protein turnover, contributing to preserving organelle integrity and cellular homeostasis.

Taken together, we have identified several vital physiological roles the ILF pathway performs within cells. First, we demonstrated that the ILF pathway controls the quantity and *quality* of polytopic proteins, acting as a critical quality control mechanism (**Figures 4, 10, 11, 17, 18, S9** and **S10**). Proteins are constantly at risk of misfolding. In order to properly fulfill its cellular function, a protein must achieve the appropriate conformation and localize to the correct cellular compartment. Due to the high diversity of proteins and the types of damage that can induce misfolding, eukaryotic cells have evolved elaborate quality control networks to remove misfolded proteins in various cellular compartments, such as the cytoplasm, nucleus,

endoplasmic reticulum, and mitochondria (Ciechanover and Kwon, 2015) to avoid proteotoxicity and preserve cellular viability. These quality control mechanisms are capable of monitoring and maintaining the cellular proteome whereby misfolded proteins can be refolded, degraded, or sequestered into specialized quality control compartments to maintain protein homeostasis, or "proteostasis" (Balch et al., 2008). Appropriate clearance of these misfolded proteins is essential as their accumulation will ultimately compromise cellular homeostasis and many human diseases, including lysosomal storage disorders (Valastyan and Lindquist, 2014), cancer (Xu et al., 2011), cystic fibrosis (Koulov et al., 2010), and numerous neurodegenerative disorders (Voisine et al., 2010) are linked to protein misfolding or aggregation. Additionally, one function of the MVB pathway is to clear misfolded surface proteins from the plasma membrane. Since the ILF pathway is analogous to the MVB pathway but functioning at lysosomal membranes, it is not surprising that the ILF pathway is also implicated in the clearance of misfolded polytopic proteins, to preserve organelle function and avoid proteotoxicity. Understanding how the ILF pathway functions as a protein quality control mechanism in recognizing and targeting misfolded proteins for degradation could unveil new therapeutic strategies or targets in various neurodegenerative diseases linked with toxic accumulation of protein aggregates including Alzheimer's, Parkinson's, and Huntington's disease.

Equally important to proteostasis is the regulation of ions and nutrients, which requires transporter function. Numerous studies have shown that the MVB pathway functions to downregulate surface transporters in response to changes in cognate substrate levels. Under normal growth conditions, surface transporters such as Gap1 (a general amino acid permease), Can1 (an arginine permease), and Mup1 (a methionine permease) are stable and active at the plasma membrane. However, in response to excess substrates, these transporters undergo ubiquitin-dependent endocytosis and delivery to the lysosomal lumen for degradation (MacDonald et al., 2012; Ghaddar et al., 2014). This represents an important mechanism for regulating nutrient transporter levels at the surface to balance between nutrient uptake from the extracellular environment and metabolism. Since the lysosome is crucial for nutrient sensing and for the storage of biomaterials, a similar mechanism is necessary to balance transporter levels and intracellular nutrient levels. Here we demonstrate that the ILF pathway performs a related function acting at the vacuolar lysosome by regulating the degradation of Vph1-GFP, a component of the V-ATPase, in response to changes in cytoplasmic pH (**Figure 6**). Importantly,

we confirm that this substrate-induced degradation is selective, whereby degradation of only the transporter recognizing the substrate is either stimulated or suppressed (**Figures 6 and S3**).

Lastly, we demonstrate that the ILF pathway can regulate protein lifetimes in response to TOR activation induced by cycloheximide treatment (**Figures 5, 12, 16, S2, S11** and **S12**). The mechanistic Target of Rapamycin (mTOR) is a critical signaling serine/threonine kinase important for a variety of cellular processes including cellular metabolism, regulating organismal growth and homeostasis, and for supplying the cell with nutrients under metabolic stress conditions (Laplante and Sabatini, 2012; Perera and Zoncu, 2016). mTOR (TOR in yeast) is essential for lysosomal (or vacuolar) nutrient sensing and metabolic regulation through their physical and functional association. mTOR interacts with several different proteins to form two distinct complexes, mTOR complex 1 (mTORC1) and mTOR complex 2 (mTORC2). Of the two complexes, mTORC1 is better characterized and often referred to as the master regulator of cell growth and proliferation. mTORC1 is responsible for modulating cellular metabolism by incorporating environmental and cellular cues, such as growth factors, energy levels, cellular stress or amino acids (Dunlop and Tee, 2009). By integrating these cues, mTORC1 can promote growth through phosphorylating substrates that promote biosynthetic processes, such as mRNA translation and lipid synthesis, or substrates that inhibit catabolic pathways like autophagy.

It has been previously shown that some surface transporters undergo ubiquitin-dependent endocytic downregulation in response to TOR activation triggered by cycloheximide (MacGurn et al., 2011). In this case, addition of cycloheximide mimics nutrient replete conditions, thus boosting intracellular amino acid levels and activating TOR. Once activated, TOR functions to control elevated nutrient levels by regulating the abundance of transporter proteins on the surface. The same logic holds true in reference to the lysosome and its membrane proteins. The addition of cycloheximide triggers a cellular response to combat the changes in nutrient availability and uptake by stimulating lysosomal transporter degradation by the ILF pathway. Furthermore, TOR is directly associated with the lysosome allowing for continuous communication and the ability for quick adaptation in response to stress conditions. Since the lysosome is a critical source of nutrients for the cell and TOR is important for integrating lysosomal and cytoplasmic nutrient information, the ILF pathway could represent one way to remodel the lysosomal membrane in response to metabolic stress.

Our studies describe another mechanism for selective cellular protein degradation that is intrinsic to homotypic organelle membrane fusion. Just as the discovery of endocytosis was paramount to our understanding of how surface transporters and receptors contribute to cell physiology, the IntraLumenal Fragment pathway will likely have similar impact on our understanding of lysosome physiology and function. We propose that the ILF pathway plays a critical role in lysosome remodeling and homeostasis by changing the membrane protein landscape to accommodate changes in cell physiology, such as clearing misfolded proteins to retain organelle function or as cells age. The ILF pathway may also reveal new contributions to overall cellular physiology, thus contributing to our fundamental understanding of metabolic regulation and may point to new therapeutic avenues in several human diseases including storage disorders, neurological diseases, and cancers.

Table 5. List of polytopic proteins studied and their primary cellular function

	Mammalian homolog	Cellular function
Lysosomal polytopic		
Fth1	NRAMP1	Iron efflux transporter
Fet5	Hephaestin	Multicopper oxidase,
Vph1	ATP6V0A1	V_0 subunit of H^+-ATPase
Cot1	ZnT2	Zinc transporter
Ncr1	NPC1	Sterol transporter
Ybt1	ABCC/MRP	Bile acid and phosphatidylcholine transporter
Ycf1	CFTR	Glutathione transporter
Sna4	?	Potential Rsp5 adaptor protein
Vba4	Major facilitator superfamily	Basic amino acid transporter
Ypq1	PQLC2	Cationic amino acid transporter
Surface polytopic		
Mup1	LAT1	Methionine permease
Can1	CAT/SLC7	Arginine permease
Hxt3	GLUT/SLC2	Glucose transporter
Aqr1	Major facilitator superfamily	Major facilitator superfamily-type transporter that excretes amino acids
Ste3	GPCRs	a-factor pheromone receptor
Itr1	HMIT	Myo-inositol transporter

5.2 Future Directions

The discovery of the IntraLumenal Fragment pathway has opened new avenues to assess protein degradation and its contributions to eukaryotic cell physiology; however several central questions persist:

Herein, we demonstrate that the ILF pathway can sort and degrade non-lysosomal membrane proteins (**Chapter 3**), but can it degrade soluble proteins, lysosomal membrane-associated proteins or lipids? For example, the EGO (Exit from G_0) GTPase complex (homologous to the mammalian Rag-GTPase complex Ragulator) is a vacuolar-membrane-associated protein complex that interacts with and activates TORC1 to mediate amino acid signaling (Binda et al., 2009; Zoncu et al., 2011; Kingsbury et al., 2014). Thus, it is likely that the ILF pathway can selectively degrade components of the EGO complex as well as TORC1 – which in yeast is constitutively located on the vacuolar membrane while mammalian (m)TORC1 is recruited to lysosomal membranes upon amino acid signaling (Zoncu et al., 2011). Just as the protein machinery (HOPS, Ypt7 and SNAREs) concentrates at the vertex domain to promote organelle membrane fusion (Wang et al., 2002) fusogenic, regulatory lipids also play a critical role in fusion events. Regulatory lipids, including phosphatidylinositol 3-phosphate (PI(3)P), phosphatidylinositol 4,5-bisphosphate ($PI(4,5)P_2$), ergosterol (a yeast sterol), and diacylglycerol (DAG), are recruited to and concentrate at the vertex domain and work together with fusion proteins to assemble the vertex ring and facilitate bilayer merger (Fratti et al., 2004). While it has yet to be formally tested, DAG appears to concentrate within the boundary membrane (Fratti et al., 2004), thus perhaps the ILF pathway can accommodate the selective turnover of DAG or other lipids if they remain present within the boundary upon organelle membrane fusion.

While we demonstrated that the ILF pathway is a critical component of the protein quality control network, how else does this pathway contribute to organelle and cell physiology? One possibility is that the ILF pathways may function to maintain lysosomal membrane integrity. The lysosomal lumen is occupied with a wide variety of hydrolases for the catabolism of various biomaterials. In order to retain these hydrolases in the lumen, the lysosomal limiting membrane must remain stable. If the lysosomal membrane destabilizes and becomes permeable, the lumenal contents including hydrolases, such as cathepsins, translocate to the cytosol. This leakage

eventually leads to cell death through a pathway called lysosomal cell death (LCD), partially due to the acidification of the cytoplasm and to the degradative activity of the released cathepsins, as cathepsins B and D are still active at neutral pH (Aits and Jäättelä, 2013; Gómez-Sintes et al., 2016).

One cause of lysosomal membrane permeabilization and LCD is oxidative stress caused by reactive oxygen species (ROS). At low levels, ROS are necessary for many biochemical pathways; however when in excess they lead to the oxidation of a variety of biomaterials leading to membrane protein inactivation, DNA mutation induction, alteration of lysosomal enzymatic activities, or lipid membrane instability (Aits and Jäättelä, 2013; Donida et al., 2017). In all cases, consequences of oxidative stress eventually cause lysosomal membrane destabilization and cell death. In addition, a relationship between lysosomal storage disorders (LSDs) and oxidative stress has recently emerged. LSDs are characterized by the abnormal accumulation of substances within the lysosomal lumen due to a genetic defect in a gene encoding a lysosomal hydrolytic enzyme, transporter protein or other gene products critical for lysosome function (Ballabio and Gieselmann, 2009). The increase in biomaterials present within the lysosomal lumen is coupled with an increase in the number and size of lysosomes, ultimately leading to lysosome dysfunction and multisystemic manifestations. Together, this may induce the excessive production of reactive species or the depletion of antioxidant capacity resulting in biomolecule oxidative stress (Donida et al., 2017). Thus, cellular damage due to oxidative stress likely contributes to the pathophysiology of numerous LSDs. The ILF pathway could potentially contribute to membrane remodeling and maintain organelle stability by removing proteins inactivated due to ROS or by changing the lipid composition to prevent the lysosome from permeabilization and consequent cathepsin leakage.

The lysosome is also largely linked with aging, whereby both physical and chemical properties of the lysosome are altered over time. In general, protein degradation declines with age, leading to an increase in the overall cellular protein content, many of which possess inappropriate posttranslational modifications (Cuervo and Dice, 2000a). While there are likely many causes for the age-related decrease in lysosomal activity and proteolysis, one contributing factor is an increase in lysosomal membrane fragility. As mentioned, lysosomal membrane proteins and lipids are sensitive to oxidative stress causing membrane instability and fragility. With age, lysosomal membranes become more fragile and sensitive to oxidative stress, ultimately

leading to an increased susceptibility for membrane permeabilization and LCD. In addition, the membrane lipid composition influences a variety of lysosomal functions, thus any change in the levels of important lipids can affect not only lysosome integrity, but also membrane fusion events and the stability of polytopic proteins (Fraldi et al., 2010; Gómez-Sintes et al., 2016). Further research is needed to identify if there are any specific age-related changes in lysosomal lipid composition, however given their central role in organelle physiology it would not be unexpected. If the ILF pathway is capable of selectively degrading lipids, stimulating their degradation might be able to overcome some of the physical alterations to the lysosome caused by aging.

A number of age-related diseases are also associated with lysosome membrane permeabilization and damage including Alzheimer's disease, Parkinson's disease, and Amyotrophic lateral sclerosis, among others. These diseases exhibit neurological pathology, as with age neurons are particularly vulnerable to lysosomal defects. The exact reasons for this sensitivity remain elusive; however it may be due in part to their limited regenerative capacity or their lack of compensatory cellular metabolic pathways. In these diseases, aggregate-prone proteins, mainly delivered through autophagy, accumulate within the lysosome representing a pathological hallmark of each disease (Bellettato and Scarpa et al., 2010; Appelqvist et al., 2013; Settembre et al., 2013). Akin to lysosomal storage disorders, abnormal substance build up in the lysosome leads to progressive loss of normal cellular function coupled with neurodegeneration. Furthermore, an imbalance in the activity of cathepsins in neurons has been detected during aging, further contributing to neurodegeneration (Gómez-Sintes et al., 2016). Perhaps stimulating the ILF pathway to selectively eliminate associated aggregate-prone proteins may facilitate new therapeutic approaches to treatment these diseases.

Is the ILF pathway evolutionarily conserved? Here, we demonstrate that the ILF pathway functions within yeast cells and well as on purified vacuoles, but does the same hold true in higher eukaryotic organisms? We speculate that the ILF pathway does exist in all eukaryotic cells as the underlying molecular machinery is evolutionarily conserved and all of the proteins studied, have mammalian orthologues. In addition, the fundamental research uncovering other cellular degradation pathways including autophagy and the MVB pathway, were first discovered in yeast and later confirmed in higher eukaryotes. Since lysosomal compartments are found to exist in all

eukaryotic organisms, using other model organisms such as *Caenorhabditis elegans*, *Arabidopsis thaliana*, or *Drosophila* could aid in confirming that the ILF pathway is evolutionarily conserved. Additionally, lumenal fragments have been observed within the lysosomes of *C. elegans* (Treusch et al., 2004; Holmes et al., 2007), *A. thaliana* (Scheuring et al., 2015) and *Drosophila* (Corrigan et al., 2014), but the events resulting in these fragments remains to be elucidated.

References

Aits, S., and Jäättelä, M. (2013) Lysosomal cell death at a glance. J. Cell Sci. *126*, 1905-1912.

Alfred, V., and Vaccari, T. (2016) When membranes need an ESCRT: endosomal sorting and membrane remodelling in health and disease. Swiss Med. Wkly. *146*, w14347.

Andrews, N.W. (2002) Lysosomes and the plasma membrane. J. Cell Biol. *158*, 389-394.

Appleqvist, H., Wäster, P., Kågedal, K., and Öllinger, K. (2013). The lysosome: from waste bag to potential therapeutic target. J. Mol. Cell Biol. *5*, 214-226.

Aris, J.P., Fishwick, L.K., Marraffini, M.L., Seo, A.Y., Leeuwenburgh, C., and Dunn, W.A. (2012) Amino acid homeostasis and chronological longevity in *Saccharomyces cerevisiae*. Subcell. Biochem. *51*, 161-186.

Arlt, H., Perz, A., and Ungermann, C. (2011) An overexpression screen in *Saccharomyces cerevisiae* identifies novel genes that affect endocytic protein trafficking. *Traffic* 12: 1592-1603.

Babst, M., Katzmann, D.J., Snyder, W.B., Wendland, B., and Emr, S.D. (2002) Endosome-associated complex, ESCRT-II, recruits transport machinery for protein sorting at the multivesicular body. Dev. Cell *3*, 283-289.

Babst, M. (2011) MVB vesicle formation: ESCRT-dependent, ESCRT-independent and everything in between. Curr. Opin. Cell Biol. *23*, 452-457.

Babst, M. (2014) Quality control at the plasma membrane: one mechanism does not fit all. J. Cell Biol. *205*, 11-20.

Baker, R.W., Jeffrey, P.D., Zick, M., Phillips, B.P., Wickner, W., and Hughson, F.M. (2015) A direct role for the Sec1/Munc18-family protein Vps33 as a template for SNARE assembly. Science *349*, 1111-1114.

Balderhaar, H.J.K., and Ungermann, C. (2013) CORVET and HOPS tethering complexes – coordinators of endosome and lysosome fusion. J. Cell Sci. *126*, 1307-1316.

Ballabio, A., and Gieselmann, V. (2009) Lysosomal disorders: From storage to cellular damage. Biochim. Biophys. Acta *1793*, 684-696.

Beck, T., Schmidt, A., and Hall, M.N. (1999) Starvation induces vacuolar targeting and degradation of the tryptophan permease in yeast. J. Cell Biol. *146*, 1227-1238.

Bellettato, C.M., and Scarpa, M. (2010) Pathophysiology of neuropathic lysosomal storage disorders. J. Inherit. Metab. Dis. *33*, 347-362.

Berger, A.C., Hanson, P.K., Nichols, J.W., and Corbett, A.H. (2005) A Yeast Model System for Functional Analysis of the Niemann-Pick Type C Protein 1 Homolog, Ncr1p. Traffic *6*, 907-917.

Berkower, C., Loayza, D., and Michaelis, S. (1994) Metabolic instability and constitutive endocytosis of STE6, the a-factor transporter of *Saccharomyces cerevisiae*. Mol. Biol. Cell *5*, 1185-1198.

Binda, M., Péli-Gulli, M-P., Bonfils, G., Panchaud, N., Urban, J., Sturgill, T.W., Loewith, R., and De Virgillo, C. (2009) The Vam6 GEF controls TORC1 by activating the EGO complex. Mol. Cell *35*, 563-573.

Blach, W.E., Morimoto, R.I., Dillin, A., and Kelly, J.W. (2008) Adapting proteostasis for disease intervention. Science *319*, 916-919.

Blanc, C., Charette, S.J., Mattei, S., Aubry, L., Smith, E.W., Cosson, P., and Letourneur, F. (2009) Dictyostelium Tom1 participates to an ancestral ESCRT-0 complex. Traffic *10*, 161-171.

Blondel, M.O., Morvan, J., Dupré, S., Urban-Grimal, D., Haguenauer-Tsapis, R., and Volland, C. (2004) Direct sorting of the yeast uracil permease to the endosomal system is controlled by uracil binding and Rsp5p-dependent ubiquitylation. Mol. Biol. Cell *15*, 883-895.

Blott, E.J., and Griffiths, G.M. (2002) Secretory lysosomes. Nat. Rev. Mol. Cell Biol. *3*, 122-131.

Bowers, K., Piper, S.C., Edeling, M.A., Gray, S.R., Owen, D.J., Lehner, P.J., and Luzio, J.P. (2006) Degradation of endocytosed epidermal growth factor and virally ubiquitinated major histocompatibility complex class I is independent of mammalian ESCRTII. J. Biol. Chem. *281*, 5094-5105.

Brett, C.L., Tukaye, D.N., Mukherjee, S., and Rao, R. (2005) The yeast endosomal $Na^+(K^+)/H^+$ exchanger Nhx1 regulates cellular pH to control vesicle trafficking. Mol. Biol. Cell *16*, 1396-1405.

Brett, C.L., and Merz, A.J. (2008) Osmotic regulation of Rab-mediated organelle docking. Curr Biol. *18*, 1072-1077.

Brett, C.L., Plemel, R.L., Lobingier, B.T., Vignali, M., Fields, S., and Merz, A.J. (2008) Efficient termination of vacuolar Rab GTPase signaling requires coordinated action by a GAP and a protein kinase. J Cell Biol. *182*, 1141-1151.

Cabrera, M., and Ungermann, C. (2008) Purification and in vitro analysis of yeast vacuoles. Methods Enzymol. *451*, 177-96.

Cabrera, M., and Ungermann, C. (2013) Guanine nucleotide exchange factors (GEFs) have a critical but not exclusive role in organelle localization of Rab GTPases. J. Biol. Chem. *288*, 28704-28712.

Carlton, J.G., and Martin-Serrano, J. (2007) Parallels between cytokinesis and retroviral budding: a role for the ESCRT machinery. Science *316*, 1908-1912.

Carmona-Gutierrez, D., Hughes, A.L., Madeo, F., and Ruckenstuhl, C. (2016) The crucial impact of lysosomes in aging and longevity. Aging Res. Rev. *32*, 2-12.

Chassefeyre, R., Martínez-Hernández, J., Bertaso, F., Bouquier, N., Blot, B., Laporte, M., Fraboulet, S., Couté, Y., Devoy, A., Isaacs, A.M., Pernet-Gallay, K., Sadoul, R., Fagni, L., and Goldberg, Y. (2015) Regulation of postsynaptic function by the dementia-related ESCRT-III subunit CHMP2B. J. Neurosci. *35*, 3155-3173.

Chen, B., Retzlaff, M., Roos, T., and Frydman, J. (2011) Cellular strategies of protein quality control. Cold Spring Harb. Perspect. Biol. *3*, a004374.

Chen, L.Q., Cheung, L.S., Feng, L., Tanner, W., and Frommer, W.B. (2015) Transport of sugars. Annu. Rev. Biochem. *84*, 865-894.

Chou, H.T., Dukovski, D., Chambers, M.G., Reinisch, K.M., and Walz, T. (2016) CATCHR, HOPS and CORVET tethering complexes share a similar architecture. Nat. Struct. Mol. Biol. *23*, 761-763.

Ciechanover, A., and Kwon, Y.T. (2015) Degradation of misfolded proteins in neurodegenerative diseases: therapeutic targets and strategies. Exp. Mol. Med. *47*, e147. doi: 10.1038/emm.2014.117.

Claessen, J.H.L., Kundrat, L., and Ploegh, H.L. (2011) Protein quality control in the ER: balancing the ubiquitin chequebook. Trends Cell Biol. *22*, 22-32.

Corrigan, L., Redhai, S., Leiblich, A., Fan, S-J., Perera, S.M.W., Patel, R., Gandy, C., Wainwright, S.M., Morris, J.F., Hamdy, F., Goberdhan, D.C.I., and Wilson, C. (2014) BMP-regulated exosomes from *Drosophila* male reproductive glands reprogram female behavior. J. Cell Biol. *206*, 671-688.

Cuervo, A.M., and Dice, J.F. (2000a) When lysosomes get old. Exp. Gerontol. *35*, 119-131.

Cuervo, A.M., and Dice, J.F. (2000b) Age-related decline in chaperone-mediated autophagy. J. Biol. Chem. *40*, 31505-31513.

D'Agostino, M., Risselada, H.J., and Mayer, A. (2016) Steric hindrance of SNARE transmembrane domain organization impairs the hemifusion-to-fusion transition. EMBO Rep. e201642209.

Davis, N.G., Horecka, J.L., and Sprague, Jr. G.F. (1993) *Cis*- and *Trans*-acting functions required for endocytosis of the yeast pheromone receptors. J Cell Biol. *122*, 53-65.

Davies, B.A., Lee, J.R.E., Oestreich, A.J., and Katzmann, D.J. (2009) Membrane protein targeting to the MVB/Lysosome. Chem. Rev. *109*, 1575-1586.

de Duve, C., and Wattiaux, R. (1966) Functions of lysosomes. Annu. Rev. Physiol. *28*, 435-492.

Diakov, T.T., and Kane, P.M. (2010) Regulation of vacuolar proton-translocating ATPase activity and assembly by extracellular pH. J. Biol. Chem. *285*, 23771-23778.

Dhonukshe, P., Baluška, F., Schlicht, M., Hlavacka, A., Šamaj, J., Friml, J., and Gadella, T.W.J. (2006) Endocytosis of cell surface material mediates cell plate formation during plant cytokinesis. Dev. Cell *10*, 137-150.

Donida, B., Jacques, C.E.D., Mescka, C.P., Rodrigues, D.G.B., Marchetti, D.P., Ribas, G., Giugliani, R., and Vargas, C.R. (2017) Oxidative damage and redox in Lysosomal Storage Disorders: Biochemical markers. Clin. Chim. Acta *466*, 46-53.

Dunlop, E.A., and Tee, A.R. (2009) Mammalian target of rapamycin complex 1: Signalling inputs, substrates and feedback mechanisms. Cell. Signal. *21*, 827-835.

Edgar, J.R., Eden, E.R., and Futter, C.E. (2014) Hrs- and CD63-dependent competing mechanisms make different sized endosomal intraluminal vesicles. Traffic. *15*, 197-211.

Efeyan, A., Zoncu, R., and Sabatini, D.M. (2012) Amino acids and mTORC1: from lysosomes to disease. Trends Mol. Med. *18*, 524-533.

Egner, R., Mahé, Y., Pandjaitan, R., and Kuchler, K. (1995) Endocytosis and vacuolar degradation of the plasma membrane-localized Pdr5 ATP-binding cassette multidrug transporter in *Saccharomyces cerevisiae*. Mol. Cell Biol. *15*, 5879-5887.

Ehrnstorfer, I.A., Geertsma, E.R., Pardon, E., Steyaert, J., and Dutzler, R. (2011) Crystal structure of a SLC11 (NRAMP) transporter reveals the basis for transition-metal ion transport. Nat. Strcut. Mol. Biol. *11*, 990-996.

Eitzen, G., Will, E., Gallwitz, D., Haas, A., and Wickner, W. (2000) Sequential action of two GTPases to promote vacuole docking and fusion. EMBO J. *19*, 6713-6720.

Epp, N., Rethmeier, R., Krämer, L., and Ungermann, C. (2011) Membrane dynamics and fusion at late endosomes and vacuoles - Rab regulation, multisubunit tethering complexes and SNAREs. Eur. J. Cell Biol. *90*, 779–785.

Fagerberg, L., Jonasson, K., von Heijne, G., Uhlén, M., and Berglund, L. (2010) Prediction of the human membrane proteome. Proteomics *10*, 1141-1149.

Fang, N.N., Chan, G.T., Zhu, M., Comyn, S.A., Persaud, A., Deshaies, R.J., Rotin, D., Gsponer, J., and Mayor, T. (2014) Rsp5/Nedd4 is the main ubiquitin ligase that targets cytosolic misfolded proteins following heat stress. Nat. Cell Biol. *16*, 1227-1237.

Fasshauer, D., Sutton, R.B., Brunger, A.T., and Jahn, R. (1998) Conserved structural features of the synaptic fusion complex: SNARE proteins reclassified as Q- and R-SNAREs. Proc. Natl. Acad. Sci. USA *95*, 15781-15786.

Ferguson, S.M. (2015) Beyond indigestion: emerging roles for lysosome-based signaling in human disease. Curr. Opin. Cell Biol. *35*, 59-68.

Feyder, S., De Craene, J-O., Bar, S., Bertazzi, D.L., and Friant, S. (2015) Membrane trafficking in the yeast *Saccharomyces cerevisiae* model. Int. J. Mol. Sci. *16*, 1509-1525.

Fraldi, A., Annunziata, F., Lombardi, A., Kaiser, H.J., Medina, D.L., Spampanato, C., Fedele, A.O., Polischuk, R., Sorrentino, N.C., Simons, K., and Ballabio, A. (2010) Lysosomal fusion and SNARE function are impaired by cholesterol accumulation in lysosomal storage disorders. EMBO J *29*, 3607-3620.

Fratti, R.A., Jun, Y., Merz, A.J., Margolis, N., and Wickner, W. (2004) Interdependent assembly of specific regulatory lipids and membrane fusion proteins into the vertex ring domain of docked vacuoles. J Cell Biol. *167*, 1087-1098.

Forgac, M. (2007) Vacuolar ATPases: rotary proton pumps in physiology and pathophysiology. Nat. Rev. Mol. Cell Biol. *8*, 917-929.

Futter, C.E., Pearse, A., Hewlett, L.J., and Hopkins, C.R. (1996) Multivesicular endosomes containing internalized EGF-EGF receptor complexes mature and then fuse directly with lysosomes. J. Cell Biol. *132*, 1011-1023.

Ghaddar, K., Merhi, A., Saliba, E., Krammer, E.M., Prévost, M., and André, B. (2014) Substrate-induced ubiquitylation and endocytosis of yeast amino acid permeases. Mol. Cell Biol. *34*, 4447-4463.

Glickman, M.H., and Ciechanover, A. (2002) The Ubiquitin-Proteasome proteolytic pathway: Destruction for the sake of construction. Physiol. Rev. *82*, 373-428.

Gómez-Sintes, R., Ledesma, M.D., and Boya, P. (2016) Lysosomal cell death mechanisms in aging. Ageing Res. Rev. *32*, 150-168.

Haas, A. (1995) A quantitative assay to measure homotypic vacuole fusion in vitro. Methods Cell Sci. *17*, 283-294.

Haigler, H.T., McKanna, J.A., and Cohen, S. (1979) Direct visualization of the binding and internalization of a ferritin conjugate of epidermal growth factor in human carcinoma cells A-431. J. Cell Biol. *81*, 382-395.

Hanson, P.I., and Cashikar, A. (2012) Multivesicular body morphogenesis. Annu. Rev. Cell Dev. Biol. *28*, 337-362

Henne, W.M., Buchkovich, N.J., and Emr, S.D. (2011) The ESCRT pathway. Dev. Cell *21*, 77-91.

Hennigar, S.R., and Kelleher, S.L. (2015) TNFα post-translationally targets ZnT2 to accumulate Zinc in lysosomes. J Cell Physiol. *10*, 2345-2350.

Hicke, L., and Riezman, H. (1996) Ubiquitination of a yeast plasma membrane receptor signals its ligand-stimulated endocytosis. Cell *84*, 277-287.

Hislop, J.N., and von Zastrow, M. (2011) Role of ubiquitination in endocytic trafficking of G-protein-coupled receptors. Traffic *12*, 137-148.

Holmes, A., Flett, A., Coudreuse, D., Korswagen, H.C., and Pettitt, J. (2007) *C. elegans* Disabled is required for cell-type specific endocytosis and is essential in animals lacking the AP-3 adaptor complex. J. Cell Sci. *120*, 2741-2751.

Hong, W. (2005) SNAREs and traffic. Biochim. Biophys. Acta *1744*, 120-144.

Horák, J. (2003) The role of ubiquitin in down-regulation and intracellular sorting of membrane proteins: insights from yeast. BBA-Biomembranes *1614*, 139-155.

Huh, W.K., Falvo, J.V., Gerke, L.C., Carroll, A.S., Howson, R.W., Weissman, J.S., and O'Shea, E.K. (2003) Global analysis of protein localization in budding yeast. Nature. *425*, 686-691.

Jaiswal, J.K., Andrews, N.W., and Simon, S.M. (2002) Membrane proximal lysosomes are the major vesicles responsible for calcium-dependent exocytosis in nonsecretory cells. J. Cell Biol. *159*, 625-635.

Jensen, L.T., Carroll, M.C., Hall, M.D., Harvey, C.J., Beese, S.E., and Culotta, V.C. (2009) Down-regulation of a manganese transporter in the face of metal toxicity. Mol. Biol. Cell *20*, 2810-2819.

Jezegou, A., Llinares, E., Anne, C., Kieffer-Jaquinod, S., O'Regan, S., Aupetit, J., Chabli, A., Sagne, C., Debacker, C., Chadefaux-Vekemans, B., Journet, A., Andre, B. and Gasnier, B. (2013) Heptahelical protein PQLC2 is a lysosomal cationic amino acid exporter underlying the action of cysteamine in cystinosis theraphy. *Proc Natl Acad Sci USA* 50: E3434-3443

Jiang, P., Nishimura, T., Sakamaki, Y., Itakura, E., Hatta, T., Natsume, T., and Mizushima, N. (2014) The HOPS complex mediates autophagosome-lysosome fusion through interaction with syntaxin 17. Mol. Biol. Cell *25*, 1327-1337.

Jones, C.B., Ott, E.M., Keener, J.M., Curtiss, M., Sandrin, V., and Babst, M. (2012) Regulation of membrane protein degradation by starvation-response pathways. Traffic *13*, 468-482.

Jun, Y., Thorngren, N., Starai, V.J., Fratti, R.A., Collins, K., and Wickner, W. (2006) Reversible, cooperative reactions of yeast vacuole docking. EMBO J *25*, 5260-5269.

Jun, Y., and Wickner, W. (2007) Assays of vacuole fusion resolve the stages of docking, lipid mixing, and content mixing. Proc. Natl. Acad. Sci. USA *104*, 13010-13015.

Jung, J., Genau, H.M., and Behrends, C. (2015) Amino acid-dependent mTORC1 regulation by the lysosomal membrane protein SLC38A9. Mol. Cell Biol. *14*, 2479-2494.

Kallunki, T., Olsen, O.D., and Jäättelä, M. (2013) Cancer-associated lysosomal changes: friends or foes? Oncogene *32*, 1995-2004.

Katzmann, D.J., Babst, M., and Emr, S.D. (2001) Ubiquitin-dependent sorting into the multivesicular body pathway requires the function of a conserved endosomal protein sorting complex, ESCRT-I. Cell *106*, 145-155.

Katzmann, D.J., Odorizzi, G., and Emr, S.D. (2002) Receptor downregulation and multivesicular-body sorting. Nat. Rev. Mol. Cell Biol. *3*, 893-905.

Katzmann, D.J., Stefan, C.J., Babst, M., and Emr, S.D. (2003) Vps27 recruits ESCRT machinery to endosomes during MVB sorting. J. Cell Biol. *162*, 413-423.

Kaushik, S., Bandyopadhyay, U., Sridhar, S., Kiffin, R., Martinez-Vicente, M., Kon, M., Orenstein, S.J., Wong, E., and Cuervo, A.M. (2011) Chaperone-mediated autophagy at a glance. J. Cell Sci. *124*, 495-499.

Kawai, K., Moriya, A., Uemura, S., and Abe, F. (2014) Functional implications and ubiquitin-dependent degradation of the peptide transporter Ptr2 in *Saccharomyces cerevisiae*. Eukaryot. Cell *13*, 1380-1392.

Kawano-Kawada, M., Pongcharoen, P., Kawahara, R., Yasuda, M., Yamasaki, T., Akiyama, K., Sekito, T., and Kakinuma, Y. (2015) Vba4p, a vacuolar membrane protein, is involved in the drug resistance and vacuolar morphology of *Saccharomyces cerevisiae*. Biosci. Biotechnol. Biochem. *40*, 279-287.

Keener, J.M., and Babst, M. (2013) Quality control and substrate-dependent downregulation of the nutrient transporter Fur4. Traffic *14*, 412-427.

Kingsbury, J.M., Sen, N.D., Maeda, T., Heitman, J., and Cardenas, M.E. (2014) Endolysosomal membrane trafficking complexes drive nutrient-dependent TORC1 signaling to control cell growth in *Saccharomyces cerevisiae*. Genetics *196*, 1077-1089.

Kiontke, S., Langemeyer, L., Kuhlee, A., Schuback, S., Raunser, S., Ungermann, C., and Kümmel, D. (2017) Architecture and mechanism of the late endosomal Rab7-like Ypt7 guanine nucleotide exchange factor complex Mon1-Ccz1. Nat. Commun. *8*, doi:10.1038/ncomms14034.

Kiss, K., Kucsma, N., Brozik, A., Tusnady, G.E., Bergam, P., van Niel, G., and Szakacs, G. (2015) Role of the N-terminal transmembrane domain in the endo-lysosomal targeting and function of the human ABCB6 protein. J Biochem. *1*, 127-139.

Klumperman, J., and Raposo, G. (2014) The complex ultrastructure of the endolysosomal system. Cold Spring Harb. Perspect. Biol. *6*, a016857.

Kolter, T., and Sandhoff, K. (2005) Principles of lysosome membrane digestion: stimulation of sphingolipid degradation by sphingolipid activator proteins and anion lysosomal lipids. Annu. Rev. Cell Dev. Biol. *21*, 81-103.

Koulov, A.V., LaPointe, P., Lu, B., Razvi, A., Coppinger, J., Dong, M-Q., Matteson, J., Laister, R., Arrowsmith, C., Yates, J.R., and Balch, W.E. (2010) Biological and structural basis for Aha1 regulation of Hsp90 ATPase activity in maintaining proteostasis in the human disease Cystic Fibrosis. Mol. Biol. Cell *21*, 871-884.

Koumanov, F., Pereira, V.J., Whitley, P.R., and Holman, G.D. (2012) GLUT4 traffic through an ESCRT-III-dependent sorting compartment in adipocytes. PLoS One *7*, e44141.

Kroemer, G., and Jäättelä, M. (2005) Lysosomes and autophagy in cell death control. Nat. Rev. Cancer *5*, 886-897.

Krsmanovic, T., Pawelec, A., Sydor, T., and Kölling, R. (2005) Control of Ste6 recycling by ubiquitination in the early endocytic pathway in yeast. Mol. Biol. Cell *16*, 2809-2821.

Laplante, M., and Sabatini, D.M. (2012) mTOR signaling in growth control and disease. Cell *149*, 274-293.

Lemus, L. and Goder, V. (2014) Regulation of endoplasmic reticulum-associated protein degradation (ERAD) by ubiquitin. Cells *3*, 824-847.

Leung, K.F., Dacks, J.B., and Field, M.C. (2008) Evolution of the multivesicular body ESCRT machinery; retention across the eukaryotic lineage. Traffic *9*, 1698-1716.

Lewis, M.J., and Pelham, H.R. (2009) Inefficient quality control of thermosensitive proteins on the plasma membrane. PLoS One *4*, e5038.

Li, M., Rong, Y., Chuang, Y., Peng, D., and Emr., S.D. (2015a) Ubiquitin-dependent lysosomal membrane protein sorting and degradation. Mol. Cell *57*, 467-478.

Li, M., Koshi, T., and Emr, S.D. (2015b) Membrane-anchored ubiquitin ligase complex is required for the turnover of lysosomal membrane proteins. J. Cell Biol. *211*, 639-652.

Li, S.C., and Kane, P.M. (2009) The yeast lysosome-like vacuole: Endpoint and crossroads. BBA-Mol. Cell Res. *1793*, 650-663.

Lim, C.Y., and Zoncu, R. (2016) The lysosomes as a command-and-control center for cellular metabolism. J. Cell Bio. *214*, 653-664.

Lin, C.H., MacGurn, J.A., Chu, T., Stefan, C.J., and Emr, S.D. (2008) Arrestin-related ubiquitin-ligase adaptors regulate endocytosis and protein turnover at the cell surface. Cell *135*, 714-725.

Lobert, V.H., and Stenmark, H. (2011) Cell polarity and migration: emerging role for the endosomal sorting machinery. Physiology (Bethesda) *26*, 171-180.

Loewith, R., and Hall, M.N. (2011) Target of Rapamycin (TOR) in nutrient signaling and growth control. Genetics *189*, 1177-1201.

Luzio, J.P., Pryor, P.R., and Bright, N.A. (2007) Lysosomes: fusion and function. Nat. Rev. Mol. Cell Biol. *8*, 622-632.

Luzio, J.P., Parkinson, M.D.J., Gray, S.R., and Bright, N.A. (2009) The delivery of endocytosed cargo to lysosomes. Biochem. Soc. Trans. *37*, 1019-1021.

MacDonald, I.R., and Ellis, R.J. (1969) Does cycloheximide inhibit protein synthesis specifically in plant tissues? Nature *222*, 791-792.

MacDonald, C., Stringer, D.K., and Piper, R.C. (2012) Sna3 is an Rsp5 adaptor protein that relies on ubiquitination for its MVB sorting. Traffic *13*, 586-598.

MacGurn, J.A., Hsu, P.C., Smolka, M.B., and Emr, S.D. (2011) TORC1 regulates endocytosis via Npr1-mediated phosphoinhibition of a ubiquitin ligase adaptor. Cell *147*, 1104-1117.

Mageswaran, S.K., Dixon, M.G., Curtiss, M., Keener, J.P., and Babst, M. (2014) Binding to any ESCRT can mediate ubiquitin-independent cargo sorting. Traffic *15*, 212-229.

Mageswaran, S.K., Johnson, N.K., Odorizzi, G., and Babst, M. (2015) Constitutively active ESCRT-II suppresses the MVB-sorting phenotype of ESCRT-0 and ESCRT-I mutants. Mol. Biol. Cell *3*, 554-568.

Mattie, S., McNally, E.K., Karim, M.A., Vali, H., and Brett, C.L. (2017) How and why intralumenal membrane fragments form during vacuolar lysosome fusion. Mol. Biol. Cell *28*, 309-321.

Maxfield, F.R., and McGraw, T.E. (2004) Endocytic recycling. Nat. Rev. Mol. Cell Biol. *5*, 121-132.

Mayer, A., and Wickner, W. (1997) Docking of yeast vacuoles is catalyzed by the Ras-like GTPase Ypt7p after symmetric priming by Sec18p (NSF). J Cell Biol. *136*, 307-317.

McNally, E.K., and Brett, C.L. *Submitted.* ESCRT-independent surface receptor and transporter protein degradation by the ILF pathway.

McNally, E.K., Karim, M.A., and Brett, C.L. (2017) Selective Lysosomal Transporter Degradation by Organelle Membrane Fusion. Dev. Cell *40*, 151-167.

McNatt, M.W., McKittrick, I., West, M., and Odorizzi, G. (2007) Direct binding to Rsp5 mediates ubiquitin-independent sorting of Sna3 via the multivesicular body pathway. Mol. Biol. Cell *18*, 697-706.

Merz, A.J., and Wickner, W. (2004) Resolution of organelle docking and fusion kinetics in a cell-free assay. Proc. Natl. Acad. Sci. USA *101*, 11548-11553.

Michaillat, L., Baars, T.L., and Mayer, A. (2012) Cell-free reconstitution of vacuole membrane fragmentation reveals regulation of vacuole size and number by TORC1. Mol. Biol. Cell *23*, 881-895.

McMahon, D. (1975) Cycloheximide is not a specific inhibitor of protein synthesis *in vivo*. Plant Physiol. *55*, 815-821.

Napolitano, G., and Ballabio, A. (2016) TFEB at a glance. J. Cell Sci. *129*, 2475-2481.

Nickerson, D.P., Russell, M.R.G., and Odorizzi, G. (2007) A concentric circle model of multivesicular body cargo sorting. EMBO Rep. *8*, 644-650.

Nickerson, D.P., Brett, C.L., and Merz, A.J. (2009) Vps-C complexes: gatekeepers of endolysosomal traffic. Curr. Opin. Cell Biol. *21*, 543-551.

Nickerson, D.P., West, M., Henry, R., and Odorizzi, G. (2010) Regulators of Vps4 ATPase activity at endosomes differentially influence the size and rate of formation of intralumenal vesicles. Mol. Biol. Cell *21*, 1023-1032.

Nikko, E., Marini, A.M., and André, B. (2003) Permease recycling and ubiquitination status reveal a particular role for Bro1 in the multivesicular body pathway. J. Biol. Chem. *278*, 50732-50743.

Nikko, E., and Pelham, H.R. (2009) Arrestin-mediated endocytosis of yeast plasma membrane transporters. Traffic *10*, 1856-1867.

Nordmann, M., Cabrera, M., Perz, A., Bröcker, C., Ostrowicz, C., Engelbrecht-Vandré, S., and Ungermann, C. (2010) The Mon1-Ccz1 complex is the GEF of the late endosomal Rab7 homolog Ypt7. Curr. Biol. *20*, 1654-1659.

O'Donnell, A.F., McCartney, R.R., Chandrashekarappa, D.G., Zhang, B.B., Thorner, J., and Schmidt, M.C. (2015) 2-Deoxyglucose impairs *Saccharomyces cerevisiae* growth by stimulating Snf1-regulated and □-arrestin-mediated trafficking of hexose transporters 1 and 3. Mol. Cell Biol. *35*, 939-955.

Palacios, F., Tushir, J.S., Fujita, Y., and D'Souza-Schorey, C. (2005) Lysosomal targeting of E-cadherin: a unique mechanism for the down-regulation of cell-cell adhesion during epithelial to mesenchymal transitions. Mol. Cell Biol. *25*, 389-402.

Palay, S.L., and Palade, G.E. (1955) The fine structure of neurons. J. Biophys. Biochem. Cytol. *1*, 69–88.

Parenti, G., Andria, G., and Ballabio, A. (2015) Lysosomal storage diseases: From pathophysiology to therapy. Annu. Rev. Med. *66*, 471-486.

Parkinson, M.D., Piper, S.C., Bright, N.A., Evans, J.L., Boname, J.M., Bowers, K., Lehner, P.J., and Luzio, J.P. (2015) A non-canonical ESCRT pathway, including histidine domain phosphotyrosine phosphatase (HD-PTP), is used for down-regulation of virally ubiquitinated MHC class I. Biochem. J. *471*, 79-88.

Peng, J., Schwartz, D., Elias, J.E., Thoreen, C.C., Cheng, D., Marsischky, G., Roelofs, J., Finley, D., and Gygi, S.P. (2003) A proteomics approach to understanding protein ubiquitination. Nat. Biotechnol. *21*, 921-926.

Perera, R.M., and Zoncu, R. (2016) The lysosome as a regulatory hub. Annu. Rev. Cell Dev. Biol. *32*, 223-253.

Piper, R.C., Cooper, A.A., Yang, H., and Stevens, T.H. (1995) VPS27 controls vacuolar and endocytic traffic through a prevacuolar compartment in *Saccharomyces cerevisiae*. J. Cell Biol. *131*, 603-607.

Pokrzywa, W., Guerriat, B., Dodzian, J., and Morsomme, P. (2009) Dual sorting of the *Saccharomyces cerevisiae* vacuolar protein Sna4p. Eukaryot. Cell, *8*, 278-286.

Prosser, D.C., Whitworth, K., and Wendland, B. (2010) Quantitative analysis of endocytosis with cytoplasmic pHluorin chimeras. Traffic *11*, 1141-1150.

Raiborg, C., and Stendmark, H. (2009) The ESCRT machinery in endosomal sorting of ubiquitylated membrane proteins. Nature *458*, 445-452.

Raiteri, L., and Raiteri, M. (2015) Multiple functions of neuronal plasma membrane neurotransmitter transporters. Prog. Neurobiol. *15*: E00089-1.

Rak, A., Fedorov, R., Alexandrov, K., Albert, S., Goody, R.S., Gallwitz, D., and Scheidig, A.J. (2000) Crystal structure of the GAP domain of Gyp1p: first insights into interaction with Ypt/Rab proteins. EMBO J *19*, 5105-5113.

Raymond, C.K., Howald-Stevenson, I., Vater, C.A., and Stevens, T.H. (1992) Morphological classification of the yeast vacuolar protein sorting mutants: evidence for a prevacuolar compartment in class E vps mutants. Mol. Biol. Cell *3*, 1389-1402.

Reddy, A., Caler, E.V., and Andrews, N.W. (2001) Plasma membrane repair is mediated by Ca^{2+}-regulated exocytosis of lysosomes. Cell *106*, 157-169.

Reggiori, F., and Pelham, H.R. (2001) Sorting of proteins into multivesicular bodies: ubiquitin-dependent and -independent targeting. EMBO J. *20*, 5176-5186.

Rodahl, L.M., Stuffers, S., Lobert, V.H., and Stenmark, H. (2009) The role of ESCRT proteins in attenuation of cell signalling. Biochem. Soc. Trans. *37*, 137-142.

Rousseau, A., and Bertolotti, A. (2016) An evolutionarily conserved pathway controls proteasome homeostasis. Nature *536*, 184-189.

Saksena, S., and Emr, S.D. (2009) ESCRTs and human disease. Biochem. Soc. Trans. *37*, 167-172.

Samson, R.Y., Obita, T., Freund, S.M., Williams, R.L., and Bell, S.D. (2008) A role for the ESCRT system in cell division in archaea. Science *322*, 1710-1713.

Scheuring, D., Schöller, M., Kleine-Vehn, J., and Löfke, C. (2015) Vacuolar staining methods in plant cells. Methods Mol. Biol. *1242*, 83-92.

Schneider, S. (2015) Inositol transport proteins. FEBS Lett. *589*, 1049-1058.

Schneider-Poetsch, T., Ju, J., Eyler, D.E., Dang, Y., Bhat, S., Merrick, W.C., Green, R., Shen, B., and Liu, J.O. (2010) Inhibition of eukaryotic translation elongation by cycloheximide and lactimidomycin. Nat. Chem. Biol. *6*, 209-217.

Schwartz, M.L., and Merz, A.J. (2009) Capture and release of partially zipped *trans*-SNARE complexes on intact organelles. J. Cell Biol. *185*, 535-539.

Schweigel-Rontgen, M. (2014) The families of zinc (SLC30 and SLC39) and copper (SCL31) transporters. Curr. Top. Membr. *73*, 321-355

Settembre, C., Fraldi, A., Medina, D.L., and Ballabio, A. (2013) Signals from the lysosome: a control centre for cellular clearance and energy metabolism. Nat. Rev. Mol. Cell Biol. *14*, 283-296.

Shields, S.B., Oestreich, A.J., Winistorfer, S., Nguyen, D., Payne, J.A., Katzmann, D.J., and Piper, R.C. (2009) ESCRT ubiquitin-binding domains function cooperatively during MVB cargo sorting. J. Cell Biol. *185*, 213-224.

Shields, S.B., and Piper, R.C. (2012) How ubiquitin functions with ESCRTs. Traffic *10*, 1306-1317.

Silverman, J.S., Muratore, K.A., and Bangs, J.D. (2013) Characterization of the late endosomal ESCRT machinery in *Trypanosoma brucei.* Traffic *14*, 1078-1090.

Smith, D.E., Clémençon, B., and Hediger, M.A. (2013) Proton-coupled oligopeptide transporter family SLC15: physiological, pharmacological and pathological implications. Mol. Aspects Med. *34*, 323-336.

Song, D., Xu, J., Bai, Q., Cai, L., Hertz, L., and Peng, L. (2014) Role of the intracellular nucleoside transporter ENT3 in transmitter and high K^+ stimulation of astrocytic ATP release investigated using siRNA against ENT3. ASN Neuro. *4*, 1759091414543439 eCollection 2014

Spang, A. (2016) Membrane Tethering Complexes in the Endosomal System. Front. Cell Dev. Biol. *4*, 35.

Stuffers, S., Brech, A., and Stenmark, H. (2009a) ESCRT proteins in physiology and disease. Exp. Cell Res. 315, 1619-1626.

Stuffers, S., Sem Wegner, C., Stenmark, H., and Brech, A. (2009b) Multivesicular endosome biogenesis in the absence of ESCRTs. Traffic *10*, 925-937.

Tarsio, M., Zheng, H., Smardon, A.M., Martinez-Munoz, G.A., and Kane, P.M. (2011) Consequences of loss of Vph1 protein-containing vacuolar ATPases (V-ATPases) for overall cellular pH homeostasis. J. Biol. Chem. *286*, 28089-28096.

Tasset, I., and Cuervo, A.M. (2016). Role of chaperone-mediated autophagy in metabolism. FEBS J. *283*, 2403-2413.

Teis, D., Saksena, S. and Emr, S.D. (2009) SnapShot: The ESCRT Machinery. *Cell* 137: 182-182.e1

Theos, A.C., Truschel, S.T., Tenza, D., Hurbain, I., Harper, D.C., Berson, J.F., Thomas, P.C., Raposo, G., and Marks, M.S. (2006) A lumenal domain-dependent pathway for sorting to intralumenal vesicles of multivesicular endosomes involved in organelle morphogenesis. Dev. Cell *10*, 343-354.

Thorngren, N., Collins, K.M., Fratti, R.A., Wickner, W., and Merz, A.J. (2004) A soluble SNARE drives rapid docking, bypassing ATP and Sec17/18p for vacuole fusion. EMBO J *23*, 2765-2776.

Trajkovic, K., Hsu, C., Chiantia, S., Rajendran, L., Wenzel, D., Wieland, F., Schwille, P., Brügger, B., and Simons, M. (2008) Ceramide triggers budding of exosome vesicles into multivesicular endosomes. Science *319*, 1244-1247.

Tran, J.H., Chen, C-J., Emr, S., and Schekman, R. (2009) Cargo sorting into multivesicular bodies in vitro. Proc. Natl. Acad. Sci. USA. *106*, 17395-17400.

Treusch, S., Knuth, S., Slaugenhaupt, S.A., Goldin, E., Grant, B.D., and Fares, H. (2004) *Caenorhabditis elegans* functional orthologue of human protein h-mucolipin-1 is required for lysosome biogenesis. Proc. Natl. Acad. Sci. USA. *101*, 4483-4488.

Urbanowski, J.L., and Piper, R.C. (1999) The iron transporter Fth1 forms a complex with the Fet5 iron oxidase and resides on the vacuolar membrane. J Biol. Chem. *274*, 38061-38070.

Urbanowski, J.L., and Piper, R.C. (2001) Ubiquitin sorts proteins into intralumenal degradative compartment of the late-endosome/vacuole. Traffic *2*, 622-630.

Valastyan, J.S., and Lindquist, S. (2014) Mechanisms of protein-folding diseases at a glance. Dis. Model Mech. *7*, 9-14.

Van Belle, D., and André, B. (2001) A genomic view of yeast membrane transporters. Curr. Opin. Cell Biol. *13*, 389-398.

Velasco, I., Tenreiro, S., Calderon, I.L., and André, B. (2004) *Saccharomyces cerevisiae* Aqr1 is an internal-membrane transporter involved in excretion of amino acids. Eukaryot. Cell *3*, 1492-1503.

Vild, C.J., Li, Y., Guo, E.Z., Liu, Y., and Xu, Z. (2015) A novel mechanism of regulating the ATPase VPS4 by its cofactor LIP5 and the endosomal sorting complex required for transport (ESCRT)-III protein CHMP5. J. Biol. Chem. *290*, 7291-7303.

Voisine, C., Søndergaard Pedersen, J., and Morimoto, R.I. (2010) Chaperone networks: Tipping the balance in protein folding diseases. Neurobiol. Dis. *40*, 12-20.

Waller-Evans, H., and Lloyd-Evans, E. (2015) Regulation of TRPML1 function. Biochem. Soc. Trans. *43*, 442-446.

Wang, C-W., Stromhaug, P.E., Kauffman, E.J., Weisman, L.S., and Klionsky, D.J. (2003a) Yeast homotypic vacuole fusion requires the Ccz1-Mon1 complex during the tethering/docking stage. J. Cell Biol. *163*, 973-985.

Wang, L., Seeley, E.S., Wickner, W., and Merz, A.J. (2002) Vacuole fusion at a ring of vertex docking sites leaves membrane fragments within the organelle. Cell *108*, 357-369.

Wang, L., Merz, A.J., Collins, K.M., and Wickner, W. (2003b) Hierarchy of protein assembly at the vertex ring domain for yeast vacuole docking and fusion. J. Cell Biol. *160*, 365-374.

Wang, S., Thibault, G., and Ng, D.T. (2011) Routing misfolded proteins through the multivesicular body (MVB) pathway protects against proteotoxicity. J. Biol. Chem. *286*, 29376-29387.

Wang, W., Gao, Q., Yang, M., Zhang, X., Yu, L., Lawas, M., Li, X., Bryant-Genevier, M., Southall, N.T., Marugan, J., Ferrer, M. and Xu, H. (2015) Up-regulation of lysosomal TRPML1 channels is essential for lysosomal adaptation to nutrient starvation. Proc. Natl. Acad. Sci. USA *11*, E1373-1381.

Watanabe-Asano, T., Kuma, A., and Mizushima, N. (2014) Cycloheximide inhibits starvation-induced autophagy through mTORC1 activation. Biochem. Bioph. Res. Co. *445*, 334-339.

Wickner, W. (2010) Membrane fusion: five lipids, four SNAREs, three chaperones, two nucleotides, and a Rab, all dancing in a ring on yeast vacuoles. Annu. Rev. Cell Dev. Biol. *26*, 115-136.

Wickner, W., and Haas, A. (2000) Yeast homotypic vacuole fusion: a window on organelle trafficking mechanisms. Ann. Rev. Biochem. *69*, 247-275.

Wickner, W., and Schekman, R. (2008) Membrane fusion. Nat. Struct. Mol. Biol. *15*, 658-664.

Xu, H., and Ren, D. (2015) Lysosome physiology. Annu. Rev. Physiol. *77*, 57-70.

Xu, J., Reumers, J., Couceiro, J.R., Smet, F.D., Gallardo, R., Rudyak, S., Cornelis, A., Rozenski, J., Zwolinska, A., Marine, J-C., Lambrechts, D., Suh, Y-A., Rousseau, F., and Schymkowitz, J. (2011) Gain of function of mutant p53 by coaggregation with multiple tumor suppressors. Nat. Chem. Biol. *7*, 285-295.

Yeo, S.C., Xu, L., Ren, J., Boulton, V.J., Wagle, M.D., Liu, C., Ren, G., Wong, P., Zahn, R., Sasajala, P., Yang, H., Piper, R.C., and Munn, A.L. (2003) Vps20p and Vta1p interact with Vps4p and function in multivesicular body sorting and endosomal transport in *Saccharomyces cerevisiae*. J Cell Sci. *116*, 3957-3970.

Zhao, Y., Macgurn, J.A., Liu, M., and Emr, S.D. (2013) The ART-Rsp5 ubiquitin ligase network comprises a plasma membrane quality control system that protects yeast cells from proteotoxic stress. Elife *2*, e00459

Zhou, R., Kabra, R., Olson, D.R., Piper, R.C., and Snyder, P.M. (2010) Hrs controls sorting of the epithelial Na+ channel between endosomal degradation and recycling pathways. J. Biol. Chem. *285*, 30523-30530.

Zhu, L., Jorgensen, J.R., Li, M., Chuang, Y-S., and Emr, S.D. (2017) ESCRTs function directly on the lysosome membrane to downregulate ubiquitinated lysosomal membrane proteins. eLife *6*, e26403 DOI: 10.7554/eLife.26403.

Zoncu, R. Bar-Peled, L., Efeyan, A., Wang, S., Sancak, Y., and Sabatini, D.M. (2011) mTORC1 senses lysosomal amino acids through an inside-out mechanism that requires the Vacuolar H^+-ATPase. Science *334*, 678-683.

Supplemental Figures

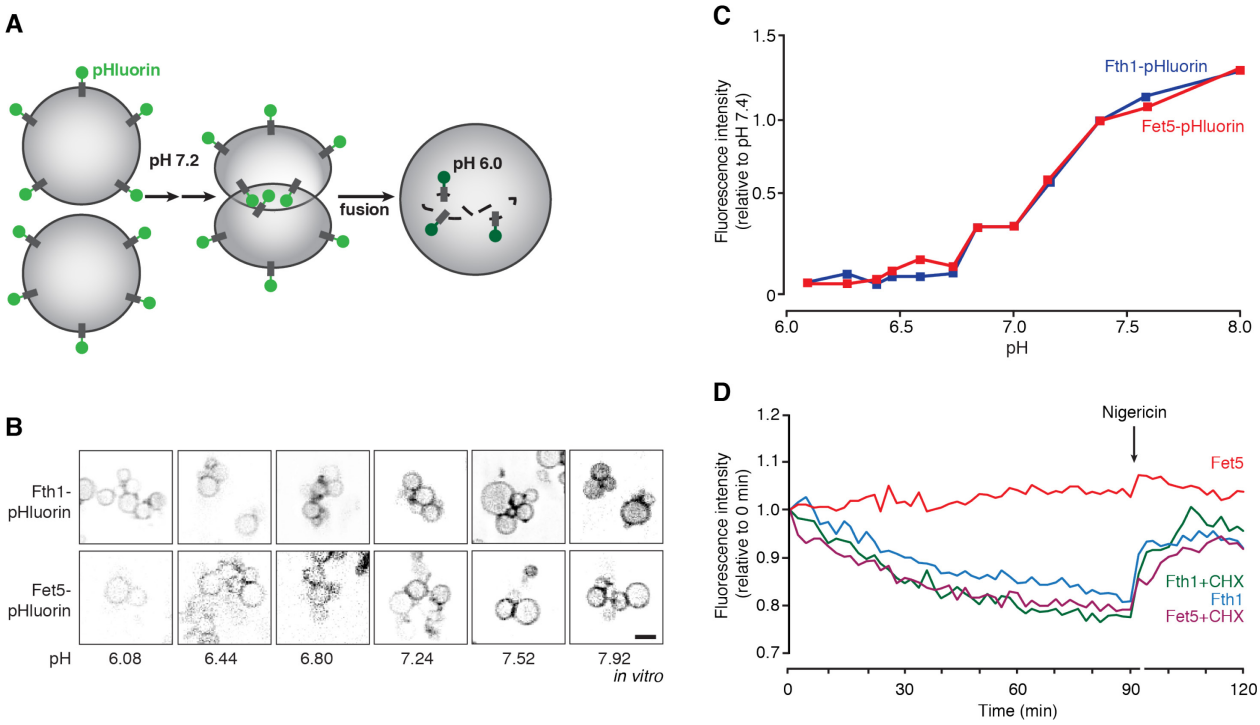

Figure S1. pHluorin-based assay to monitor polytopic protein internalization during fusion

(A) Model of the pHluroin assay with the pHluorin tag cytoplasmically tagged and after internalization, pHluroin fluorescence is quenched. **(B)** Micrographs of isolated vacuoles expressing Fth1-pHluorin or Fet5-pHuolin in reaction buffer titrated to increasing pH values (from 6.08 to 7.92) to visually demonstrate the pHluorin tag is responsive to changes in pH. The same acquisition and editing settings were used for all micrographs. **(C)** pHluorin fluorescence intensity was measured in isolated vacuole samples titrated to different reaction buffer pH and plotted as a calibration curve demonstrating that the pHluorin tag is cytoplasmic facing and pH sensitive. Values shown are relative to the fluorescence intensity measured at pH 7.4. **(D)** Relative pHluroin fluorescence of isolated vacuoles expressing Fet5-pHluorin or Fth1-pHluorin over the course of the fusion reaction treated in the absence or presence of 100 µM cycloheximide (CHX). After vacuoles were permitted to fuse for 90 minutes, 50 µM nigericin was added to demonstrate this is an assay of transporter internalization. Data shown are representative traces with values normalized to time zero (n = 2). Scale bar, 2 µm (*in vitro*).

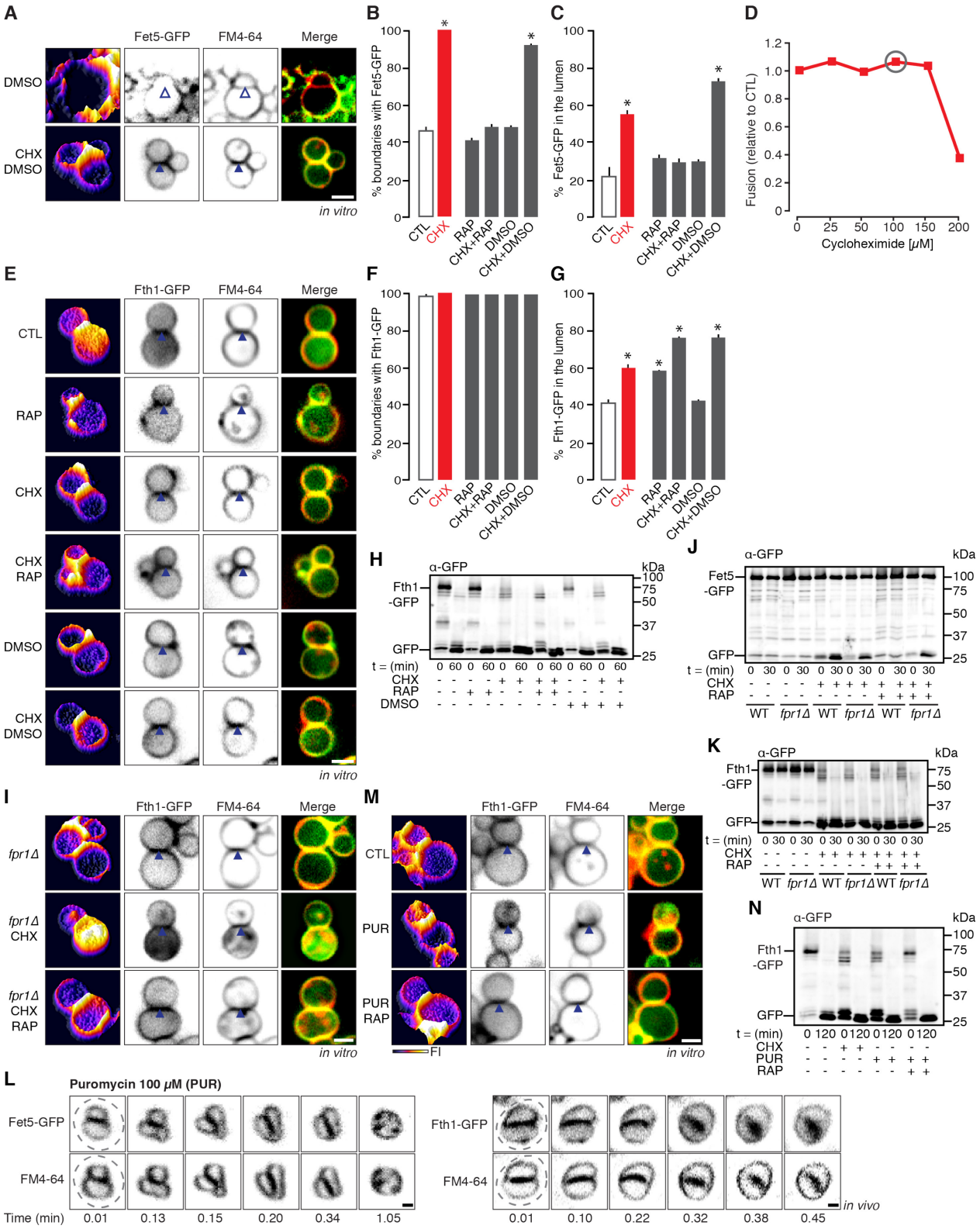
A
Fet5-GFP
FM4-64
Merge
DMSO
CHX DMSO
in vitro
B
% boundaries with Fet5-GFP
CTL
CHX
RAP
CHX+RAP
DMSO
CHX+DMSO
C
% Fet5-GFP in the lumen
D
Fusion (relative to CTL)
Cycloheximide [μM]
E
Fth1-GFP
CTL
RAP
CHX
CHX RAP
F
% boundaries with Fth1-GFP
G
% Fth1-GFP in the lumen
H
α-GFP
kDa
Fth1 -GFP
GFP
t = (min)
CHX
RAP
DMSO
J
Fet5 -GFP
WT
fpr1Δ
K
Fth1 -GFP
I
fpr1Δ
fpr1Δ CHX
fpr1Δ CHX RAP
M
PUR
PUR RAP
FI
N
L
Puromycin 100 μM (PUR)
Fet5-GFP
FM4-64
Time (min)
0.01
0.13
0.15
0.20
0.34
1.05
Fth1-GFP
0.10
0.22
0.32
0.38
0.45
in vivo

Figure S2. Rapamycin blocks cycloheximide-induced protein degradation by the ILF pathway

(A) Micrographs of docked vacuoles expressing Fet5-GFP pretreated with DMSO in the absence or presence of cycloheximide (CHX). **(B)** Percent of boundaries observed that contain Fet5-GFP and **(C)** GFP fluorescence intensity within the lumen of docked vacuoles under control (CTL), rapacmycin (RAP), or DMSO conditions in the absence or presence of cycloheximide (CHX) based on micrographic analysis ($n \geq 205$). **(D)** *In vitro* homotypic vacuole fusion of isolated vacuoles was measured after reactions were pretreated increasing concentrations of cycloheximide. Grey circle indicates CHX concentration (100 μM) used in all other experiments shown. **(E)** Micrographs of docked vacuoles expressing Fth1-GFP in the presence or absence of RAP, CHX or both. **(F)** Percent of boundaries containing Fth1-GFP and **(G)** lumenal GFP fluorescence were calculated from micrographic analysis ($n \geq 189$). **(H)** Western blot analysis of Fth1-GFP degradation in the absence (CTL) or presence of CHX, RAP or DMSO. **(I)** Micrographs of isolated vacuoles expressing Fth1-GFP in wildtype or *fpr1Δ* strain in the absence (CTL) or presence of CHX or RAP. **(J)** Western blot analysis of Fet5-GFP degradation in wildtype or *fpr1Δ* strain under CTL, CHX, and RAP conditions. (K) Western blot analysis of Fth1-GFP degradation in wildtype or *fpr1Δ* strain under CTL, CHX, and RAP conditions. **(L)** Images from time-lapse videos of vacuole fusion events within live yeast cells expressing either Fet5-GFP or Fth1-GFP in the presence of 100 μM puromycin. **(M)** Micrographs of docked vacuoles expressing Fth1-GFP in the absence or presence of PUR and RAP. **(N)** Western blot analysis of Fth1-GFP degradation under CTL, CHX, PUR and RAP conditions. Dotted lines outline each cell as observed by DIC. Scale bars, 1 μm. GFP fluorescence intensity profile plots (left panel). Scale bars, 1 μm (*in vivo*) or 2 μm (*in vitro*); *, $P < 0.05$.

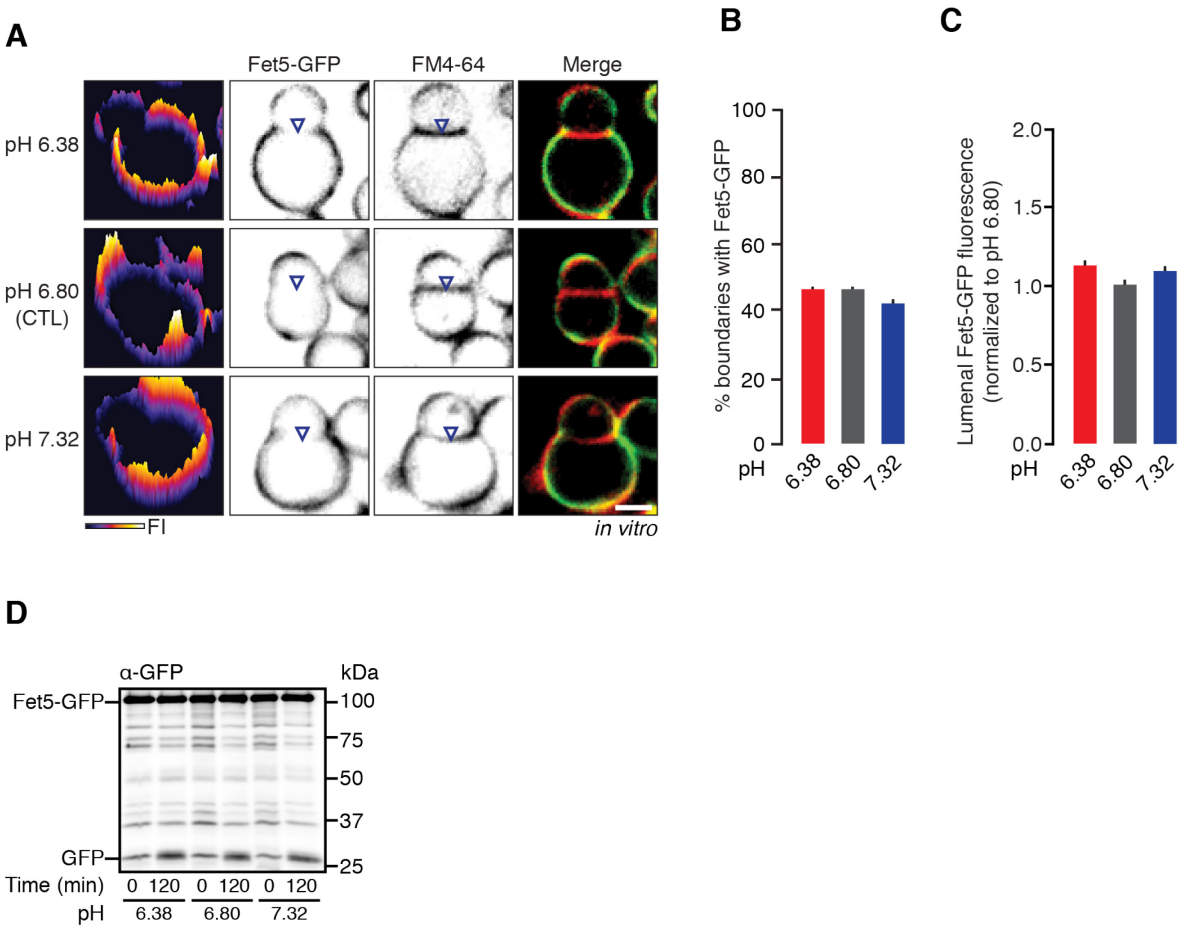

Figure S3. Fet5-GFP sorting and degradation are not affected by changes in pH

(A) Micrographs of docked vacuoles expressing Fet5-GFP imaged 60 minutes into the *in vitro* fusion reaction titrated to different pH values. **(B)** Percent of boundaries containing Fet5-GFP and **(C)** relative lumenal GFP fluorescence (normalized to pH 6.80; standard conditions) were calculated from micrographic data ($n \geq 83$). **(D)** Western blot comparing degradation kinetics of Fet5-GFP before and after fusion of isolated vacuoles at different pH values. Scale bars, 2 µm (*in vitro*).

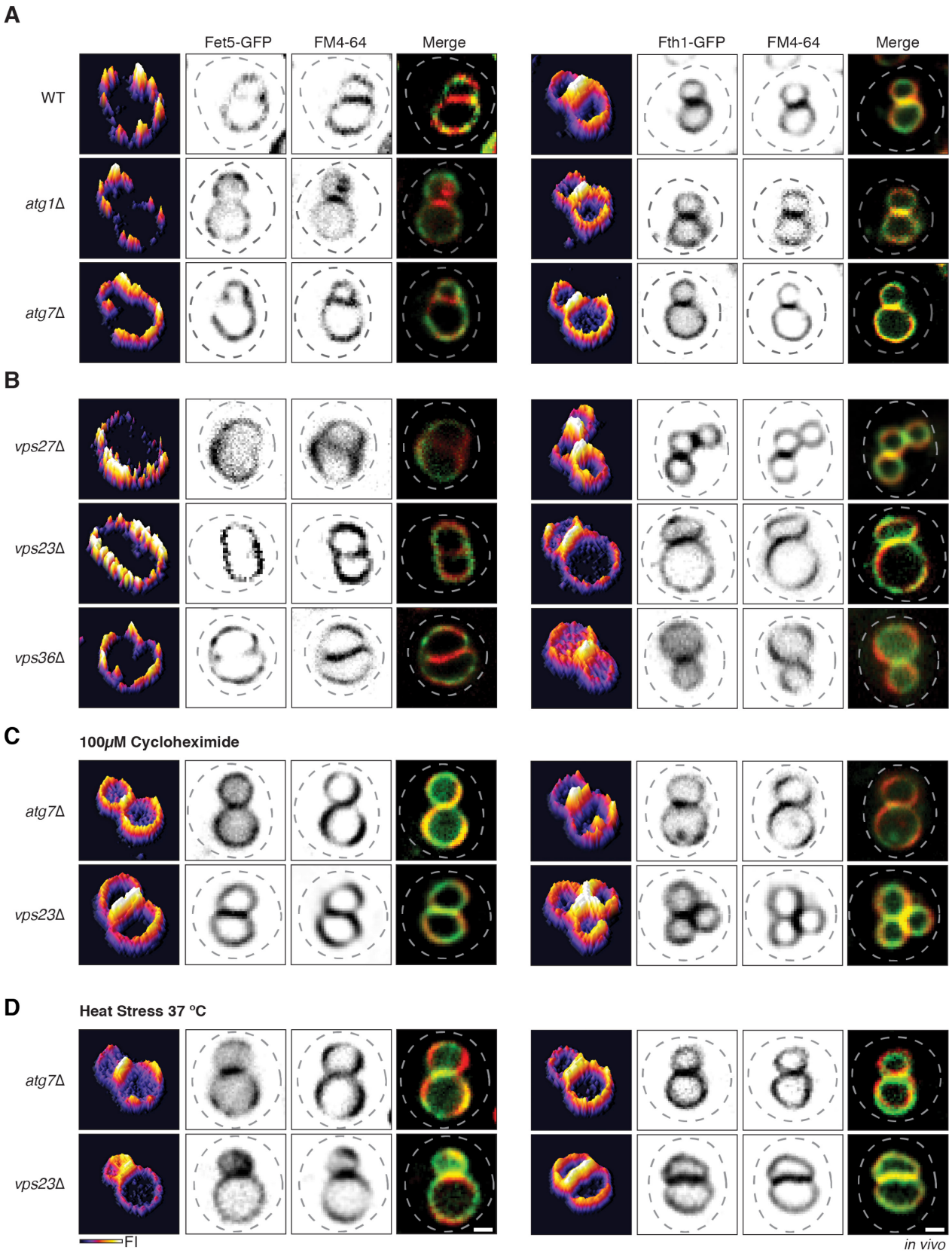
A
Fet5-GFP
FM4-64
Merge
Fth1-GFP
FM4-64
Merge
WT
atg1Δ
atg7Δ
B
vps27Δ
vps23Δ
vps36Δ
C
100μM Cycloheximide
atg7Δ
vps23Δ
D
Heat Stress 37 °C
atg7Δ
vps23Δ
FI
in vivo

Figure S4. Autophagy and ESCRT machinery are not required for lysosomal polytopic protein sorting by the ILF pathway within cells

Micrographs of docked vacuoles within cells expressing Fet5-GFP or Fth1-GFP in **(A)** autophagy or **(B)** ESCRT machinery mutants. Micrographs of yeast cells treated **(C)** with cycloheximide or **(D)** after heat stress in *atg7Δ* and *vps23Δ* mutants. Dotted lines outline each cell as observed by DIC. Scale bars, 1 μm (*in vivo*).

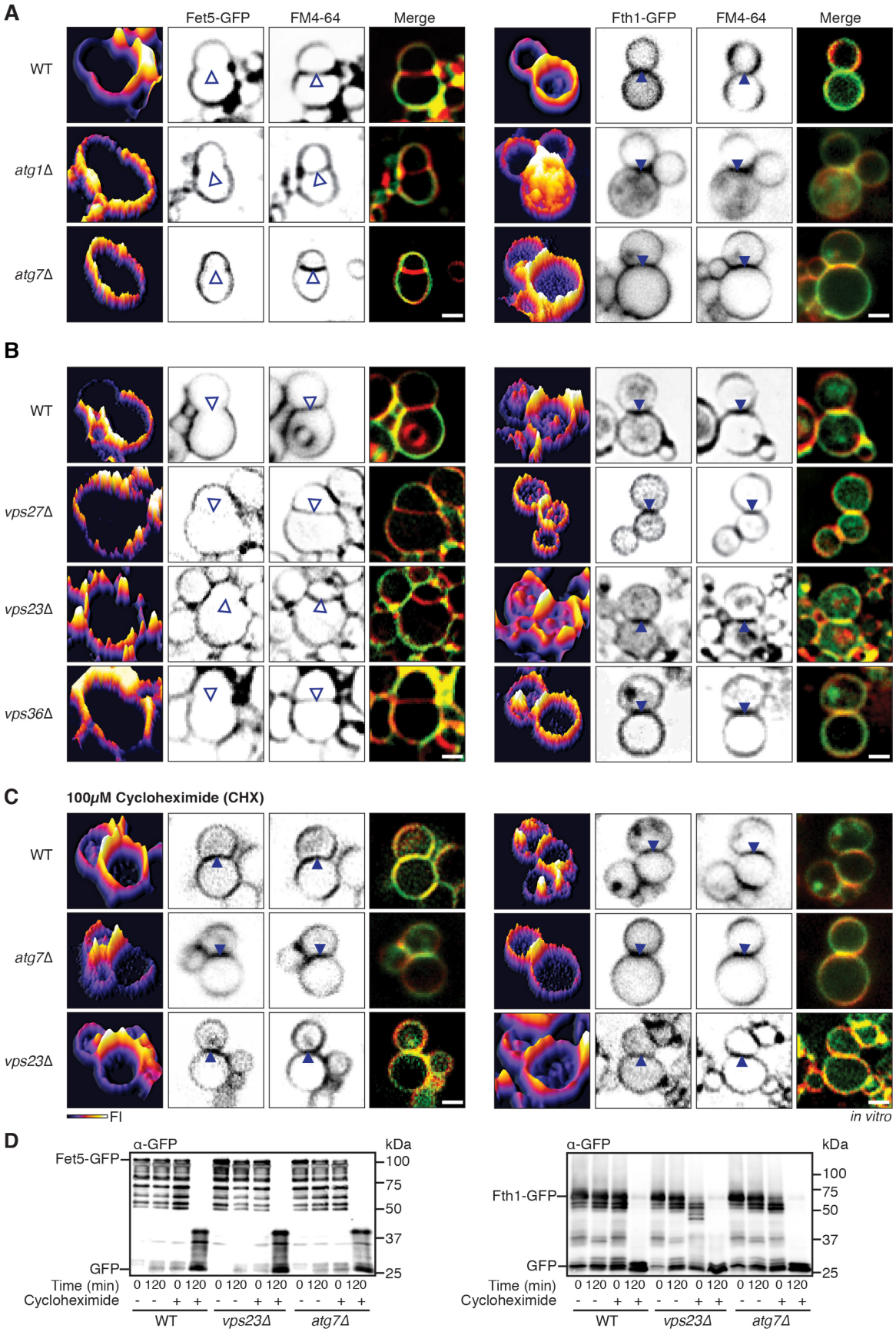
A
Fet5-GFP
FM4-64
Merge
Fth1-GFP
FM4-64
Merge
WT
atg1Δ
atg7Δ
B
WT
vps27Δ
vps23Δ
vps36Δ
C
100μM Cycloheximide (CHX)
WT
atg7Δ
vps23Δ
FI
in vitro
D
α-GFP
kDa
Fet5-GFP
GFP
100
75
50
37
25
Time (min)
0 120 0 120 0 120 0 120 0 120 0 120
Cycloheximide
- - + + - - + + - - + +
WT
vps23Δ
atg7Δ
α-GFP
kDa
Fth1-GFP
GFP
100
75
50
37
25
Time (min)
0 120 0 120 0 120 0 120 0 120 0 120
Cycloheximide
- - + + - - + + - - + +
WT
vps23Δ
atg7Δ

Figure S5. The ILF pathway does not require autophagy and MVB machinery for protein sorting *in vitro*

Micrographs of docked vacuoles expressing Fet5-GFP or Fth1-GFP imaged 60 minutes into the in vitro fusion reaction with mutations in the **(A)** autophagy or **(B)** ESCRT machinery. **(C)** Micrographs of docked vacuoles expressing Fet5-GFP or Fth1-GFP and **(D)** western blot analysis of degradation in *atg7*Δ and *vps23*Δ mutants in the absence (CTL) or presence of cycloheximide (CHX). Scale bars, 2 μm (*in vitro*).

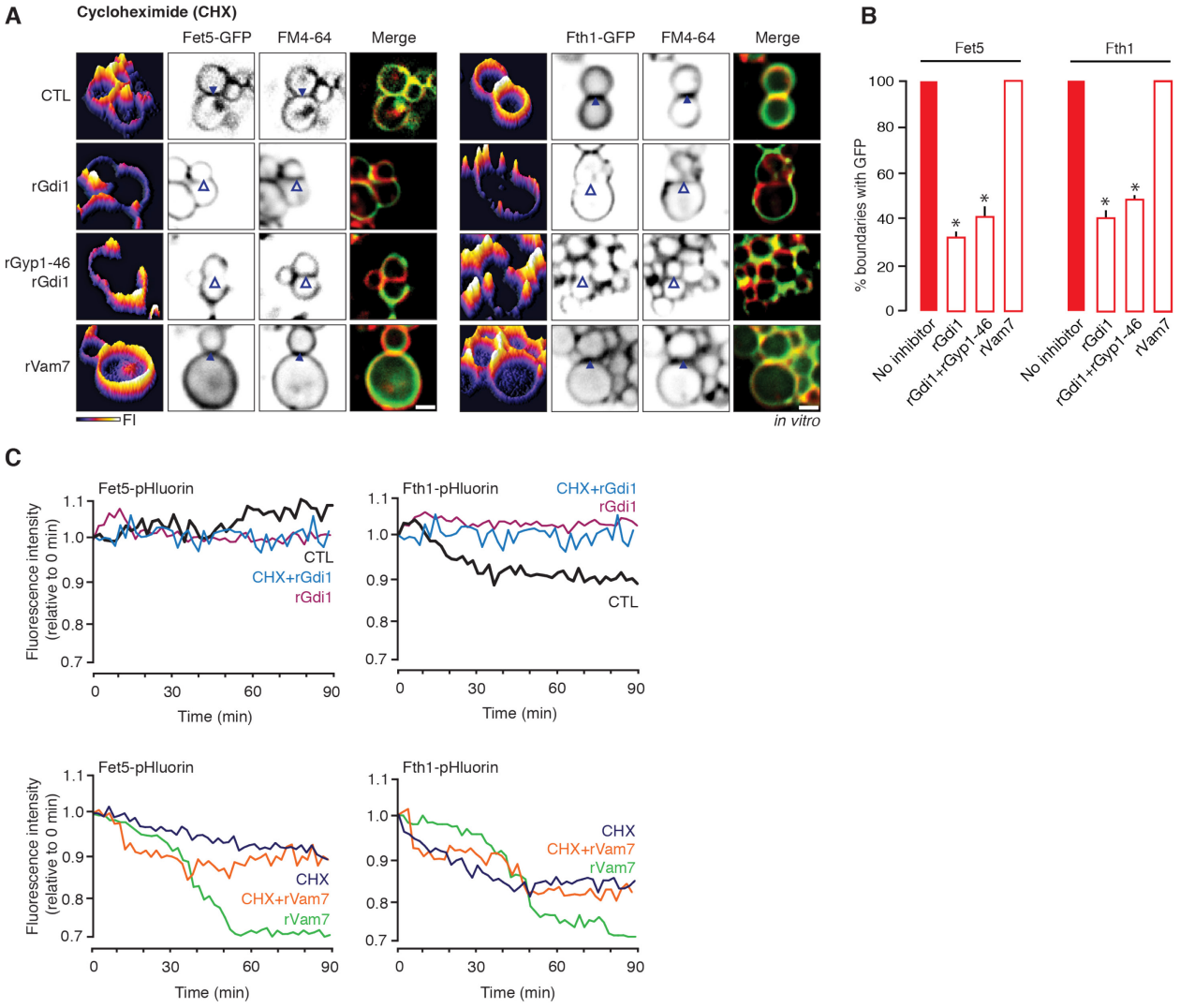

Figure S6. The docking machinery is responsible for cycloheximide-induced polytopic protein degradation by the ILF pathway

(A) Micrographs of docked vacuoles expressing Fet5-GFP or Fth1-GFP during the *in vitro* fusion reaction pretreated with cycloheximide (CHX) in the absence (CTL) or presence of 4 µM rGdi, 4 µM rGdi and 3.2 µM Gyp1-46, or 100 nM rVam7. **(B)** Percent of boundaries containing Fet5-GFP or Fth1-GFP under these conditions was calculated from micrographic analysis ($n \geq 203$). **(C)** Relative pHluorin fluorescence of isolated vacuoles expressing Fet5-pHluorin or Fth1-pHluorin during *in vitro* the fusion reaction incubated with rGdi or rVam7 in CTL or CHX treatment. Scale bars, 2 µm (*in vitro*); *, $P < 0.05$.

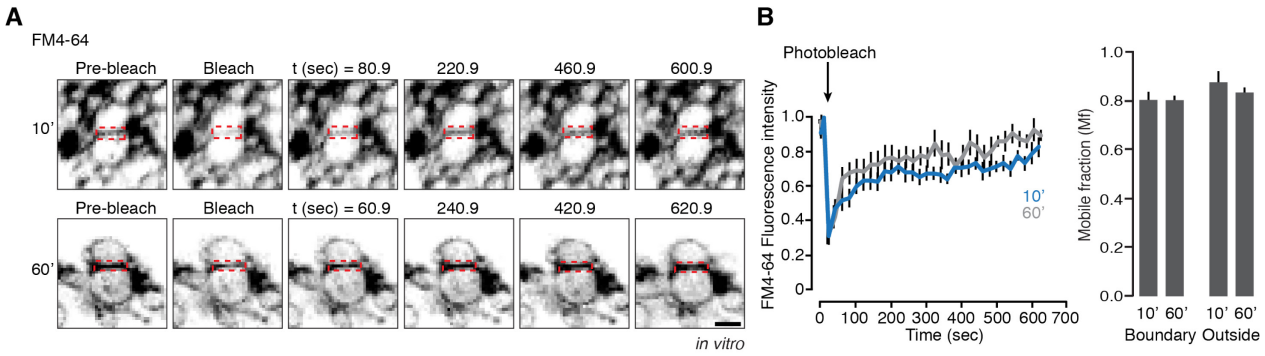

Figure S7. FRAP analysis of FM4-64 stained lysosomal vacuole membranes

(A) FRAP analysis of the boundary membrane between docked GFP-free vacuoles stained with FM4-64 10 and 60 minutes after vacuoles were permitted to fuse. **(B)** FM4-64 fluorescence intensity plots demonstrating fluorescence recovery in photobleached boundary membrane ROIs and Mf quantifications for boundary and outside membrane ROIs were calculated from micrographic data ($n \geq 12$). The red dotted box outlines ROIs subjected to photobleaching. Scale bar, 2 µm (*in vitro*).

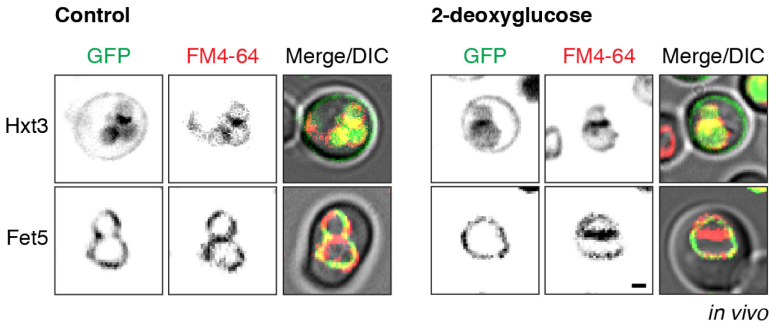

Figure S8. Fet5-GFP sorting is not affected by 2-deoxyglucose

Fluorescence and DIC micrographs of live wild type cells expressing GFP-tagged Hxt3 or Fet5 before (control) and after addition of 2-deoxyglucose for 30 minutes. Scale bars, 1 µm (*in vivo*). See also **Figure 10.**

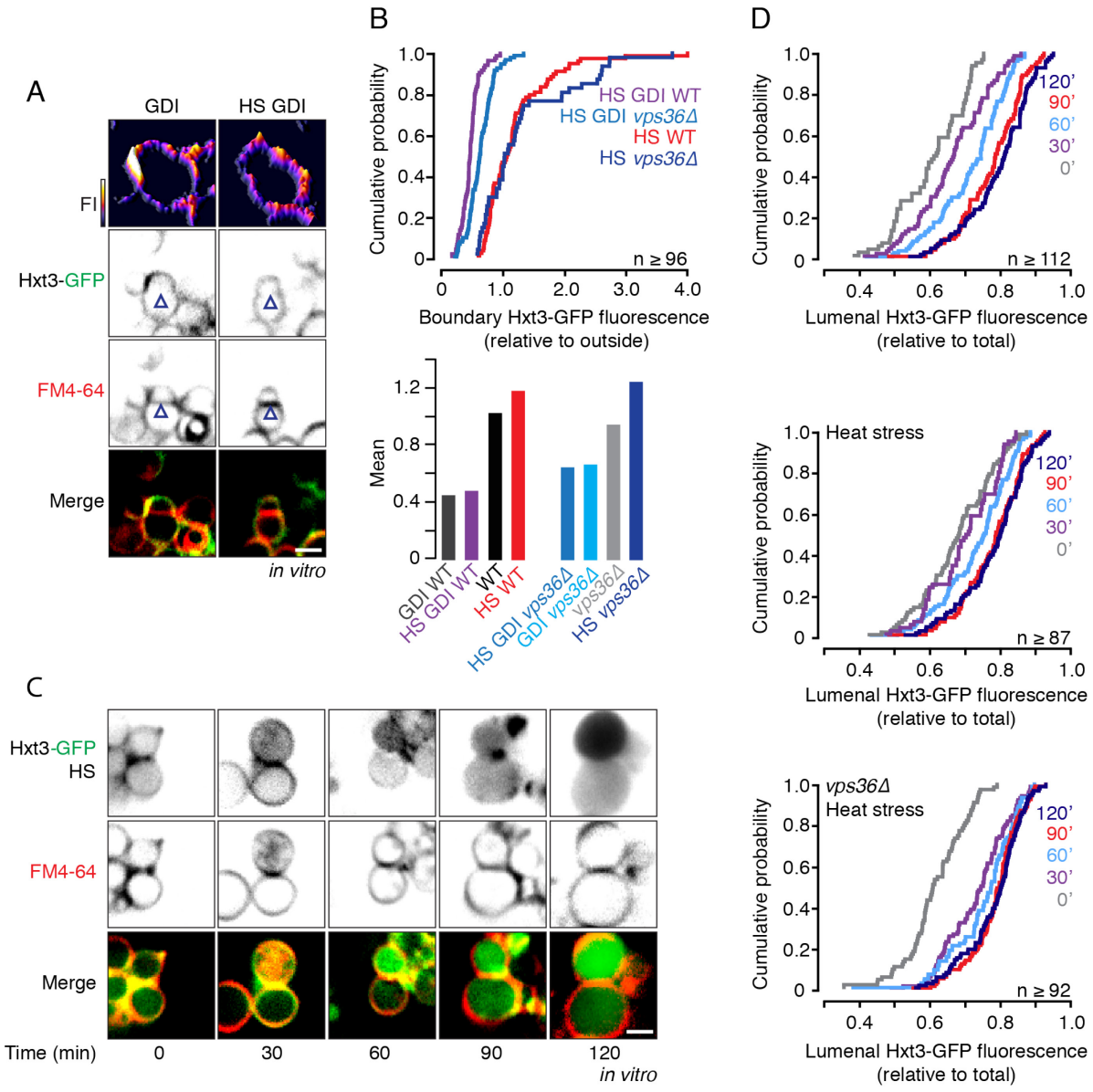
A
GDI
HS GDI
FI
Hxt3-GFP
FM4-64
Merge
in vitro
B
Cumulative probability
HS GDI WT
HS GDI vps36Δ
HS WT
HS vps36Δ
n ≥ 96
Boundary Hxt3-GFP fluorescence
(relative to outside)
Mean
GDI WT
HS GDI WT
WT
HS WT
HS GDI vps36Δ
GDI vps36Δ
vps36Δ
HS vps36Δ
C
Hxt3-GFP
HS
FM4-64
Merge
Time (min)
0
30
60
90
120
in vitro
D
Cumulative probability
120'
90'
60'
30'
0'
n ≥ 112
Lumenal Hxt3-GFP fluorescence
(relative to total)
Heat stress
n ≥ 87
vps36Δ
Heat stress
n ≥ 92

Figure S9. Hxt3-GFP is sorted and packaged for degradation by the ILF pathway independently of ESCRT machinery *in vitro*

(A) Fluorescence micrographs of lysosomes isolated from wild type yeast cells expressing Hxt3-GFP in the presence of fusion inhibitors (GDI) alone or in the presence of heat stress (HS) treatment. **(B)** Cumulative probability plots (top) of Hxt3-GFP fluorescence measured at boundaries between lysosomes isolated from wild type (WT) or *vps36*Δ cells after fusion in the presence or absence of heat stress (HS) alone or with fusion inhibitors (GDI) and respective mean (bottom) values as shown in **Figure 10C**. **(C)** Fluorescence micrographs of lysosomes isolated from wild type cells expressing Hxt3-GFP after 30 minutes of fusion in the presence of rGdi1 and rGyp1-46 (GDI) alone or with heat stress (HS) treatment. **(D)** Cumulative probability plots of Hxt3-GFP fluorescence measured within the lumen of lysosomes isolated from WT or *vps36*Δ cells after 0, 30, 60, 90 or 120 minutes of fusion in the presence of heat stress, as shown in **Figure 10E**. Scale bars, 2 μm (*in vitro*).

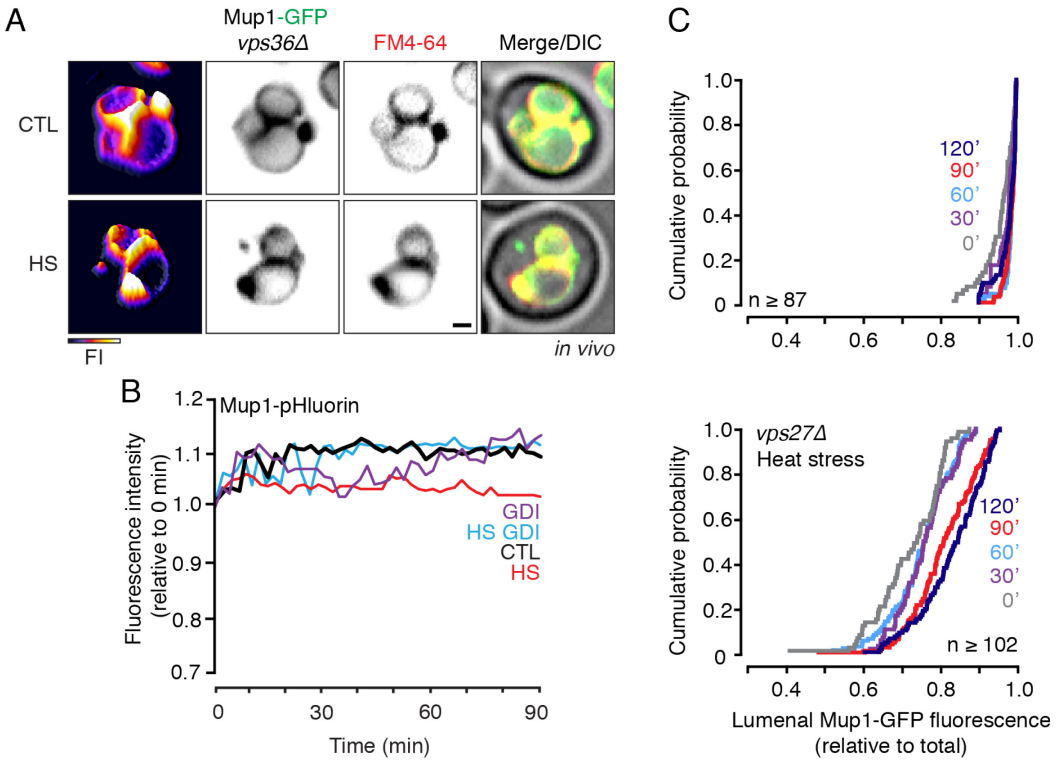

Figure S10. The ILF pathway sorts and internalizes the ESCRT client protein Mup1-GFP when MVB formation is impaired

(A) Fluorescence and DIC micrographs of live *vps36*Δ cells expressing GFP-tagged Mup1 before (CTL) and after heat stress (HS) for 30 minutes. 3-dimensional fluorescence intensity (FI) plots of Mup1-GFP are shown. **(B)** Fluorescence of lysosomes isolated from wild type cells expressing Mup1-pHluorin during the *in vitro* fusion reaction under control conditions (CTL) or after heat stress (HS) treatment in presence or absence of rGdi1 and rGyp1-46 (GDI). **(C)** Cumulative probability plots of Mup1-GFP fluorescence measured within the lumen of lysosomes isolated from WT (top) or *vps27*Δ (bottom) cells with heat stress treatment after 0, 30, 60, 90 or 120 minutes of fusion, as shown in **Figure 11F.** Scale bars, 1 μm (*in vivo*).

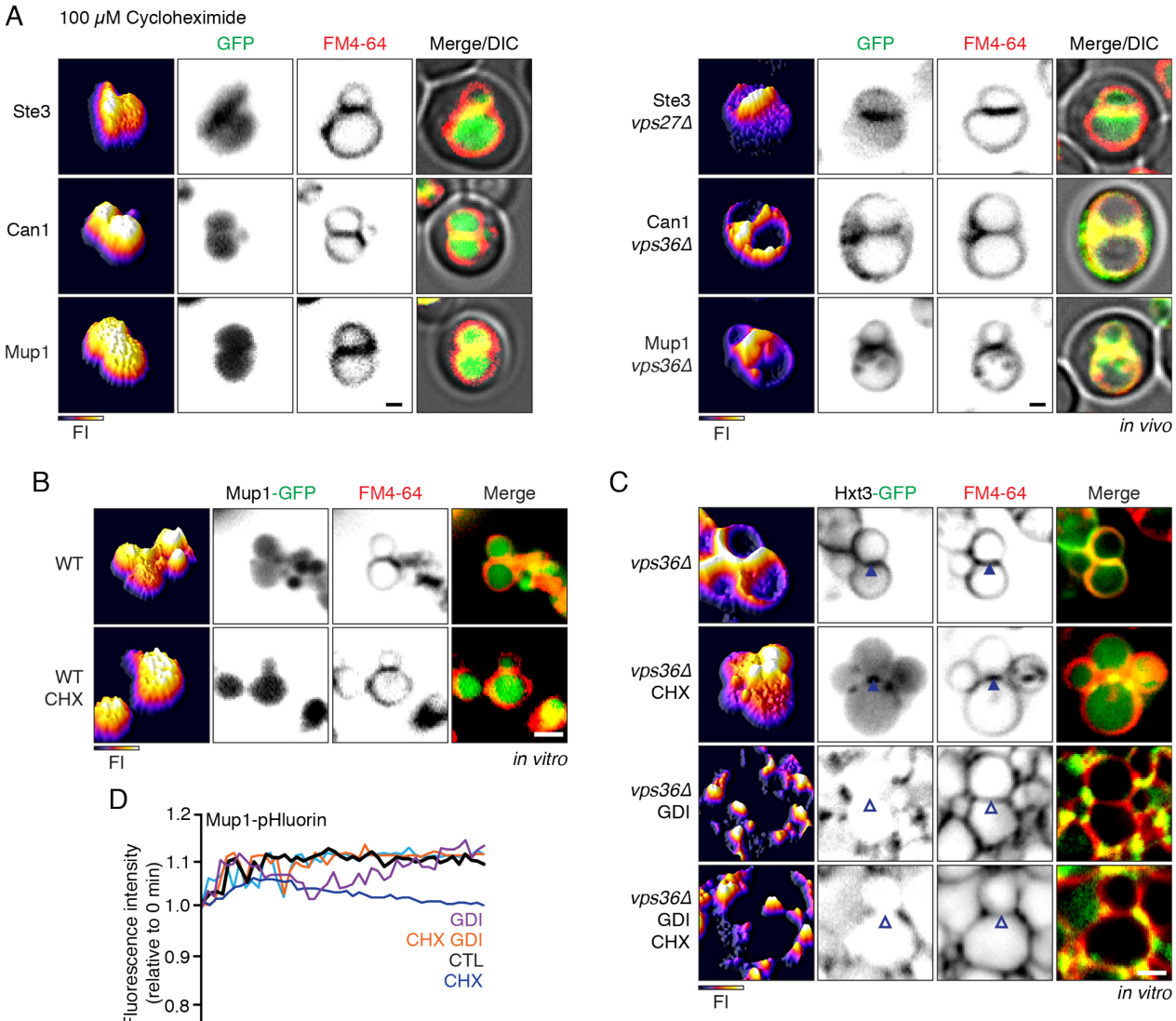
A
100 μM Cycloheximide
GFP
FM4-64
Merge/DIC
Ste3
Can1
Mup1
FI
Ste3 vps27Δ
Can1 vps36Δ
Mup1 vps36Δ
in vivo
B
Mup1-GFP
FM4-64
Merge
WT
WT CHX
FI
in vitro
C
Hxt3-GFP
FM4-64
Merge
vps36Δ
vps36Δ CHX
vps36Δ GDI
vps36Δ GDI CHX
FI
in vitro
D
Mup1-pHluorin
Fluorescence intensity (relative to 0 min)
1.2
1.1
1.0
0.9
0.8
0.7
0
30
60
90
Time (min)
GDI
CHX GDI
CTL
CHX

Figure S11. The ILF pathway sorts and internalizes surface polytopic proteins in response to TOR signaling

(A) Fluorescence and DIC micrographs of live wild type (left) and *vps27*Δ or *vps36*Δ (right) cells expressing GFP-tagged Ste3, Can1 or Mup1 after incubation with 100 μM cycloheximide for 70 minutes. **(B)** Fluorescence micrographs of lysosomes isolated from wild type Mup1-GFP cells in the absence (WT) or presence of pretreatment with cycloheximide (CHX). **(C)** Fluorescence micrographs of lysosomes isolated from *vps36*Δ cells expressing Hxt3-GFP in the absence or presence of cycloheximide (CHX) or rGdi1 and rGyp1-46 (GDI). 3-dimensional fluorescence intensity (FI) plots of Mup1-GFP or Hxt3-GFP are shown. Arrowheads indicate GFP-tagged protein enrichment (closed) or exclusion (open) within the boundary membrane. **(D)** Fluorescence of lysosomes isolated from wild type cells expressing Mup1-pHluorin during the *in vitro* fusion reaction under control conditions (CTL) or after cycloheximide (CHX) treatment in the presence or absence of rGdi1 and rGyp1-46 (GDI). Scale bars, 1 μm (*in vivo*) or 2 μm (*in vitro*). See also **Figure 12.**

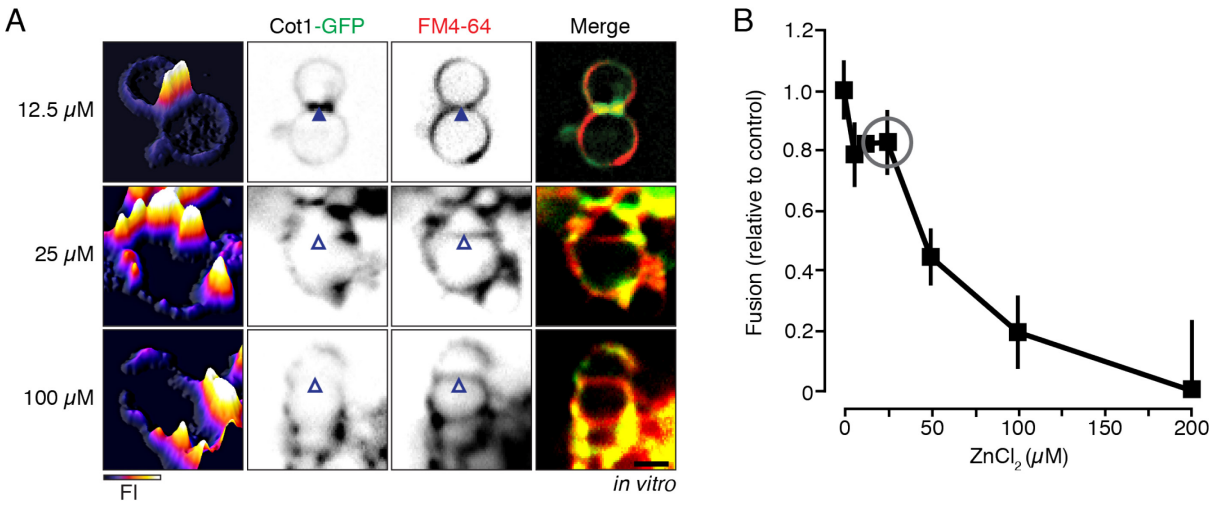

Figure S12. Conditions used to trigger Cot1-GFP degradation by the vReD pathway do not impair the membrane fusion reaction

(A) Fluorescence micrographs of isolated vacuoles from cells expressing Cot1-GFP pretreated for 5 minutes with different concentrations of $ZnCl_2$ prior to addition to the fusion reaction and further incubation for 30 minutes. **(B)** *In vitro* homotypic vacuole fusion of isolated vacuoles was measured after reactions were pretreated for 5 minutes at 27 °C with increasing concentrations of $ZnCl_2$. Grey circle indicates $ZnCl_2$ concentration (25 µM) used in all other experiments shown. Scale bar, 2 µm (*in vitro*). See also **Figure 15**.

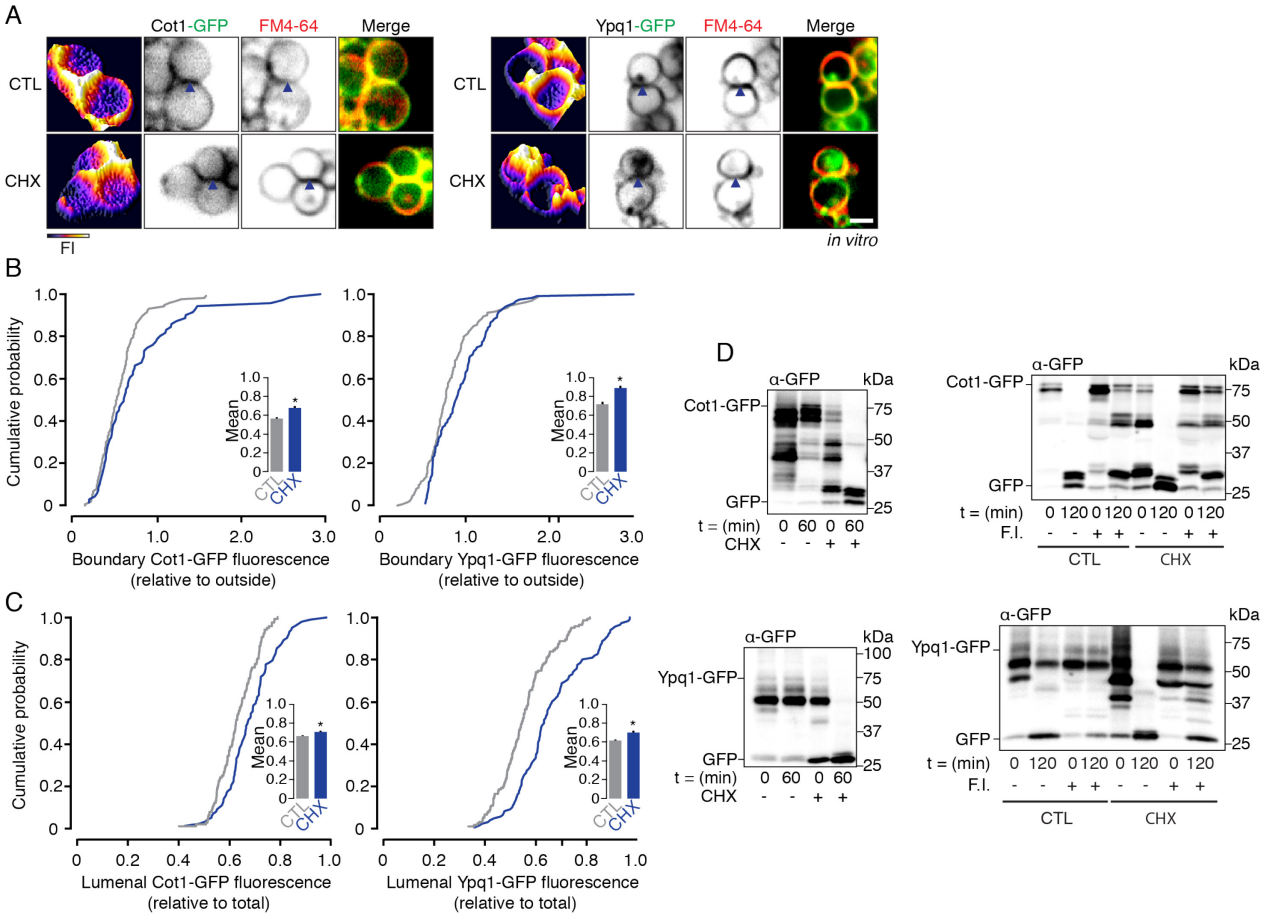

Figure S13. The ILF pathway degrades Cot1 and Ypq1 in response to TOR signaling on isolated vacuoles

(A) Fluorescence micrographs of vacuoles isolated from cells expressing Cot1-GFP or Ypq1-GFP under standard fusion conditions (CTL) or when vacuoles were pretreated with cycloheximide (CHX). Boundary membranes containing GFP fluorescence are indicated by closed arrowheads and GFP fluorescence profile are plotted (left panel). Scale bar, 2 µm (*in vitro*). Cumulative probability curves of GFP fluorescence intensity within the boundary membrane **(B)** or vacuolar lumen **(C)** of micrographs presented in **A**. ($n \geq 142$). **(D)** Western blots comparing Cot1-GFP and Ypq1-GFP degradation kinetics before and after fusion under standard conditions (CTL) or when isolated vacuoles were pretreated with cycloheximide (CHX) **(E)** in the absence or presence of fusion inhibitors rGdi1 and rGyp1-46 (F.I.). See also **Figure 16**.

Supplemental Movie Legends

Movie S1, related to Figure 2

Movie of a vacuole fusion event demonstrating the sorting and internalization of Vph1-GFP into the vacuolar lumen. GFP and FM4-64 fluorescence, and the two channels merged are shown.

Movie S2, related to Figure 2

Movie of a vacuole fusion event demonstrating the exclusion of Fet5-GFP from the boundary membrane although a membrane fragment was formed. GFP and FM4-64 fluorescence, and the two channels merged are shown.

Movie S3, related to Figure 2

Movie of a vacuole fusion event demonstrating the sorting and internalization of Fth1-GFP into the vacuolar lumen. GFP and FM4-64 fluorescence, and the two channels merged are shown.

Movie S4, related to Figure 3

Movie of a vacuole fusion event demonstrating the sorting and internalization of Fet5-GFP into the vacuolar lumen after heat stress. GFP and FM4-64 fluorescence, and the two channels merged are shown.

Movie S5, related to Figure 3

Movie of a vacuole fusion event demonstrating the sorting and internalization of Fth1-GFP into the vacuolar lumen after heat stress. GFP and FM4-64 fluorescence, and the two channels merged are shown.

Movie S6, related to Figure 4

Movie of a vacuole fusion event demonstrating the sorting and internalization of Fet5-GFP into the vacuolar lumen after cycloheximide treatment. GFP and FM4-64 fluorescence, and the two channels merged are shown.

Movie S7, related to Figure 4

Movie of a vacuole fusion event demonstrating the sorting and internalization of Fth1-GFP into the vacuolar lumen after cycloheximide treatment. GFP and FM4-64 fluorescence, and the two channels merged are shown.

Movie S8, related to Figure 10

Movie of a vacuole fusion event demonstrating the internalization of *vps36*Δ cells expressing Hxt3-GFP into the vacuolar lumen. GFP and FM4-64 fluorescence, and the two channels merged are shown.

Movie S9, related to Figure 11

Movie of a vacuole fusion event demonstrating the internalization of *vps27*Δ cells expressing Mup1-GFP into the vacuolar lumen. GFP and FM4-64 fluorescence, and the two channels merged are shown.

Movie S10, related to Figure 12

Movie of a vacuole fusion event demonstrating the internalization of *vps27*Δ cells expressing Mup1-GFP into the vacuolar lumen after cycloheximide treatment. GFP and FM4-64 fluorescence, and the two channels merged are shown.

Movie S11, related to Figure 12

Movie of a vacuole fusion event demonstrating the internalization of Hxt3-GFP into the vacuolar lumen after cycloheximide treatment. GFP and FM4-64 fluorescence, and the two channels merged are shown.

Movie S12, related to Figure 13

Movie of a vacuole fusion event demonstrating the sorting and internalization of Ypq1-GFP into the vacuolar lumen. GFP and FM4-64 fluorescence, and the two channels merged are shown.

Movie S13, related to Figure 13

Movie of a vacuole fusion event demonstrating the internalization of *vps36*Δ cells expressing Ypq1-GFP into the vacuolar lumen. GFP and FM4-64 fluorescence, and the two channels merged are shown.

Movie S14, related to Figure 13

Movie of a vacuole fusion event demonstrating the sorting and internalization of Cot1-GFP into the vacuolar lumen. GFP and FM4-64 fluorescence, and the two channels merged are shown. Scale bar, 1 μm.

Movie S15, related to Figure 13

Movie of a vacuole fusion event demonstrating the internalization of *vps27*Δ cells expressing Cot1-GFP into the vacuolar lumen. GFP and FM4-64 fluorescence, and the two channels merged are shown.

Movie S16, related to Figure 14

Movie of a vacuole fusion event demonstrating the exclusion of Vba4-GFP from the boundary membrane although a membrane fragment was formed. GFP and FM4-64 fluorescence, and the two channels merged are shown.

Movie S17, related to Figure 14

Movie of a vacuole fusion event demonstrating the internalization of *vps36*Δ cells expressing Vba4-GFP into the vacuolar lumen. GFP and FM4-64 fluorescence, and the two channels merged are shown.

Movie S18, related to Figure 16

Movie of a vacuole fusion event demonstrating the exclusion of Vba4-GFP from the boundary membrane although a membrane fragment was formed and the presence of puncta closely apposed to the vacuolar membrane after cycloheximide treatment. GFP and FM4-64 fluorescence, and the two channels merged are shown.

Movie S19, related to Figure 17

Movie of a vacuole fusion event demonstrating the internalization of Vba4-GFP into the vacuolar lumen after heat stress. GFP and FM4-64 fluorescence, and the two channels merged are shown.